

NOTE TO USERS

This reproduction is the best copy available.

UMI[®]

FUZZY LOGIC CONTROL OF COMPRESSOR SURGE IN A TURBOJET ENGINE MODEL

by

**MARK LADERMAN, B. ENG.
RYERSON UNIVERSITY**

A thesis presented to Ryerson University
in partial fulfillment of the requirement for the degree of
Master of Applied Science in the Program of
Mechanical Engineering

Toronto, Ontario, Canada, 2004
© Mark Laderman, 2004

PROPERTY OF
RYERSON UNIVERSITY LIBRARY

UMI Number: EC52969

INFORMATION TO USERS

The quality of this reproduction is dependent upon the quality of the copy submitted. Broken or indistinct print, colored or poor quality illustrations and photographs, print bleed-through, substandard margins, and improper alignment can adversely affect reproduction.

In the unlikely event that the author did not send a complete manuscript and there are missing pages, these will be noted. Also, if unauthorized copyright material had to be removed, a note will indicate the deletion.

UMI[®]

UMI Microform EC52969

Copyright 2008 by ProQuest LLC.

All rights reserved. This microform edition is protected against unauthorized copying under Title 17, United States Code.

ProQuest LLC
789 E. Eisenhower Parkway
PO Box 1346
Ann Arbor, MI 48106-1346

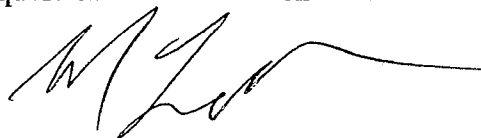
AUTHOR'S DECLARATION

I hereby declare that I am the sole author of this thesis.

I authorize Ryerson University to lend this thesis to other institutions or individuals for the purpose of scholarly research.

A handwritten signature in black ink, appearing to be 'M. Lee', written over the text of the second paragraph.

I further authorize Ryerson University to reproduce this thesis by photocopying or by other means, in total or in part, at the request of other institutions or individuals for the purpose of scholarly research.

A second handwritten signature in black ink, identical to the one above, written over the text of the third paragraph.

BORROWER'S PAGE

Ryerson University requires the signatures of all persons using or photocopying this thesis. Please sign below, and give address and date.

[illegible]

ABSTRACT

Fuzzy Logic Control of Compressor Surge in a Turbojet Engine Model

© Mark Laderman, 2004
Master of Applied Science
in the Program of
Mechanical Engineering
Ryerson University

Stable operation of a gas turbine engine's axial compressor is constrained by compressor surge and rotating stall. In order to avoid these flow instabilities, an active fuzzy logic control approach is applied to a turbojet engine model. The actuator surfaces used in the controller are the inlet guide vanes, movable stator blades, and variable spool speed with regards to the compressor; in addition, consideration is given to varying the engine inlet and exit geometries. For design purposes, in the simulation, the rotor blade geometry is also allowed to be variable. This thesis also examines the stability and control of the Moore-Greitzer model, and Gravdahl and Egeland's close coupled valve active controller. The Moore-Greitzer model is used as a black box to create a surge detection and avoidance fuzzy logic controller that does not require a *stall line*. The controller responds to the fluctuations in the axial mass flow coefficient and the pressure coefficient across the compressor system, and adjusts the throttle characteristic or the closed coupled valve characteristic.

ACKNOWLEDGEMENTS

The author would like to express his gratitude to his supervisors, Dr. Guangjun Liu and Dr. David Greatrix for their unfailing support and guidance before and during the process of this work. Special thanks are given to the author's Aerospace Engineering colleagues at Ryerson University: Stephen Borneman, Andrew Roach and Kyle Davidson for their beneficial discussions on modeling and control techniques. The author wishes to extend a thank you to Jerry Karpynczyk and other fellow members of the Ryerson Propulsion Research Facility. As well, the author wishes to thank Cliff Chan and fellow members of the Ryerson University Systems and Control Laboratory.

TABLE OF CONTENTS

ABSTRACT	vii
ACKNOWLEDGEMENTS	ix
TABLE OF CONTENTS	x
LIST OF FIGURES	xii
LIST OF TABLES	xiv
NOMENCLATURE	xv
 1. INTRODUCTION AND LITERATURE REVIEW	 1
1.1 MOTIVATION	2
1.2 BACKGROUND ON AXIAL COMPRESSORS	2
1.2.1 ROTATING STALL	3
1.2.2 SURGE	4
1.2.3 COMPRESSOR PERFORMANCE MAP	4
1.2.4 SURGE MARGIN	5
1.3 BACKGROUND ON COMPRESSOR MODELS	6
1.4 BACKGROUND ON ACTIVE CONTROL	8
1.5 BACKGROUND ON FUZZY LOGIC CONTROL	9
1.5 APPROACH	11
1.6 SUMMARY	13
 2. TURBOJET ENGINE MODELING	 14
2.1 TURBOJET ENGINE MODEL	15
2.1.1 INTAKES AND NOZZLES	15
2.1.1.1 SUBSONIC DIFFUSER INTAKE	16
2.1.1.2 LOW SUPERSONIC PITOT INTAKE	18
2.1.1.3 HIGH SUPERSONIC MULTIPLE SHOCK INTAKE	19
2.1.1.4 CONVERGING NOZZLE	21
2.1.1.5 CONVERGING-DIVERGING NOZZLE	23
2.1.2 COMPRESSORS AND TURBINES	24
2.1.2.1 BLADE GEOMETRY	25
2.1.2.2 INLET GUIDE VANES	28
2.1.2.3 ROTOR STAGE	29
2.1.2.4 STATOR STAGE	31
2.1.2.5 STAGE PRESSURE RATIO	32
2.1.3 BURNER AND AFTERBURNER	33
2.2 GREITZER COMPRESSOR MODEL	35
2.2.1 STABILITY ANALYSIS OF GREITZER MODEL	36
2.3 MOORE – GREITZER MODEL	38
2.3.1 IMPLICATIONS OF MOORE-GREITZER MODEL	40
2.4 GRAVDAHL AND EGELAND CCV MOORE-GREITZER MODEL	40
2.4.1 STABILITY ANALYSIS OF MG MODEL WITH CCV CONTROL	42
2.5 FUZZY LOGIC COMPRESSOR MODEL	43
2.5.1 CREATING THE MEMBERSHIP FUNCTIONS	44
2.5.2 CONSTRUCTING THE RULE BASE	44

3. FUZZY LOGIC CONTROLLERS	47
3.1 FUZZY LOGIC CONTROL	48
3.1.1 FUZZY SETS	49
3.1.2 MEMBERSHIP FUNCTIONS	50
3.1.3 FUZZY INFERENCE AND DEFUZZIFICATION	52
3.2 SPOOL SPEED CONTROLLER	54
3.3 IGV AND STATOR BLADE ANGLE CONTROLLERS	59
3.3.1 ADJUSTABLE IGV TO OPERATE AT DESIGN INCIDENCE ANGLE	59
3.3.2 ADJUSTABLE IGV TO OPERATE AT DEFINED REACTION	62
3.3.3 STATOR CONTROL AT DESIGN INCIDENCE ANGLE	63
3.3.4 COMBINATION CONTROL	63
3.3.5 MULTIPLE STAGE CONTROL	64
3.4 IGV WITH ADJUSTABLE RPM	64
3.5 ACTIVE SURGE CONTROLLER	65
3.5.1 IGV SURGE CONTROL	68
3.5.2 IGV AND VARIABLE ROTOR GEOMETRY CONTROL	72
3.6 DETECTION/AVOIDANCE CONTROLLER	72
4. SIMULATION RESULTS	75
4.1 IGV AND STATOR BLADE ANGLE CONTROLLERS	76
4.1.1 ADJUSTABLE IGV TO OPERATE AT DESIGN INCIDENCE ANGLE	76
4.1.2 ADJUSTABLE IGV TO OPERATE AT DEFINED REACTION	79
4.1.3 ADJUSTABLE STATOR TO OPERATE AT DESIGN INCIDENCE ANGLE	80
4.1.4 COMBINED CONTROL	80
4.2 SPOOL SPEED CONTROL	83
4.3 SURGE LINE CONTROLLER	83
4.3.1 IGV ONLY	84
4.3.2 IGV AND VARIABLE ROTOR GEOMETRY	85
4.3.3 IGV AND VARIABLE ROTOR GEOMETRY WITH DISTURBANCE	88
4.4 DETECTION/AVOIDANCE CONTROLLER	92
5. CONCLUSIONS	95
5.1 SUMMARY OF CONTRIBUTIONS	99
5.2 CONCLUSIONS	99
5.3 FUTURE WORK	96
REFERENCES	100
APPENDIX A: ADDITIONAL SIMULATION DATA	105
APPENDIX B: SIMULATION CODE	105

LIST OF FIGURES

Figure 1.1: Compressor performance map	5
Figure 1.2: MG model compared to gas turbine jet engine	8
Figure 1.3: (a) Crisp set for temperature (b) Fuzzy set for temperature	10
Figure 2.1: Turbojet engine model	15
Figure 2.2: Inlet diffuser geometry	17
Figure 2.3: Supersonic inlet with multiple shock waves variable geometry	19
Figure 2.4: Flow angles with sign conventions	26
Figure 2.5: Rotor turn angle and blade angles relationship	27
Figure 2.6: Velocity triangle for inlet guide vane stage	28
Figure 2.7: Rotor blade and hub dimensions	29
Figure 2.8: Velocity triangle for rotor stage	30
Figure 2.9: Velocity triangle for stator stage	32
Figure 2.10: Stability of the linearized Greitzer Model	37
Figure 2.11: Compressor and throttle characteristics	42
Figure 2.12: MFs for blade speed	44
Figure 2.13: MFs for the probability of a flow instability	45
Figure 3.1: Fuzzy control logic flowchart	48
Figure 3.2: Crisp set theory (a) A and not A (b) A union B (c) A intersection B	50
Figure 3.3: Membership functions (a) Triangle MF (b) Trapezoidal MF (c) Gaussian MF (d) Open ended Gaussian MF	51
Figure 3.4: Triangular membership functions of output	52
Figure 3.5: Max-min inference method	53
Figure 3.6: (a) Max-dot inference method (b) Product-sum inference method	53
Figure 3.7: Simple symmetric triangular membership functions for altitude input	55
Figure 3.8: MF for spool speed scaling factor	55
Figure 3.9: Three-dimensional control surface for spool speed controller	56
Figure 3.10: Acceptable values for the mass flow coefficient expressed as a MF	57
Figure 3.11: Two-dimensional control surface for spool speed control of mass coefficient	58
Figure 3.12: MF for outputted spool speed scaling factor	58
Figure 3.13: Three-dimensional control surface for spool speed control of mass coefficient	59
Figure 3.14: Two dimensional control surface for adjustable IGV to operate at design incidence angle	61
Figure 3.15: Combination control flow chart: (a) multiple error / single controller (b) multiple error / multiple controller	64
Figure 3.16: Multiple control surfaces flow chart	65
Figure 3.17: Surge line and surge margin	66
Figure 3.18: MF for incidence angle error for IGV surge controller	69
Figure 3.19: Two-dimensional plot of incidence error controller	70
Figure 3.20: Input MF of work coefficient error for IGV surge controller	70
Figure 3.21: Output MF for change in IGV for surge controller	71
Figure 3.22: Two-dimensional control surface for IGV surge controller	71
Figure 3.23: Three-dimensional control surface for IGV surge control	72
Figure 3.24: Three-dimensional control surface for MG surge detection model	74

Figure 4.1: IGV and stator blade variable geometry	76
Figure 4.2: Change in rotor blade incidence angle	78
Figure 4.3: Change in IGV angle.....	78
Figure 4.4: Velocity triangles and blade geometry for adjustable IGV operating at design incidence angle: (a) time zero (b) simulation end.....	79
Figure 4.5: Velocity triangles for an optimized rate of reaction (50%).....	79
Figure 4.6: Velocity triangles and blade geometry for adjustable stator operating at design incidence angle: (a) time zero (b) simulation end.....	80
Figure 4.7: Incidence angles resulting from flow entering the rotor blades	81
Figure 4.8: Incidence angles resulting from flow entering the stator blades	81
Figure 4.9: Change in stator blade stagger angle.....	82
Figure 4.10: Incidence angles resulting from flow entering the rotor blades	82
Figure 4.11: Degree of reaction	83
Figure 4.12: Change in work coefficient	84
Figure 4.13: Incidence angles resulting from flow entering the rotor blades	85
Figure 4.14: Change in IGV angle.....	86
Figure 4.15: Compressor characteristic	86
Figure 4.16: Change in work coefficient error value.....	87
Figure 4.17: Change in incidence angle of flow entering rotor blade	87
Figure 4.18 Change in deviation angle of flow leaving rotor blade	88
Figure 4.19: Velocity triangles and blade geometry for adjustable IGV and variable rotor geometry: (a) time zero (b) simulation end	88
Figure 4.20: Change in work coefficient error for disturbed case	89
Figure 4.21: Compressor characteristic for disturbance case	90
Figure 4.22: Change in IGV blade angle for disturbed case.....	90
Figure 4.23: Change in rotor blade incidence angle for disturbed case.....	91
Figure 4.24: Change in rotor blade deviation angle for disturbed case	91
Figure 4.25: Response (controller turned on at $\xi = 1000$)	93
Figure 4.26: Compressor and throttle characteristics for Simulation 1 (no CCV)	94

LIST OF TABLES

Table 1.1: Overview of compressor model properties.....	7
Table 2.1: User-defined variables for subsonic diffuser intake.....	16
Table 2.2: User-defined variables for converging nozzle.....	21
Table 2.3: User-defined variables for axial-flow compressor.....	26
Table 2.4: User-defined variables for burner and afterburner.....	34
Table 2.5: Operating ranges of fuzzy inputs.....	43
Table 2.6: Operating ranges of fuzzy output.....	43
Table 2.7: Rule base matrices for three-input / one-output system.....	46
Table 3.1: Crisp theory compared with fuzzy set theory.....	50
Table 3.2: Rule base matrices for three-input / one-output system.....	56
Table 3.3: Operating ranges of fuzzy inputs and output.....	73
Table 3.4: Rule base matrix for two-input / one-output system.....	74
Table 4.1: Numerical values for simulations.....	77
Table 4.2: Numerical values used in simulations.....	94

NOMENCLATURE

Roman

a	speed of sound
a_t	MG reciprocal time-lag of blade passage
d_h	rotor hub diameter
d_t	rotor blade tip-to-tip diameter
deH	deHaller number
c_p	specific heat
f	fuel-air ratio
h	altitude
i	compressor blade incidence angle
k	ratio of specific heats
l_c	MG nondimensional compressor length
l_e	MG nondimensional length of exit duct
l_i	MG nondimensional length of inlet duct
m	compressor duct flow parameter
\dot{m}_a	mass flow of air
\dot{m}_f	mass flow of fuel
n	incidence angle slope factor
q_r	heat of reaction in burner
$r_{d,ent}$	diffuser entrance radius,
$r_{d,exit}$	diffuser exit radius,
t_b / c	thickness-to-chord ratio,
u	rotor blade speed at mid-point radius
v	axial velocity (compressor)
w	whirl velocity
A_c	flow area
B	Greitzer B-parameter
C_x	axial velocity through MG model
H	MG compressor characteristic semi height
I	spool and rotor moment of inertia
J	MG squared amplitude of rotating stall
K_{sh}	blade shape parameter

$K_{t,i}$	design incidence angle thickness correct factor
K_T	throttle coefficient
L_c	length of ducts and compressor
L_d	diffuser length
L_E	length of exit duct
L_I	length of inlet duct
M	Mach number
$M_{n,0}$	normal component of Mach number
N	spool speed
N_s	number of compressor stages
P	pressure
\bar{P}_o	stagnation pressure
P	power to drive the compressor
R	mean compressor radius
R'	degree of reaction for compressor stage
R_d	gas constant for air (diffuser)
T	temperature
T_o	stagnation temperature
T	thrust
V	velocity
V_P	plenum volume
U	mean rotor velocity
W	MG compressor characteristic semi width

Greek

α	flow angle into blade
β	compressor blade metal angle
β_i	oblique shock angle (high supersonic intake)
β_{IGV}	IGV angle
δ	compressor blade deviation angle
γ_v	CCV gain
γ_T	throttle gain
η	efficiency
μ	Mach angle

θ	compressor blade turn angle
θ_i	ramp angle (high supersonic intake)
ρ	density
σ	compressor cascade solidity
τ	torque of the rotor
ξ	MG time in terms of radians of wheel travel
ψ	work coefficient
ψ_c	MG shut-off value of compressor characteristic
ζ	compressor blade stagger angle
Φ	mass flow coefficient
Θ	divergence semi-angle of the duct cross-section (intake)
Ψ	pressure coefficient
Ψ_c	compressor characteristic
Ψ_e	equivalent compressor characteristic
Ψ_v	CCV characteristic
Ψ_T	inverse throttle characteristic

Subscript

ab	afterburner
b	burner
c	compressor
d	diffuser
e	equivalent compressor
in	blade inlet angle
o	initial value
out	blade outlet angle
n	nozzle
r	rotor
s	stator
t	turbine
v	CCV
IGV	inlet guide vane
T	throttle
∞	atmospheric conditions

Diacritic Symbol

- rate of change
- * design value

Acronyms

CCV	close coupled valve
FLC	fuzzy logic controller
IGV	inlet guide vane
MF	membership function
MG	Moore-Greitzer

CHAPTER 1

INTRODUCTION AND LITERATURE REVIEW

The main focus of this chapter is to illustrate the differences between active and avoidance control with regards to surge in an axial compressor. This chapter provides background information on axial compressors and the flow instabilities, rotating stall and surge that can occur within the compressor. A literature review of some of the more predominant papers in the field of compressor modeling and active control is also provided. Finally, fuzzy logic control is introduced as an alternative to classical control theory along with a brief literature review on current fuzzy logic applications.

1.1 MOTIVATION

The work in this thesis is motivated by the fundamental instability problems of surge and rotating stall which limit the range of operation of the compressor stage in a gas turbine engine. The current industry solution for the instability problems is based on surge avoidance, where the operating point of the compressor is kept below the surge line using a surge margin. Aircraft engines are most effective when the compressor is operating at or near these aero-mechanical limits. Therefore, there is a potential for increasing the efficiency of the compressor by narrowing the gap between the current margin line and the surge line. This approach raises the need for an active controller that can quickly stabilize a compressor that crosses into the surge region. Active surge control in approach is fundamentally different to surge avoidance. In active surge control, feedback is used to stabilize the unstable regime of the compressor map. Another alternative to surge avoidance is surge detection and avoidance. Using a detection strategy, the drawbacks of the loosely defined surge margin can be avoided.

1.2 BACKGROUND ON AXIAL COMPRESSORS

A compressor transfers kinetic energy from an aero-mechanically-driven rotor to a steady flow of air. The pressure of the air is raised by converting the acceleration imparted by the rotating parts of the compressor via diffusion. In an axial-flow compressor the air flows through in the direction parallel to the axis of rotation. The interest in this field largely involves axial compressors rather than centrifugal, mainly due to the fact that the majority of aircraft engines utilize axial compressors (Gravdahl and Egeland, 1997b).

The kinetic energy of the rotor is converted into pressure energy of the air through the alternate rows of fixed stator blades and moving rotor blades. The moving blades are root-mounted to the turbine driven rotor; the fixed blades, which function as the diffusers, are attached to the compressor casing. Air is drawn into the compressor intake and enters the first cascade of moving rotor blades, where its absolute velocity is increased. The increase in velocity results from the action of the rotor blades, which, because of the applied torque, causes a whirl or rotational velocity to the air in the direction of the rotor

INTRODUCTION AND LITERATURE REVIEW

blade motion. In addition to the gain of whirl velocity, the divergent shapes of the passage between the blades results in a small pressure rise.

On leaving the rotor blades, the air enters the fixed stator blades where the whirl velocity is reduced and a further pressure rise occurs. The air leaves the stator blades with approximately the velocity it had before entering the moving blades, but at an increased pressure. A set of one ring of rotor blades and one ring of stator blades is called a stage and a stage pressure ratio is normally about 1.1:1. Due to the practical limit of the achievable pressure ratio - about 1.5 - of each stage of an axial compressor (Bathie, 1996), many stages are necessary to obtain a useful overall pressure ratio. The flow through a compressor will be examined in more detail in Section 2.1.2 of this report.

1.2.1 ROTATING STALL

An aircraft wing is said to *stall* when its angle of incidence is increased to the point where the air no longer flows smoothly over the wing but breaks away from the surface and becomes turbulent. When this happens the lift drops sharply and the drag increases. Rotating compressor blades are subject to stalling in a similar manner if the angle of incidence between the blade and the direction of the airflow is varied beyond critical limits. A design incidence angle that results in the smallest pressure loss coefficient can be calculated for each compressor cascade. As a general rule during operation the actual incidence angle should only deviate by \pm ten degrees from the design value, keeping the loss coefficient within an acceptable range of less than or equal to twice the minimum loss coefficient (Aungier, 2003).

Rotating stall is a two-dimensional, local instability phenomenon in which one or more local regions of stagnant flow rotate around the circumference of the compressor. These cells have a constant rotational speed between 20% and 70% of the rotor speed. Rotating stall induces large vibratory stresses in the blading, and depending on the stalled characteristics, can result in a large drop in performance and efficiency (Moore, 1984). The reduced flow rates can lead to undesirable thermal loads in the turbine.

FUZZY LOGIC CONTROL OF COMPRESSOR SURGE IN A TURBOJET ENGINE MODEL

Should the mass flow be reduced when the compressor is turning at low speed, because of the back pressure from the combustion chamber, stalling will start at the first row of moving blades and then progress aft. In the event of a reduction of mass flow when the compressor is turning at high speeds, a sudden change of aircraft attitude affecting the airflow at intake, a condition can arise in which stalling occurs in the high-pressure stages of the compressor (Greitzer, 1976).

1.2.2 SURGE

Aircraft wings not only have a stalling angle but also a stalling speed; the angle between the airflow and the wing chord line changes with speed, becoming greater as the speed drops. If the air mass flow through a compressor is reduced, the axial velocity of the air passing through the compressor is reduced accordingly. As the air velocity falls, stalling occurs at some blade stages and, if the condition is severe, other stages stall in unison and surging results. Surging signifies a complete breakdown of flow through the compressor.

Surge is characterized by large amplitude fluctuations of the nominal compressor pressure rise, and unsteady annulus-average mass flow through the compressor. Toward low mass flows, stable operation is constrained by surge. Surge can lead to failure in the system due to large mechanical and thermal loads in the blading and casing. Avoidance of surge improves maintainability, life span, and the performance of the compressor.

1.2.3 COMPRESSOR PERFORMANCE MAP

In normal operation of a compressor, the flow is nominally steady and axisymmetric. The pressure rise is dependent on the speed of rotation, but the efficient range is limited. As the flow through the compressor is throttled from the design point to the stall limits, the steady axisymmetric flow pattern becomes unstable. This instability can take on one of two forms, either surge or rotating stall depending upon the engine speed.

The performance of a compressor is plotted as pressure ratio versus mass flow for different rotational speeds as shown in Figure 1.1. The plot is divided into two regions by the stall (or surge) line. This line defines the operation limits of the engine. To the

INTRODUCTION AND LITERATURE REVIEW

left of the stall line the flow is no longer steady. In this region large oscillations of the mass flow rate may occur (surge) or severe self-induced circumferential flow distortions may rotate around the annulus (rotating stall), or a combination of both may appear (Greitzer, 1980).

It is important to know which mode of instability will occur since their consequences can be quite different. Rotating stall induces large vibratory stresses in the blading that is unacceptable for structural reasons. In addition, there is a drop in performance and an increase in turbine operating temperature. Surge causes high blade and casing stress levels as well as possible system failure (Willems et. al, 1998). For low flow regimes, the operating range is limited by surge and rotating stall. For high mass flow the operating range is bounded by the limited capacity of the compressor.

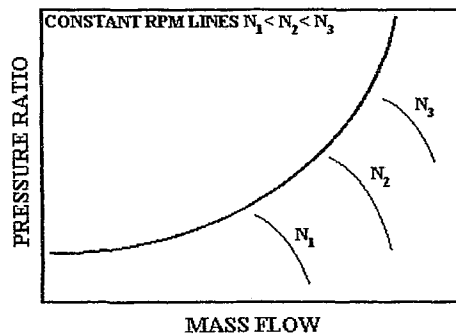


Figure 1.1: Compressor performance map

As mass flow is reduced the pressure rise increases. A point is reached at which the pressure rise is a maximum and further reduction in mass flow leads to an abrupt and definite change in the flow pattern in the compressor. Beyond this point the compressor enters into either a stall or a surge. Regardless of the flow instability this point is called the surge point.

1.2.4 SURGE MARGIN

Surge avoidance prevents the compressor from operating in a region near and beyond the surge line by preventing the compressor from crossing the surge margin. Stable

FUZZY LOGIC CONTROL OF COMPRESSOR SURGE IN A TURBOJET ENGINE MODEL

operation can be guaranteed by operating the compressor at a safe distance from the unstable region (avoidance control). In this strategy, a surge margin is defined at some distance below the surge line. The safety margin is set by the sensors and actuator limitations, and the uncertainty in the location of the surge line. If the compressor's operating point crosses the surge margin, the controller must compensate quickly by adjusting the current flight settings. According to Cumpsty (1989), in a multistage axial compressor in a turbojet it is normal to insist on a 25% surge margin.

1.3 BACKGROUND ON COMPRESSOR MODELS

An essential step in controller design is to understand the physical phenomena in the system and to develop a mathematical model that describes the most important phenomena. Table 1 provides an overview of various model properties; one-dimensional models describe axisymmetric flows, while two-dimensional models predict flow variations in both axial and circumferential directions.

The models described in Badmus, et al. (1994) and Botros (1995) start from a general description by applying principles of conservation of mass, energy, and momentum for a perfect gas. Both models can be applied to generic compressor systems to describe the dynamic behaviour of axial and centrifugal compressors during surge. In comparison to the other models studied, these models are relatively complex.

The theoretical compressor model developed by Moore and Greitzer approximates fully developed surge and rotating stall observed in laboratory-scale gas turbines. For dynamic analysis and controller design in axial compressors, the low-dimensional Greitzer, Moore, and Moore-Greitzer models are frequently used. The Greitzer model (1976) can predict the onset of stall and the Moore model (1984) can foresee the onset of surge. Moore and Greitzer combined their models (1986) to predict both flow instabilities. The majority of literature available on compressor modeling refers to this model as a starting point for new developments and variations. For instance Haynes, et al. (1994) introduces the effect of blade row time-lags to the Moore-Greitzer model to describe the occurrence of higher order rotating stall modes at different mass flows. The Botros and Gravdahl-

INTRODUCTION AND LITERATURE REVIEW

Egeland (1997a) models incorporate rotor speed variations in order to include spool dynamics in the Moore-Greitzer model. Numerous other variations of the Moore-Greitzer model have been developed to contain variable throttle values, bleed valves and actuators.

Model	Flow Description	Compressor Type	Instability Described
Badmus, et al.	1D Compressible	AC	S
Botros	1D Incompressible	AC	S
Greitzer	1D Incompressible	A	S
Hansen, et al.	1D Incompressible	C	S
Fink, et al.	1D Incompressible	C	S
Moore	2D Incompressible	A	R
Adomaitis	2D Incompressible	A	R
Moore-Greitzer	2D Incompressible	A	SR
Haynes, et al.	2D Incompressible	A	SR
Gravdahl-Egeland	2D Incompressible	A	SR
A: Axial Compressor, C: Centrifugal Compressor, S: Surge, R: Rotating Stall			

Table 1.1: Overview of compressor model properties

Haynes, et al. (1994) showed that rotating stall mainly occurs in low-speed axial compressors, whereas surge occurs at relatively high speeds in axial as well as radial compressors. Although not as common, Fink, et al. (1992) reported results of rotating stall in radial compressors. The occurring type of instability can be affected by the plenum volume; rotating stall may result from surge when the size of the plenum is progressively reduced. Also surge may propagate by throttling the compressor to lower mass flows. Both flow phenomena are related and techniques that delay the onset of one instability is seen to be effective in delaying the other.

Instabilities in axial compressors generally are better understood than those in centrifugal compressors and the Moore-Greitzer model has emerged as the workhorse of axial flow compressor modeling. For these reasons, this model is used later in this report as a black box representation of a jet engine compressor.

FUNCTIONAL LOGIC CONTROL OF COMPRESSOR SURGE IN A TURBOJET ENGINE MODEL

In the MG model, an incompressible fluid is pressurized in the compressor and is discharged into a closed tank that contains a compressible gas. This tank discharges via a throttle valve into another larger reservoir. The essential elements in the system are the compressor that realizes the pressurization, the inertness of the incompressible fluid in the compressor and throttle ducts, the mass storage capacity of the system in the closed tank - the plenum - and the throttle, which represents the system pressure requirements. This system is analogous to a gas turbine engine, where the plenum is the combustion chamber and the throttle represents the turbine. The idealized system is shown in Figure 1.2. The Moore-Greitzer model is a simplified model of a single shaft gas turbine.

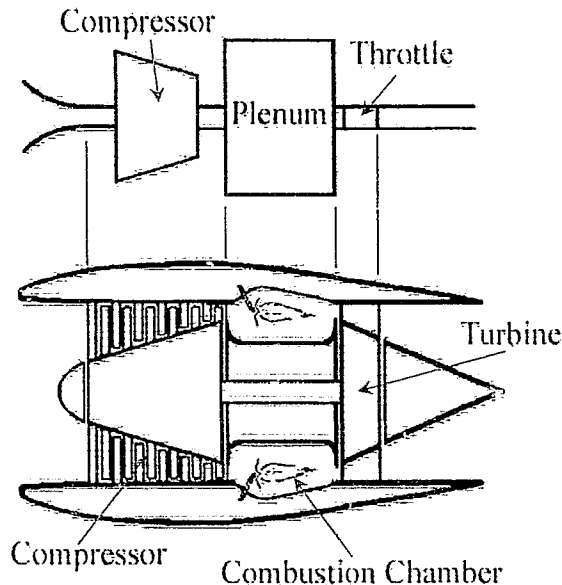


Figure 1.2: MG model compared to gas turbine jet engine

1.4 BACKGROUND ON ACTIVE CONTROL

An early publication on active stabilization of surge is by Ffowcs Williams and Huang (1989). Ffowcs Williams and Huang use a modified Greitzer model that contains a movable wall in the plenum. The wall surface is part of a mass-spring system responding to the unsteady pressure fluctuations in the plenum. The surge controller is able to stabilize the system both before and after surge had occurred. Similar results are also found in Epstein et al. (1989), where control is achieved by the use of complex valued

INTRODUCTION AND LITERATURE REVIEW

proportional feedback from plenum pressure perturbations to both a moveable plenum wall and the throttle.

Epstein et al. (1989) names several actuators that might also be used to implement their algorithm: unsteady jets or wiggling stators far upstream, wiggling inlet guide vanes and downstream pressure perturbation using loudspeakers or pulsing the combustor. In Simon and Valavani (1991) and Simon (1993), a close coupled valve (CCV) is the actuator used for active surge control. The pressure drop over the valve downstream of the compressor reshapes the compressor characteristic creating a combined characteristic of compressor and valve resulting in a stable operating point. The same CCV idea is utilized by Gravdahl (1998) and Gravdahl and Egeland (1997b) where an adaptive control law stabilises a system that undergoes pressure and flow disturbances. Fully automated active control strategies such as opening and closing of bleed ports either lower the back-pressure, or increase the mass flow rate whenever rotating stall is imminent.

Steady bleeding with preset amounts of bleed opening is effective, but can be wasteful. In modern engines with small cores the mass flow rate is already small. Liaw and Abed (1992) relate the amount of bleeding to the stall amplitude such that the loss of high-pressure air through bleeding is minimized. Badmus et al. (1995b) implemented the Liaw and Abed Controller at the Georgia Tech Axial Compressor Facility, and demonstrated that it works successfully.

1.5 BACKGROUND ON FUZZY LOGIC CONTROL

A fuzzy logic controller (FLC) can be utilized to avoid flow instabilities. In very simplistic terminology, fuzzy logic allows situations or problems to be described by linguistic variables rather than precise numeric values. Linguistic variables are adjectives that are used to describe the situation, such as “tall” or “cold”. The use of a linguistic variable frees a given element from the rigid traditional set theory. With traditional set theory the element is either completely within the set or completely out of the set. With a fuzzy set, a given element can be partially in a set to a given degree. The degree to which an element is within a set is defined as the element’s degree of membership. Elements

FUZZY LOGIC CONTROL OF COMPRESSOR SURGE IN A TURBOJET ENGINE MODEL

are no longer classified using the Boolean zero-or-one logic, with the use of a membership function an element can have a degree of membership of any real number between zero and one (Tanaka, 1997).

Using crisp logic, the definition of hot water might be water at temperatures above 80°F. By this definition water at 70°F would not be considered to be hot. Using a fuzzy logic linguistic variable, water at 70°F might be said to be warm, or by the use of a membership function the water might be said to be hot to a degree of 0.75.

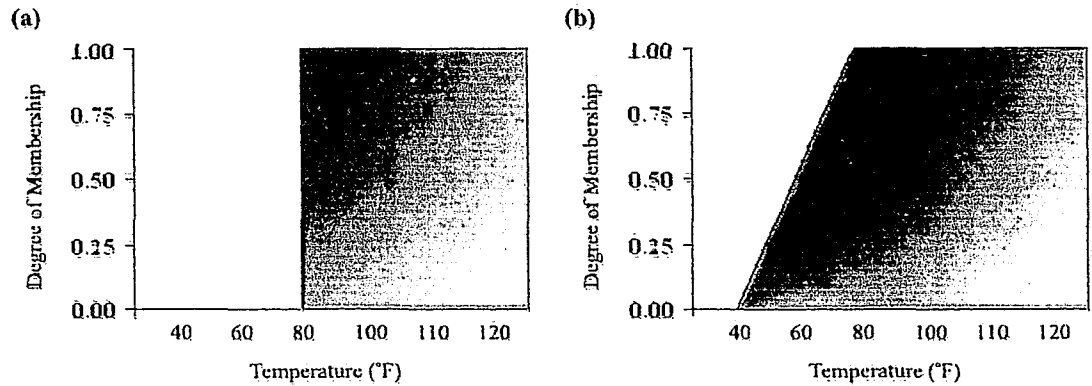


Figure 1.3: (a) Crisp set for temperature (b) Fuzzy set for temperature

If the degree of membership shown in Figure 1.3 were to be described mathematically, for the crisp set it would be:

$$\text{Degree of Hotness} = \begin{cases} 1 & \text{for } x \geq 80^\circ\text{F} \\ 0 & \text{for } x < 80^\circ\text{F} \end{cases} \quad 1.1$$

And the degree of membership for the fuzzy set would be:

$$\text{Degree of Hotness} = \begin{cases} 1 & \text{for } x \geq 80^\circ\text{F} \\ (x - 60)/2 & \text{for } 80^\circ\text{F} > x \geq 60^\circ\text{F} \\ 0 & \text{for } x < 60^\circ\text{F} \end{cases} \quad 1.2$$

INTRODUCTION AND LITERATURE REVIEW

The process of calculating the degree of membership of a variable relative to its membership function is called the *fuzzification* process. Clearly it can be seen that more information is contained in the fuzzy definition of water temperature than the traditional definition. The ability of fuzzy logic to capture and convey 'grey' levels of truth is one of the main advantages over conventional Boolean logic.

Fuzzy logic is an attractive technique for the control of poorly understood, unmodeled, or complex systems where the experience of human operators is available to provide qualitative "rules of thumb" (Lee, 1990). These rule-bases can also be developed from numerical simulations of mathematical models. Swaminathan, et al. (1997) derived a fuzzy rule-base from the Moore-Greitzer model and successfully tested it at the Georgia Tech axial compressor facility. The pressure fluctuations upstream of the compressor were measured at three sensor locations and classified into three fuzzy sets: positive, approximately zero, and negative. The fuzzified measurements were then passed through the inference engine, to determine the value of the throttle opening (the opening and closing of a bleed valve). The Georgia Tech compressor quickly experiences rotating stall, when the main throttle opening is reduced to 50% of the design value. A combination of passive controller, that modifies the inlet, and the fuzzy controller allowed the system to operate at 40% of the design throttle setting. When rotating stall did develop in the compressor, the amplitude of the stall with the fuzzy control was found to be much smaller than with other classical control methods.

A particular problem with engine control and nonlinear systems in general, is that the gains of the controller have to be scheduled over the operating envelope. At each design point, the controller is required to meet a set of performance objectives. A mathematical model that describes the complete behaviour of a system does not exist, and since the control strategy depends strongly on the current operating point, linear PID control models are not suitable (Hindmon, 1998). A reduced order model or complex look-up tables, generated from the results of extensive testing and an engineer's experience, are the basis for most engine control strategies. The automotive industries of Japan, Korea, Sweden and France have found success in fuzzy logic engine control as a replacement for the limitations of reduced order models or the look-up table method (von Altrock, 1997).

FUZZY LOGIC CONTROL OF COMPRESSOR SURGE IN A TURBOJET ENGINE MODEL

Chipperfield, et al. (2002) use fuzzy logic towards improving the performance and simultaneously enhancing the flexibility of the control strategy of a gas turbine aero-engine. FLC is used to regulate fuel flow, nozzle geometry and inlet guide vane (IGV) positioning. The resulting controllers were shown to offer improved thrust responses while still satisfying stability and structural design constraints. The fuzzy scheduling system was also able to marginally improve the turbine blade temperature and the surge margin while maintaining the thrust mapping.

Despite many successes FLC has not been regarded as a rigorous discipline due to the lack of formal techniques that guarantee stability, performance, and robustness. This is particularly true for flight control applications where certification standards require a very stringent assessment of the system qualities and performance (Chipperfield, et al., 2002). Blumel, et al. (1999) evaluated the robustness of their fuzzy trajectory controller for a non-linear missile model, showing that it achieved the desired tracking performance with no overshoot and almost no steady state error.

1.5 APPROACH

The objective of the present work is to utilize fuzzy logic control to allow the compressor of a turbojet model to operate at close proximity to the stall line, in order to increase compressor performance. A turbojet engine model is created in MATLAB using velocity triangles to approximate the flow through the multiple stage compressor and turbine. Various fuzzy logic controllers are implemented via the MATLAB Fuzzy Logic Engine. The fuzzy logic controllers tune variables such as the inlet guide vane positioning, the stator blade stagger angles, the spool speed, and the compressor inlet velocity. Static variables that are commonly not tuned during flight can be tuned during these simulations for design purposes. A known surge line is utilized to tune the engine conditions in order to operate at a set surge margin.

Two gas turbine models for surge transients are also implemented in MATLAB, the Moore-Greitzer model and the Gravdahl and Egeland modified Moore-Greitzer model. The fuzzy logic controller used for these models measures the fluctuations in the axial

INTRODUCTION AND LITERATURE REVIEW

mass flow coefficient, Φ , and the pressure coefficient, Ψ , across the compressor system. The magnitude of the fluctuations is normalized and converted into a change in either throttle or CCV gain via a fuzzy membership function. The gains are directly proportional to the throttle or valve opening. This method of control does not require prior knowledge of the surge line as it reacts upon measurable fluctuations within the compressor.

Finally a fuzzy logic model of a gas turbine compressor that predicts the probability of flow instability is designed. The compressor is represented by linguistic variables that are expressed as membership functions. The design of the rule base is discussed and presented in a series of design matrices.

1.6 SUMMARY

The outline of this thesis is as follows:

- **Chapter 2:** A detailed description is provided on the turbojet engine model, the Moore-Greitzer model, the Gravdahl and Egeland modified model, and the fuzzy logic compressor model.
- **Chapter 3:** Designs of the fuzzy logic controllers for the turbojet engine models are presented. These designs include spool speed control, compressor blade incidence angle control, compressor reaction control, active surge control, and detection/avoidance control.
- **Chapter 4:** Various simulation results are presented.
- **Chapter 5:** Conclusions.
- References, additional simulation results, and examples of the MATLAB code are provided at the end of this thesis.

CHAPTER 2

TURBOJET ENGINE MODELING

The first section of this chapter outlines the six sections of a turbojet engine model, shown in Figure 2.1. It is assumed that the flow-field properties are uniform across any cross section and vary only in the flow direction, and thus this is a quasi-one-dimensional flow engine model. Special attention is placed on the engine compressor, as it is the dynamics of the compressor which is the main study of this thesis. The evolution of the Greitzer, the Moore-Greitzer and finally the Gravdahl and Egeland modified Moore-Greitzer compressor models are traced in the second portion of this chapter. The chapter is concluded with a look at fuzzy logic modeling of a gas turbine compressor stage.

TURBOJET ENGINE MODELING

2.1 TURBOJET ENGINE MODEL

Each section of the turbojet model is contained in its own module. Each module is called from the main program, along with the desired controller algorithm (outlined in Chapter 3), which loops continuously as the engine is in *flight*. A module that calculates the atmospheric conditions is called at the beginning of each program loop, if the altitude of the engine is adjusted during the simulation.

All of the user defined variables are defined within the main program. A summary of these user defined variables can be found in the tables at the beginning of each subsection that focuses on the breakdown of the engine stages.

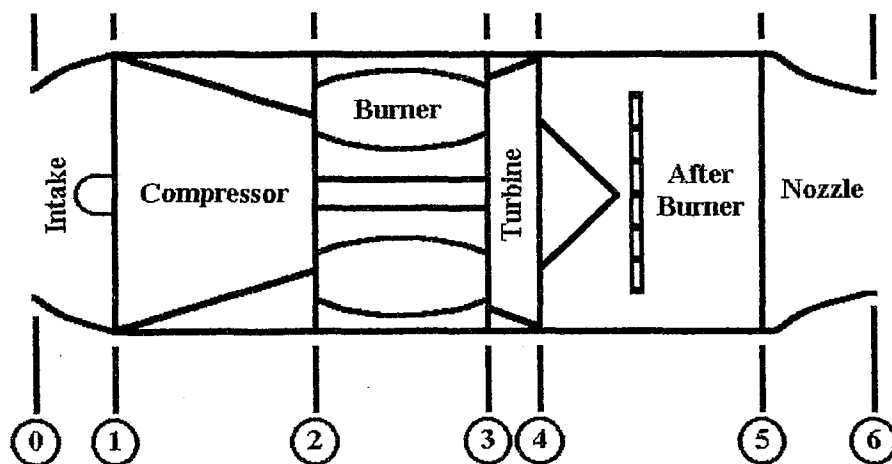


Figure 2.1: Turbojet engine model

2.1.1 INTAKES AND NOZZLES

The purpose of any aircraft gas turbine intake is to provide a sufficient air supply to the compressor at a low subsonic velocity without exhibiting large losses in total pressure for different flight speeds, altitudes, and attitudes. Though the outlined turbojet model would most commonly fly under subsonic conditions, for the sake of completeness, three variable geometry inlets are modeled for both subsonic and supersonic flight.

FUZZY LOGIC CONTROL OF COMPRESSOR SURGE IN A TURBOJET ENGINE MODEL

To aid the regulation of the engine thrust, variable geometry nozzles are utilized for this turbojet model. Again, both the converging nozzle commonly found in subsonic flight and the converging-diverging nozzle used for supersonic flight is included.

2.1.1.1 SUBSONIC DIFFUSER INTAKE

This simplified subsonic intake is a diffuser with a circular cross-sectional area. The area of the diffuser increases with a linear relation defined by the inlet and exit areas. The area expands in cross-section from the mouth of the intake in order to diffuse the subsonic flow. The model assumes that flow separation will not occur around the inlet lip of the intake. As well, it is assumed that this intake will be free of transonic flow zones associated with shockwaves and boundary layer problems.

The diffuser intake increases the static pressure and reduces the kinetic energy of the flow. The geometry of the intake is shown in Figure 2.2 and the required user defined variables are summarized in Table 2.1.

Variable	Unit	Symbol	Constant
Diffuser entrance radius	m	$r_{d,ent}$	NO
Diffuser exit radius	m	$r_{d,exit}$	NO
Diffuser Length	m	L_d	YES
Ratio of specific heats	-	k_d	YES
Gas constant for air	J/kg · K	R_d	YES
Intake efficiency	-	η_d	YES

Table 2.1: User-defined variables for subsonic diffuser intake

During simulation, the user will be notified if the velocity entering this intake type approaches sonic velocity and the simulation will halt if sonic air speed is reached. In order to control the air velocity entering the compressor, the controller may adjust both the diffuser inlet and outlet cross-sectional area; either or both of these variables can also be left as constant values. Upper and lower bounds are set for each cross-section and the user is warned if the subsonic diffuser inlet area becomes larger than the outlet area. The

TURBOJET ENGINE MODELING

length of the diffuser, though not commonly done in practice may also be modified during simulation.

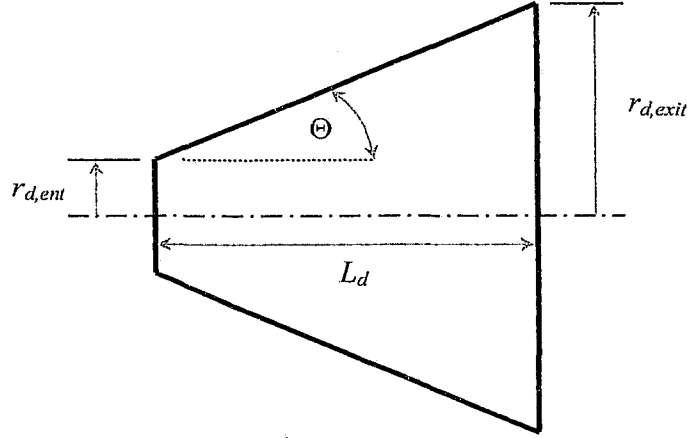


Figure 2.2: Inlet diffuser geometry

To ensure separation does not occur within the diffuser a limit is placed on the divergence semi-angle of the duct cross-section. Thus the diffuser geometry must meet the following constraint (Archer, 1996):

$$\Theta = \arctan\left(\frac{r_{d,exit} - r_{d,ent}}{L_d}\right) < (1 - M_0^2) \frac{5\pi}{180} \quad 2.1$$

It is assumed that both the density and mass flow through the diffuser are constant. The air density within the diffuser can then be calculated using the Ideal Gas Law:

$$\rho_d = \frac{P_0}{R_d T_0} \quad 2.2$$

The mass flow can be calculated using the expression for conservation of mass flow.

$$\dot{m}_d = (\rho VA)_{ent} = \rho_d M_0 \sqrt{k_d R_d T_0} \pi (r_{d,ent})^2 = (\rho VA)_{exit} \quad 2.3$$

By rearranging Equation 2.3 the diffuser exit velocity can be calculated:

$$V_1 = V_{d,exit} = \dot{m}_d / \rho_d \pi (r_{d,exit})^2 \quad 2.4$$

The pressure rise at the diffuser exit is calculated using Bernoulli's Equation and the change in temperature at the diffuser exit is based on the ratio of exit and inlet pressure (White, 1999).

$$P_1 = \frac{\rho}{2} (V_\infty^2 - V_1^2) + P_0 \quad 2.5$$

$$T_1 = \frac{P_1}{P_\infty} T_0 \quad 2.6$$

Using the diffuser exit temperature, the simulation verifies that the diffuser exit velocity is below the set subsonic Mach number (default value of 0.80 M).

The stagnation pressure and temperature at the diffuser exit is calculated based on the inlet Mach number and a user defined diffuser efficiency (Archer, 1996).

$$T_{o1} = T_0 \left(1 + \frac{k_d - 1}{2} M_0^2 \right) \quad 2.7$$

$$P_{o1} = P_0 \left(1 + \eta_d \left(\frac{T_{o1}}{T_0} - 1 \right) \right)^{\frac{k_d}{k_d - 1}} \quad 2.8$$

2.1.1.2 LOW SUPERSONIC PITOT INTAKE

This type of intake generates a strong shock wave (a normal shock) across the mouth of the intake. This intake is designed to fly at transonic Mach numbers not much higher than 1. The flow behind a standing normal shock is always subsonic and thus the intake duct is the same subsonic diffuser intake described in Section 2.1.1.1. If the flow into the pitot intake drops below Mach 1 then no shock will occur and the flow enters the diffuser unchanged; and if the flow rises above Mach 1.4, the simulation is halted. While the flow velocity remains within the intake's operation range, it is assumed that the inlet will always generate a strong normal shock wave across the mouth of the intake that is governed by the following equations for a normal shock (Anderson, 1991):

TURBOJET ENGINE MODELING

$$P_{0n} = P_0 \left(1 + \frac{2k_d}{k_d + 1} (M_0^2 - 1) \right) \quad 2.9$$

$$T_{0n} = T_0 \left(\frac{P_{0n}}{P_0} \left[\frac{2 + (k_d - 1)M_0^2}{(k_d + 1)M_0^2} \right] \right) \quad 2.10$$

$$M_{0n} = \sqrt{\frac{1 + [(k_d - 1)/2]M_0^2}{k_d M_0^2 - (k_d - 1)/2}} \quad 2.11$$

where the subscript $0n$ refers to the state after the normal shock where the now subsonic flow enters the diffuser. For simplicity, the ratio of specific heats used in the calculations across the shock waves is assumed to be equal to the value used in the diffuser.

2.1.1.3 HIGH SUPERSONIC MULTIPLE SHOCK INTAKE

This intake employs a spike center body ahead of the intake mouth as shown in Figure 2.3. The spike is made up of a series of adjustable ramps that cause an oblique shock at each ramp junction. The number of ramp junctions as well as each ramp angle can be defined by the user. In order to guarantee that no separation occurs, the ramp angles must be less than 45.5° (Anderson, 1991). After the flow passes through the n number of oblique shocks a normal shock will occur at the mouth of the diffuser and the model will revert to the intake described in Section 2.1.1.2 as the flow will now be subsonic beyond the normal shock. If the flow over the spike is subsonic then the model will revert to the model outlined in Section 2.1.1.1.

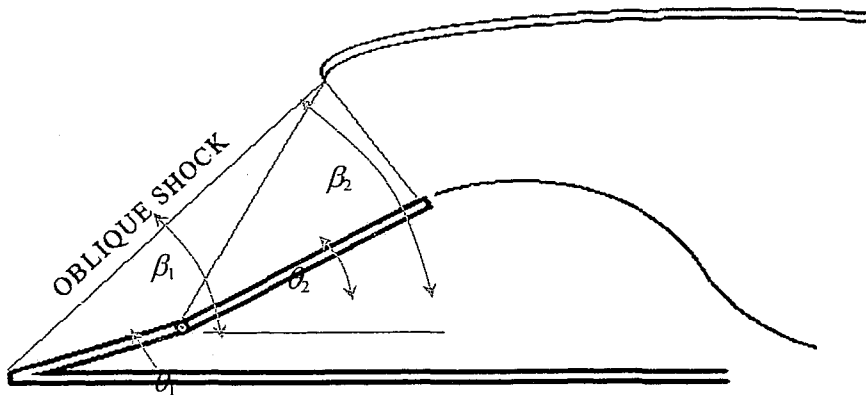


Figure 2.3: Supersonic inlet with multiple shock waves variable geometry

FUZZY LOGIC CONTROL OF COMPRESSOR SURGE IN A TURBOJET ENGINE MODEL

A step method is used for solving the following theta-beta-Mach solution for the oblique shock waves:

$$\tan \theta_i = 2 \cot \beta_i \frac{M^2 \sin^2 \beta_i - 1}{M^2 (k_d + \cos 2\beta_i) + 2} \quad 2.12$$

where θ_i is the ramp angle in question and β_i is the resulting shock angle caused by the flow at the Mach number, M and i is an integer value corresponding to the oblique shock along the inlet spike. The Mach angle defined as:

$$\mu = \sin^{-1} \frac{1}{M} \quad 2.13$$

is used as the initial guess for the shock angle and is substituted into the right-hand side of Equation 2.12. If the difference between the right-hand side of Equation 2.12 using the Mach angle as an initial guess and the left-hand side of Equation 2.12 is within the defined tolerance then the shock angle has been found. If the angle has yet to be found the guess is increased by a defined step size and the equation is retested. Since the Mach angle must always be smaller than the shock angle this step method will always guarantee convergence.

The normal component of the upstream Mach number, $M_{n,0}$ is a function of the upstream Mach number and the Mach angle,

$$M_{n,0} = M_0 \sin \beta_i \quad 2.14$$

The normal component of the Mach number behind the shock wave is expressed as:

$$M_{n,0.1} = \sqrt{\frac{1 + [(k_d - 1)/2] M_{n,0}^2}{k_d M_{n,0}^2 - (k_d - 1)/2}} \quad 2.15$$

The actual downstream Mach number can be found from the oblique shock geometry:

TURBOJET ENGINE MODELING

$$M_{0.1} = \frac{M_{n,0.1}}{\sin(\beta_i - \theta_i)} \quad 2.16$$

The subscript 0.1 refers to the state after the first oblique shock where the supersonic flow will then pass through either another oblique shock (resulting in state 0.2, etc.) or the normal shock at the mouth of the diffuser. The change in temperature and pressure across each oblique shock wave is calculated as follows:

$$P_{0.2} = P_{0.1} \left[1 + \frac{2k_d}{k_d + 1} (M_{n,0.1}^2 - 1) \right] \quad 2.17$$

$$T_{0.2} = \frac{P_{0.2}}{P_{0.1}} \left[\frac{2 + (k_d - 1)M_{n,0.1}^2}{(k_d + 1)M_{n,0.1}^2} \right] \quad 2.18$$

With each ramp angle increase that the flow passes, the above method is repeated, and the flow temperature and pressure increases as the flow velocity decreases. After the oblique shocks are passed, the intake model becomes identical to that describe in Section 2.1.1.2.

2.1.1.4 CONVERGING NOZZLE

The cross-sectional area at the nozzle inlet is assumed to be large so that the velocity is negligibly small, meaning that the pressure and temperature at the nozzle inlet are assumed to be the stagnation pressure and temperature P_{0s} and T_{0s} respectively (Bathie, 1996). The required user defined variables are summarized in Table 2.2.

Variable	Unit	Symbol	Required
Nozzle exit radius	m	$r_{n,exit}$	NO
Ratio of specific heats	-	k_n	YES
Gas constant for air	J/kg · K	R_n	YES

Table 2.2: User-defined variables for converging nozzle

FUZZY LOGIC CONTROL OF COMPRESSOR SURGE IN A TURBOJET ENGINE MODEL

The nozzle choke condition is defined as follows (Bathie, 1996):

$$P_5^* = P_{o5} \left(\frac{2}{k_n + 1} \right)^{\frac{k_n}{k_n - 1}} \quad 2.19$$

The nozzle is choked if $P_5^* > P_\infty$ and then the nozzle exit pressure, temperature and velocity is calculated as follows:

$$P_6 = P_5^* \quad 2.20$$

$$T_6 = T_{o5} \left(\frac{2}{k_n + 1} \right) \quad 2.21$$

$$V_6 = \sqrt{k_n R_n T_6} \quad 2.22$$

If the nozzle is not choked then the nozzle exit pressure, temperature and velocity is calculated as follows:

$$P_6 = P_\infty \quad 2.23$$

$$T_6 = T_{o5} \left(\frac{P_6}{P_{o5}} \right)^{\frac{k_n - 1}{k_n}} \quad 2.24$$

$$V_6 = \sqrt{2(T_5 - T_6) \frac{k_n R_n}{k_n - 1}} \quad 2.25$$

In order to calculate the thrust produced by the engine, two values defined in the burner module must be known: the fuel-air ratio, f , and the mass flow of the fuel-air mixture entering the nozzle, \dot{m}_5 . Thrust is then calculated using the following expression (Bathie, 1996):

$$\mathbf{T} = (P_6 - P_\infty) (\pi r_{n,exit}^2) + \dot{m}_5 [(1 + f) V_6 - V_\infty] \quad 2.26$$

TURBOJET ENGINE MODELING

2.1.1.5 CONVERGING-DIVERGING NOZZLE

The converging-diverging nozzle requires the user-defined variables as for the converging nozzle, along with the addition of the nozzle inlet area defined as $r_{n,ent}$. The temperature and pressure and the nozzle inlet is calculated from the stagnation values (Anderson, 1991):

$$T_5 = T_{o5} - \frac{V_5^2}{2c_{p_n}} \quad 2.27$$

$$P_5 = \frac{P_{o5}}{\left(\frac{T_{o5}}{T_5} \right)^{\frac{k_n}{k_n-1}}} \quad 2.28$$

The maximum possible mass flow occurs in a duct when its throat is at the sonic condition. The duct is then said to be choked and can carry no additional mass flow unless the throat is widened. It is assumed that for maximum thrust, the throat area of the nozzle is variable and will automatically set itself to the critical throat area, A^* , defined by the following expression (White, 1999):

$$A^* = \frac{\pi r_{n,ent}^2}{\frac{1}{M_5} \left[\frac{1 + \frac{1}{2}(k_n - 1)M_5^2}{\frac{1}{2}(k_n + 1)} \right]^{\frac{0.5(k_n+1)}{k_n-1}}} \quad 2.29$$

The simulation will halt if the nozzle exit area is smaller than the critical throat area; assuming that this condition is met the program runs a step solver to find the nozzle exit Mach number using the following relationship, starting with an initial guess of $M_6 = 1$ (White, 1999):

$$\frac{\pi r_{n,exit}^2}{A^*} = \frac{1}{M_6} \left[\frac{1 + \frac{1}{2}(k_n - 1)M_6^2}{\frac{1}{2}(k_n + 1)} \right]^{\frac{0.5(k_n+1)}{k_n-1}} \quad 2.30$$

The nozzle exit temperature and pressure is calculated using the following equations:

$$T_6 = \frac{T_{o5}}{1 + \frac{k_n - 1}{2} M_6^2} \quad 2.31$$

$$P_6 = \frac{P_{o5}}{\left(\frac{T_{o5}}{T_6} \right)^{\frac{k_n}{k_n - 1}}} \quad 2.32$$

Thrust is calculated using the same method as for the converging nozzle, as outlined in Section 2.1.1.4.

2.1.2 COMPRESSORS AND TURBINES

An axial compressor is made up of many alternating rows of rotating and stationary blades called rotors and stators, respectively. The first stationary row (which comes before the first rotor row) is comprised of the inlet guide vanes or IGVs. Each successive rotor-stator pair is called a compressor stage. Hence compressors with many blade rows are termed multistage compressors.

The rotor adds swirl to the flow, thus increasing the total energy carried in the flow by increasing the angular momentum (adding to the kinetic energy associated with the tangential or swirl velocity). The stator removes swirl from the flow, but it is not a moving blade row and thus cannot add any net energy to the flow. Rather, the stator converts the kinetic energy associated with swirl to internal energy (raising the static pressure of the flow). The IGV also adds no energy to the flow. It is designed to add swirl in the direction of rotor motion to lower the Mach number of the flow relative to the rotor blades, and thus improve the aerodynamic performance of the rotor.

The thermodynamics and fluid mechanics for a stage of compressor blades are basically the same for a stage of turbine blades. For a turbine stage the stationary blade, commonly known as the nozzle, precedes the rotor blade. As well, the relative velocities in an axial-flow turbine are generally substantially higher than in an axial-flow compressor, with a greater change in enthalpy per stage (Dixon, 1998). In the turbine nozzle, the tangential velocity is increased in the direction of rotation with a corresponding drop in the static

TURBOJET ENGINE MODELING

pressure. In the rotor row, the tangential velocity is decreased. Fewer stages are needed for an axial-flow turbine than in an axial-flow compressor because in the compressor the flow is decelerating in the passageways with a corresponding rise in pressure, whereas in the turbine the gas is accelerating. The diffuser action of a compressor allows for only moderate changes in the compressor passageways to avoid separation (Bathie, 1996).

Velocity triangles are used in the following sections to relate the flow properties through an axial flow compressor with the blade design parameters in the relative frame (rotating with the moving blades), to the properties in the stationary or absolute frame. It is assumed that the area of the annulus through which the flow passes is nearly constant and the density changes are small so that the axial velocity is approximately constant.

The same velocity triangles, shown in the following section for a compressor, can be applied to a turbine. If the tangential velocity increases across a blade row (where positive tangential velocity is defined in the same direction as the rotor motion) then work is added to the flow (a compressor). If the tangential velocity decreases across a blade row (where positive tangential velocity is defined in the same direction as the rotor motion) then work is removed from the flow (a turbine).

2.1.2.1 BLADE GEOMETRY

Table 2.3 outlines the user-defined variables required for one stage of an axial-flow compressor. These same variables are used for one stage of an axial-flow turbine. It should be noted that flow enters and exits the blades at the flow angles calculated by the velocity triangles outlined in the following subsections. The flow angles are not the same as the blade (or metal) angles which are the actual angles of the physical structure. These angles must be kept very similar in order to avoid separation of the flow. This will be dealt with in more detail in Chapter 3. Blade and flow angles are illustrated in Figure 2.4, along with the required sign conventions.

FUZZY LOGIC CONTROL OF COMPRESSOR SURGE IN A TURBOJET ENGINE MODEL

Variable	Unit	Symbol	Constant
IGV initial position	rad	β_{IGV_o}	NO
Rotor Speed	rpm	N	NO
Ratio of specific heats	-	k_n	YES
Gas constant for air	J/kg · K	R_n	YES
Blade Angle at Inlet*	rad	$\beta_{S,in}$	NO
Blade Angle at Outlet*	rad	$\beta_{S,out}$	NO
Thickness-to-chord ratio*	-	t_b / c	YES
Location of maximum camber-to-chord ratio*	-	a / c	YES
Solidity - chord-to-blade pitch ratio *	-	σ	YES
Rotor blade tip-to-tip diameter	m	d_t	YES
Rotor hub diameter	m	d_h	YES

*These variables are defined for both the Rotor and Stator blade, differentiated by the subscripts R and S

Table 2.3: User-defined variables for axial-flow compressor

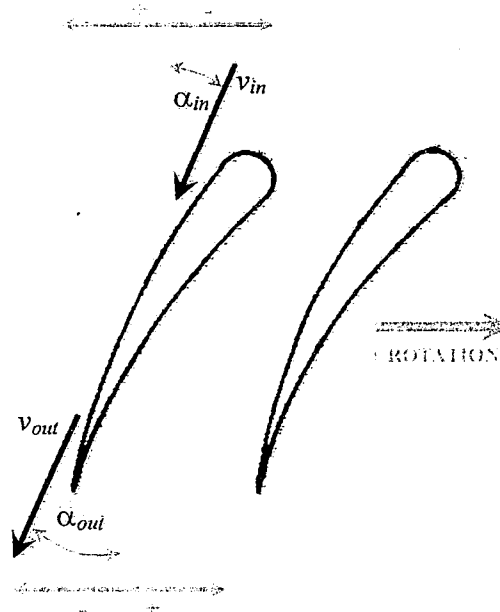


Figure 2.4: Flow angles with sign conventions

TURBOJET ENGINE MODELING

From Triangle ABC in Figure 2.5, the blade turn angle θ can be defined in terms of the leading and trailing blade angles β_{in} and β_{out} :

$$\beta_{out} + \theta + (180^\circ - \beta_{in}) = 180^\circ \quad 2.33$$

$$\theta = \beta_{in} - \beta_{out} \quad 2.34$$

The blade stagger angle can be defined in terms of the leading edge blade angle and the turn angle as:

$$\zeta = \beta_{in} - \frac{\theta}{2} \quad 2.35$$

The flow will enter and exit a stage at an angle very close to the actual blade angles. The difference between the flow entering the blade and the actual blade angle is referred to as the angle of incidence, defined as:

$$i = \alpha_{in} - \beta_{in} \quad 2.36$$

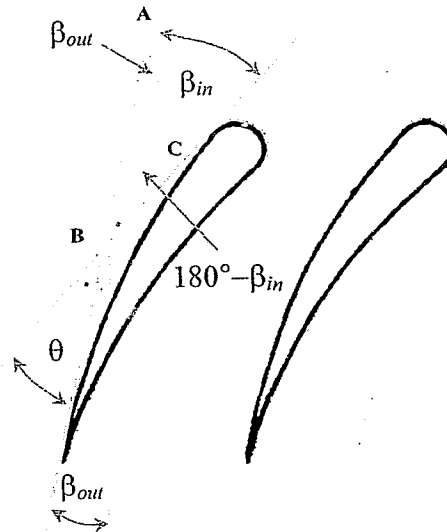


Figure 2.5: Rotor turn angle and blade angles relationship

The difference between the flow leaving the blade and the actual blade angle at the blade exit is called the deviation, and is defined as:

$$\delta = \alpha_{out} - \beta_{out} \quad 2.37$$

2.1.2.2 INLET GUIDE VANES

The model contains the option of adding inlet guide vanes (IGVs) ahead of the first compressor stage. The IGVs are a row of stator blades that direct the air flow into the first row of rotor blades. The IGV blade angle can be set as a constant or can be adjusted. Limits are set on the IGV blade angle, 0 to 60 degrees (where 0 degrees represents a blade parallel to the flow, which would not affect the fluid as it passes over). It is assumed that there are no temperature losses over the IGV stage.

Figure 2.6 shows the velocity triangles for the IGV stage. The simulation will halt if the incoming axial air flow velocity v_1 entering the compressor from the intake is sonic. It is assumed the flow velocity at the trailing edge of the IGV, v_2 , leaves the blade at the blade exit angle. The following trigonometric relationship relates the flows:

$$v_2 = \frac{v_1}{\cos \beta_{IGV}} \quad 2.38$$

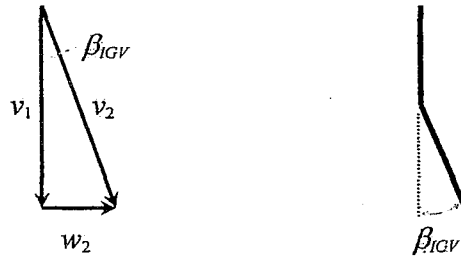


Figure 2.6: Velocity triangle for inlet guide vane stage

The whirl velocity is shown as w_2 ; it is the tangential velocity calculated in the stationary frame as:

TURBOJET ENGINE MODELING

$$w_2 = v_1 \tan \beta_{IGV} \quad 2.39$$

2.1.2.3 ROTOR STAGE

The rotor blade speed is subtracted from the IGV induced whirl velocity to determine the tangential velocity in the rotating frame:

$$w_{r2} = w_2 - u \quad 2.40$$

The rotor blade speed u is the mid-point radius multiplied by the angular velocity which can be expressed as:

$$u = \frac{(d_t + d_h)}{2} \frac{N\pi}{60} \quad 2.41$$

where d_t and d_h are the rotor blade-tip-diameter and the diameter of the hub respectively as shown in Figure 2.7. The blade-tip-speed must not exceed the speed of sound in order to avoid shock wave formation; the rotor blade tip speed is limited to Mach 0.85. Speed of sound is a function of temperature; temperature rises near the rear of a compressor, which permits a higher blade tip speed. Multiple spools can be added to the engine model and coupled with high speed turbines.

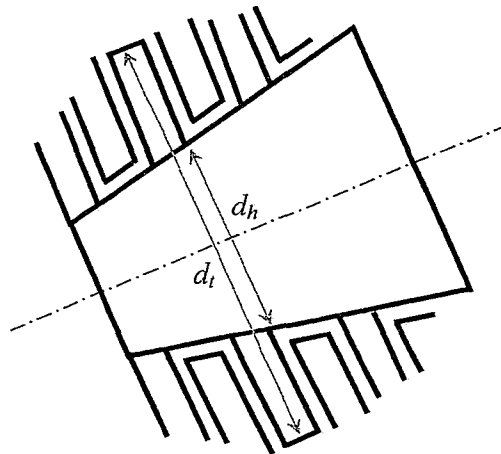


Figure 2.7: Rotor blade and hub dimensions

FUZZY LOGIC CONTROL OF COMPRESSOR SURGE IN A TURBOJET ENGINE MODEL

Based on the assumption that the axial velocity through the compressor stage is constant, the relative velocity entering the rotor stage in the rotating frame can be calculated using the Pythagorean Theorem:

$$v_{r2} = \sqrt{v_1^2 - w_{r2}^2} \quad 2.42$$

The corresponding flow angle is calculated as:

$$\alpha_{r2} = \arctan \frac{w_{r2}}{v_1} \quad 2.43$$

The relationship between the absolute velocity, relative velocity and blade velocity is shown in the rotor stage velocity triangle in Figure 2.8.

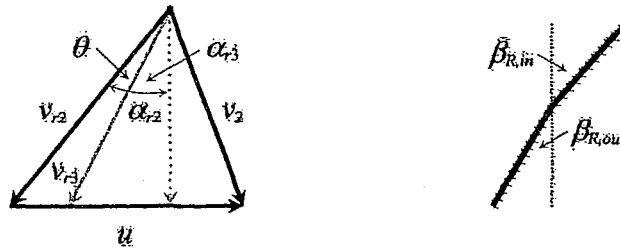


Figure 2.8: Velocity triangle for rotor stage

The exit angle of the rotor blade can be constant or variable. Such a variable geometry is not commonly found in practice, but for the purpose of this design simulation program the rotor blade turning angle, θ_R , can be adjusted. The turning angle redirects the air flow over the rotor blade. The relationship between the rotor inlet blade angle and the rotor exit blade angle is illustrated in Figure 2.8, and the angle at which the flow leaves the rotor blade is calculated as:

$$\alpha_{r3} = \alpha_{r2} + \theta_R \quad 2.44$$

The velocity exiting the rotor blade in the rotating frame can now be calculated as:

TURBOJET ENGINE MODELING

$$v_{r3} = \frac{v_1}{\cos \alpha_{r3}} \quad 2.45$$

The tangential velocity component of the rotor blade exit velocity in the rotating frame is given by:

$$w_{r3} = v_1 \tan \alpha_{r3} \quad 2.46$$

2.1.2.4 STATOR STAGE

The blade speed is added to the flow exiting the rotor, transforming the vectors back into the stationary frame of reference. The tangential component entering the stator stage becomes:

$$w_3 = u + w_{r3} \quad 2.47$$

The flow angle into the stator blade uses the whirl velocity calculated above (once again, the assumption is made that the axial velocity through the compressor stage is constant):

$$\alpha_3 = \arctan \frac{w_3}{v_1} \quad 2.48$$

and the resulting velocity entering the stator stage in the stationary frame is calculated by:

$$v_3 = \frac{v_1}{\cos \alpha_3} \quad 2.49$$

The velocity exiting the stator blade is first turned through the turning angle, θ_s , which like the rotor turning angle can be constant or variable. The flow exit angle is first calculated as:

$$\alpha_4 = \alpha_3 - \theta_s \quad 2.50$$

and the exit velocity is calculated as:

$$v_4 = \frac{v_1}{\cos \alpha_4} \quad 2.51$$

with a tangential whirl velocity of:

$$w_4 = v_1 \sin \alpha_4 \quad 2.52$$

The velocity triangle for the stator stage is shown in Figure 2.9. The increase in the tangential component of the stationary velocity in the direction of the rotor indicates compression, while a decrease of the tangential component would represent the expansion of gas found in a turbine stage.

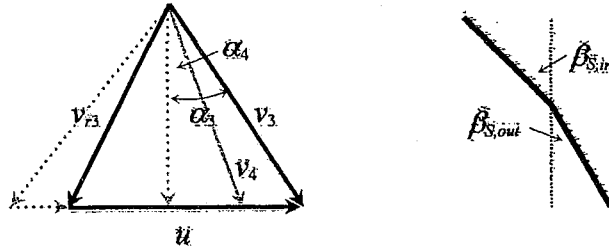


Figure 2.9: Velocity triangle for stator stage

2.1.2.5 STAGE PRESSURE RATIO

The torque of the rotor at the mid-point of the blade is first calculated using the change in whirl velocities of the stationary velocity components (Bathie, 1996):

$$\bar{\tau} = \dot{m} \frac{(d_i + d_h)}{2} (w_2 - w_3) \quad 2.53$$

where the mass flow through the rotor is found from:

$$\dot{m} = \rho A V = \frac{P_1}{R_c T_1} \pi \left(\frac{d_i^2 + d_h^2}{4} \right) v_1 \quad 2.54$$

Now the required power to drive the compressor can be calculated (Bathie, 1996):

TURBOJET ENGINE MODELING

$$P = \frac{2\pi N\tau}{60 \dot{m}} \quad 2.55$$

The power will be negative, once again confirming compression.

The stagnation temperature at the compressor outlet is found by first calculating the stagnation temperature at the compressor inlet:

$$T_{o1} = T_1 + \frac{v_1^2}{2c_{p_c}} \quad 2.56$$

The rise of stagnation temperature at the compressor outlet is found by using the required power (Bathie, 1996):

$$T_{o2} = T_{o1} - \frac{P}{c_{p_c}} \quad 2.57$$

The stage pressure ratio is calculated using the adiabatic relationship of the stagnation temperature and stagnation pressure:

$$P_{ratio} = \left(\frac{T_{o2}}{T_{o1}} \right)^{\frac{k_c}{k_c-1}} \quad 2.58$$

2.1.3 BURNER AND AFTERBURNER

A simplified model for calculation of the stagnation temperature and pressure at the burner exit is used. Table 2.4 summarizes the user-defined variables needed for both the burner and the afterburner. The afterburner between the turbine and exit nozzle is optional. Additional fuel is pumped into the afterburner and the stagnation temperature is increased and the stagnation pressure is decreased via the same method as the burner which is outlined as followed:

FUZZY LOGIC CONTROL OF COMPRESSOR SURGE IN A TURBOJET ENGINE MODEL

$$T_{o3} = \frac{\eta_b \dot{q}_r + T_{o2} c_{p_c}}{(1+f) c_{p_{be}}} \quad 2.59$$

$$P_{o3} = \eta_b P_{o2} \quad 2.60$$

where the specific heat for the burner is calculated as:

$$c_{p_b} = \frac{k_b}{k_b - 1} R_b \quad 2.61$$

the specific heat at the burner exit is estimated as:

$$c_{p_{be}} = 2c_{p_b} - c_{p_c} \quad 2.62$$

and the fuel to air ratio is calculated by:

$$f = \frac{\dot{m}_f}{\dot{m}_a} \quad 2.63$$

Variable	Unit	Symbol	Constant
Ratio of specific heats for burner	-	k_b	YES
Ratio of specific heats for afterburner	-	k_{ab}	YES
Gas constant for air	J/kg · K	R_b	YES
Gas constant for fuel-air mixture	J/kg · K	R_{ab}	YES
Mass flow of fuel into burner	kg/s	$\dot{m}_{f,b}$	NO
Mass flow of fuel into afterburner	kg/s	$\dot{m}_{f,ab}$	NO
Burner efficiency	-	η_b	YES
Afterburner efficiency	-	η_{ab}	YES
Heat of reaction in burner	J/kg of fuel	\dot{q}_r	YES

Table 2.4: User-defined variables for burner and afterburner

TURBOJET ENGINE MODELING

2.2 GREITZER COMPRESSOR MODEL

The main advantage of Greitzer's original model over other models at the time was that Greitzer developed a systematic rule for determining which instability would occur in the compressor, using Greitzer's B-parameter,

$$B = \frac{U}{2\varpi_H L_C} = \frac{U}{2a} \sqrt{\frac{V_p}{A_C L_C}} \quad 2.64$$

where U is the mean rotor velocity, ϖ_H is the Helmholtz resonator frequency, V_p is the plenum volume, A_C is the flow-through area, and L_C is the effective compressor and duct length. Surge tends to occur for high speeds and large plenum volumes where $B > B_{critical}$ and rotating stall tends to occur for lower speeds and smaller plenum volumes when $B < B_{critical}$. The value for $B_{critical}$ is compressor-dependent.

Referring to Figure 1.2, Greitzer modeled the compressor and mass-flow throttle as actuator discs, assuming low Mach numbers and low pressure ratios compared to ambient conditions. Small inertial forces in the throttle duct are assumed, and the compressor pressure rise is considered to be quasi-steady. The two states of the model are the nondimensionalized mass flow referred to as the axial mass flow coefficient, Φ , and the nondimensionalized pressure difference known as the pressure coefficient, Ψ . The mass flow coefficient in this case is the axial velocity parameter, C_x/U , where C_x is the axial velocity:

$$\Phi = \frac{\rho C_x A_C}{\rho U A_C} = \frac{C_x}{U} \quad 2.65$$

The pressure coefficient is the pressure difference across the plenum normalized by the density and square of the blade speed:

$$\Psi = \frac{P_1 - P_2}{\rho U^2} \quad 2.66$$

The Greitzer model is defined as:

$$\frac{d\Phi}{d\xi} = B(\Psi_c(\Phi) - \Psi) \quad 2.67$$

$$\frac{d\Psi}{d\xi} = \frac{1}{B}(\Phi - \Phi_T(\Psi)) \quad 2.68$$

where the compressor characteristic is defined as:

$$\Psi_c(\Phi) = \psi_{c_0} + H \left[1 + \frac{3}{2} \left(\frac{\Phi}{W} - 1 \right) - \frac{1}{2} \left(\frac{\Phi}{W} - 1 \right)^3 \right] \quad 2.69$$

and the throttle characteristic is given by:

$$\Phi_T(\Psi) = \gamma_T \sqrt{\Psi} \quad 2.70$$

where γ_T is the throttle gain, which is proportional to the throttle valve opening. The inverse throttle characteristic is used for determining the stability of the model and is given by:

$$\Psi_T(\Phi) = \Phi_T^{-1}(\Phi) = \frac{1}{\gamma_T^2} \Phi^2 \quad 2.71$$

2.2.1 STABILITY ANALYSIS OF GREITZER MODEL

Linearizing Equations 2.67 and 2.68 around the equilibrium point defined by the intersection of the inverse throttle characteristic Ψ_T and the compressor characteristic Ψ_c , the following model is found (Greitzer, 1980):

$$\begin{bmatrix} \dot{\Phi} \\ \dot{\Psi} \end{bmatrix} = \underbrace{\begin{bmatrix} Ba_c & -B \\ 1/B & -1/Ba_T \end{bmatrix}}_A \begin{bmatrix} \Phi \\ \Psi \end{bmatrix} \quad \text{where } a_c = \frac{\partial \Psi_c}{\partial \Phi} \text{ and } a_T = \frac{\partial \Psi_T}{\partial \Phi} \quad 2.72$$

From Equation 2.72 the eigenvalues, λ , of A are found to be:

TURBOJET ENGINE MODELING

$$\lambda = \frac{-\left(\frac{1}{Ba_T} - Ba_C\right) \pm \sqrt{\left(\frac{1}{Ba_T} - Ba_C\right)^2 - 4\left(1 - \frac{a_C}{a_T}\right)}}{2} \quad 2.73$$

The stability properties of the equilibrium state depend on the relative magnitude of the terms B , a_T , and a_C . Greitzer uses $T_a \equiv \left(\frac{1}{Ba_T} - Ba_C\right)$ to determine dynamic stability, and $T_b \equiv \left(1 - \frac{a_C}{a_T}\right)$ to determine static stability. The term T_b will be negative if the slope of the compressor characteristic is greater than the slope of the throttle characteristic at the point of intersection.

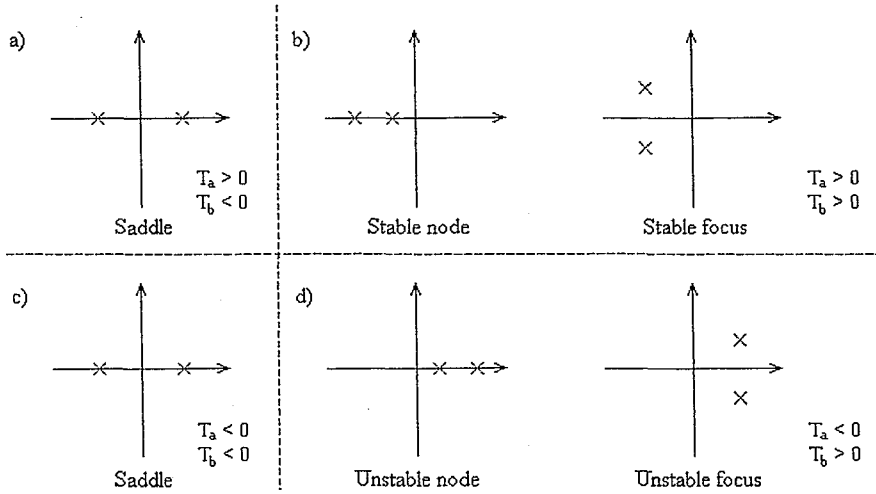


Figure 2.10: Stability of the linearized Greitzer Model

If $T_b < 0$ the system has one eigenvalue in the left half-plane and one eigenvalue in the right-half plane, and the equilibrium state is thus a saddle-point, which is unstable (shown in Figure 2.10a and 2.10c). This type of instability is called *static* by Greitzer. If $T_b > 0$ and $T_a < 0$ (as seen in Figure 2.10d) the equilibrium state can be one of two types, dependent on the numerical value of B . If $T_b^2 < 4T_a$ the equilibrium state will be an unstable focus (dynamic instability), and if $T_b^2 > 4T_a$ the equilibrium state will be an

FUZZY LOGIC CONTROL OF COMPRESSOR SURGE IN A TURBOJET ENGINE MODEL

unstable node (static instability). If $T_b > 0$ and $T_a > 0$ (as seen in Figure 2.10b) the system is stable, and depending on B , will either be a stable focus or a stable node. Whether the instability is dynamic or static, the nonlinear system will go into surge oscillations.

As predicted by the value of B , an engine is more likely to surge as the speed is increased. Increasing the blade speed leads to an increase in B for the same system parameters, so that a configuration is more likely to surge as the rotational speed is increased. A natural way to account for the number of axial compressor stages is to use $B' = NB$ where N is the number of compressor stages.

2.3 MOORE – GREITZER MODEL

In Moore and Greitzer's later works, Greitzer's model is expanded to include the state J , the square of the amplitude of angular disturbance of the axial flow coefficient, Φ . Finite-amplitude rotating stall cannot evolve without producing a finite disturbance in Φ or the total-to-static pressure rise coefficient, Ψ . In the case of pure surge, when $J = 0$, the model shown in Equations 2.74, 2.75, and 2.76 reduces to that of Greitzer's original model for surge. This three-state model is capable of describing the growth of rotating stall and surge during a compressor mass-flow transient.

$$\frac{d\Psi}{d\xi} = \frac{W/H}{4B^2} \left[\frac{\Phi}{W} - \frac{1}{W} F_r^{-1}(\Psi) \right] \frac{H}{l_c} \quad 2.74$$

$$\frac{d\Phi}{d\xi} = \left[-\frac{\Psi - \varphi_{c_s}}{H} + 1 + \frac{3}{2} \left(\frac{\Phi}{W} - 1 \right) \left(1 - \frac{1}{2} J \right) - \frac{1}{2} \left(\frac{\Phi}{W} - 1 \right)^3 \right] \frac{H}{l_c} \quad 2.75$$

$$\frac{dJ}{d\xi} = J \left[1 - \left(\frac{\Phi}{W} - 1 \right)^2 - \frac{1}{4} J \right] \frac{3a_t H}{(1 + ma_t) W} \quad 2.76$$

All distances have been nondimensionalized by the mean compressor radius, R , such that l_c is defined as the total aerodynamic length of the compressor and ducts in wheel radii. Time is denoted by radians of wheel travel:

TURBOJET ENGINE MODELING

$$\xi = Ut / R \quad 2.77$$

The functional form between Φ and Ψ is simply the compressor performance map determined by experimental data and approximated by the following:

$$\Psi = \psi_{c_o} + H \left[1 + \frac{3}{2} \left(\frac{\Phi}{W} - 1 \right) - \frac{1}{2} \left(\frac{\Phi}{W} - 1 \right)^3 \right] \quad 2.78$$

where H is the semi-height, W is the semi-width, and ψ_{c_o} is the shut-off value of the cubic axisymmetric performance characteristic. The parameter a_i is the reciprocal time-lag of the blade passage defined by the following:

$$a_i = R / N_s \tau U \quad 2.79$$

where U is the wheel speed at mean diameter, and N_s is the number of compressor stages. The coefficient of pressure-rise lag, τ , is a time constant associated with the internal lags in the compressor. A reasonable estimation for τ is the inertia of fluid in the passage.

The compressor-duct flow parameter, m , reflects the length of the exit duct where $m = 2$ would refer to a *long* exit duct and $m = 1$ would refer to a *short* exit duct. F_T^{-1} is the inverse of the throttle characteristic which is a function of total-to-static pressure rise. A realistic throttle characteristic is of parabolic form:

$$F_T = \frac{1}{2} K_T \Phi_T^2 \quad 2.80$$

where K_T is the throttle coefficient. From Equation 2.80 Φ_T is simply the inverse of F_T and the inverse of the throttle characteristic can be expressed as:

$$F_T^{-1} = \Phi_T = \gamma_T \sqrt{\Psi} \quad 2.81$$

2.3.1 IMPLICATIONS OF MOORE-GREITZER MODEL

For rotating stall, the time derivative vanishes. This occurs when J has the constant equilibrium value:

$$J = J_e = 4 \left[1 - \left(\frac{\Phi}{W} - 1 \right)^2 \right] \quad 2.82$$

When J_e from Equation 2.82 is substituted into the right-hand side of Equation 2.75, the result is the steady performance map arising from Equation 2.78, which may be used to infer the performance effect of rotating stall. In the case of pure surge, $\dot{J} = 0$, and once J is zero it will remain zero forever unless the compressor is physically reset.

It appears impossible for rotating stall to evolve without producing some disturbance in Φ or Ψ . If J changes then the model shows that Φ or Ψ must also change. The angular-disturbance amplitude J grows at a rate which initially depends only on the disturbance itself, but then tries to approach the equilibrium position in Equation 2.82. The model shows that pure modes of surge (time variation) or rotating stall (angle variation) can exist without the other. However, in general the time and angular fluctuations are coupled. The angular variation grows towards a time dependent equilibrium, while the damping rate of any time variation depends on the strength of the angular variation.

2.4 GRAVDAHL AND EGELAND CCV MOORE-GREITZER MODEL

The approach of active surge/stall control is to use feedback to stabilize the unstable regime of the compressor map. It is common to use bleed valves as surge avoidance actuators. The compressed high energy in nominal bleed-off operation is not wasted in aircraft engines, as it is utilized by other aircraft systems. Unscheduled bleed-off may however result in some lost energy.

By stabilizing an unstable area of the compressor map using feedback, one allows for compression operation in the peak efficiency and pressure rise regions located in the

TURBOJET ENGINE MODELING

neighbourhood of the surge line. Active control broadens the operating range of the compressor by effectively shifting the surge line and the surge avoidance line, thereby enabling the machine to now operate in regions that were previously unreliable (de Jager 1995). A close coupled valve (CCV) incorporated into the present engine model represents this active bleed control capability.

The CCV has a characteristic given by:

$$\Psi_v(\Phi) = \frac{1}{\gamma_v^2} \Phi^2 \quad 2.83$$

where $\gamma_v > 0$ is CCV gain which is proportional to the valve opening. The pressure rise across the compressor is modified according to:

$$\frac{p_E - p_1}{\rho U^2} = N_s F(\phi) - \frac{1}{2a_t} \left(2 \frac{\partial \phi}{\partial \xi} + \frac{\partial \phi}{\partial \theta} \right) - \Psi_v(\Phi) \quad 2.84$$

where p_1 and p_E are the static pressure at the entrance and exit of the equivalent compressor, ρ is the constant inlet density, U is the compressor speed at mean diameter, N_s is the number of compressor stages, $F(\phi)$ is the pressure rise coefficient in the blade passage, and θ is the angular coordinate around the wheel. Following the derivation of Moore and Greitzer (1986), the following MG modified model is found (for the full derivation, see Gravdahl and Egeland, 1998):

$$\frac{d\Psi}{d\xi} = \frac{W/H}{4B^2} \left[\frac{\Phi}{W} - \frac{1}{W} \Phi_T(\Psi) \right] \frac{H}{l_c} \quad 2.85$$

$$\frac{d\Phi}{d\xi} = \frac{H}{l_c} \left[-\frac{\Psi - \phi_{c_0}}{H} - \frac{1}{2} \left(\frac{\Phi}{W} - 1 \right)^3 + 1 + \frac{3}{2} \left(\frac{\Phi}{W} - 1 \right) \left(1 - \frac{1}{2} J \right) - \frac{1}{\gamma_v^2} \left(\frac{W^2 J}{2H} + \frac{\Phi^2}{H} \right) \right] \quad 2.86$$

$$\frac{dJ}{d\xi} = J \left[1 - \left(\frac{\Phi}{W} - 1 \right)^2 - \frac{1}{4} J - \frac{1}{\gamma_v^2} \frac{4W\Phi}{3H} \right] \frac{3a_c H}{(1 + ma_c) W} \quad 2.87$$

In the case of pure surge, J is set to zero and Equations 2.84, 2.85, and 2.86 become:

$$\frac{d\Psi}{d\xi} = \frac{1}{4B^2 l_c} [\Phi - \Phi_r(\varphi)] \quad 2.88$$

$$\frac{d\Phi}{d\xi} = \frac{1}{l_c} \left(\underbrace{\Psi_c(\Phi) - \Psi_v(\Phi)}_{\Psi_r(\Phi)} - \Psi \right) \quad 2.89$$

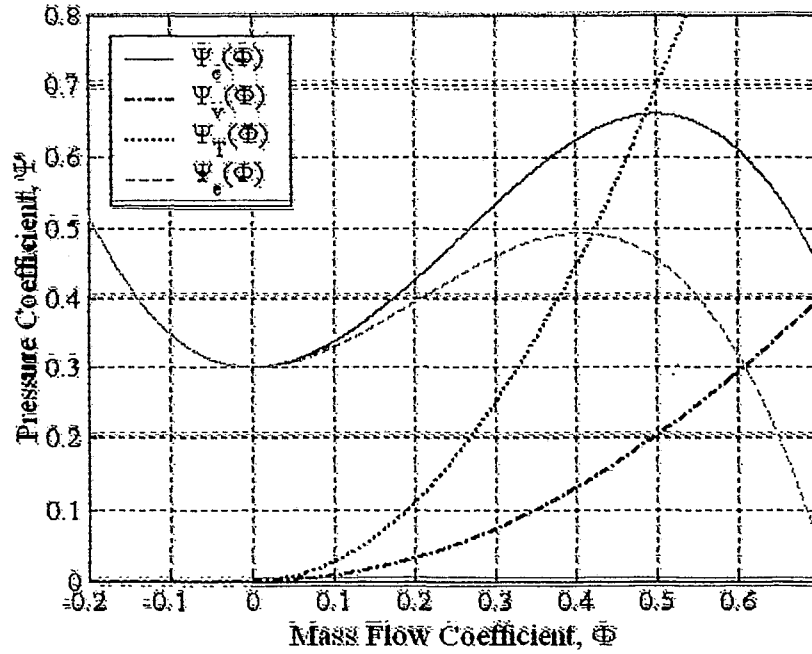


Figure 2.11: Compressor and throttle characteristics

2.4.1 STABILITY ANALYSIS OF MG MODEL WITH CCV CONTROL

The compressor is in equilibrium when $\dot{\Phi} = \dot{\Psi} = \dot{J} = 0$. If $J(0) = 0$ then $J = 0$ and the equilibrium values Φ_0 and Ψ_0 are given by the intersection of $\Psi_r(\Phi) = \Psi_c(\Phi) - \Psi_v(\Phi)$ and the throttle characteristic (see Figure 2.11). If $J(0) > 0$, and the throttle

TURBOJET ENGINE MODELING

characteristic crosses Ψ_c to the left of the local maximum, the compressor may enter rotating stall, and the equilibrium values ϕ_0 and ψ_0 are given by the intersection of the throttle characteristic and the stall characteristic $\Psi_{cs}(\Phi)$. This is dependent on the Greitzer B -parameter; as discussed earlier, a small value for B results in rotating stall, and a large B gives surge.

2.5 FUZZY LOGIC COMPRESSOR MODEL

The two states of the MG model, the axial mass flow coefficient, Φ , and the pressure coefficient, Ψ , can be simplified down to the three variable and measurable quantities which they are based upon: blade speed [rpm]; axial velocity [m/s]; and pressure ratio across the stage. With these three values a three-input, one-output model can be created to predict the probability of flow instability (either compressor surge or rotating stall) using a fuzzy logic model. The operating ranges of the inputs are summarized in Table 2.5, and the operating range of the fuzzy output, being the probability of a flow instability, is summarized in Table 2.6. The basis of selection for these values come from the operation of the above turbojet and compressor models.

Blade Speed	Range [RPM]	Axial Velocity	Range [m/s]	Pressure Ratio	Range
Slow	0 to 6.5k	Slow	0 to 150	Low	1 to 1.5
Average	0k to 13k	Average	0 to 300	Average	1 to 2
Fast	6.5k to 13k	Fast	150 to 300	High	1.5 to 2

Table 2.5: Operating ranges of fuzzy inputs

Instability	Range
None	0 to 0.3
Low	0.1 to 0.4
Medium	0.3 to 0.7
High	0.5 to 1
Danger	0.7 to 1

Table 2.6: Operating ranges of fuzzy output

FUZZY LOGIC CONTROL OF COMPRESSOR SURGE IN A TURBOJET ENGINE MODEL

This type of modeling requires a working knowledge of the system. The more empirical data available on the operation of a particular compressor the better, as the programmer will have a better picture for comparison as the fuzzy model is adjusted during creation.

2.5.1 CREATING THE MEMBERSHIP FUNCTIONS

A membership function is a curve that defines how each point in the input space is mapped to a membership value (or degree of membership) between 0 and 1. The function itself can be any arbitrary curve whose shape can be defined as a function that suits the problem. A more advanced discussion on membership functions can be found in Chapter 3. For this example model, triangular membership functions are defined for each classified category of input and output. The base of each triangular membership function rests on the intervals of each category, and the apex of the triangle is located above the midpoint of the interval. The membership functions for blade speed and the probability of a flow instability are plotted in Figure 2.12 and Figure 2.13, respectively.

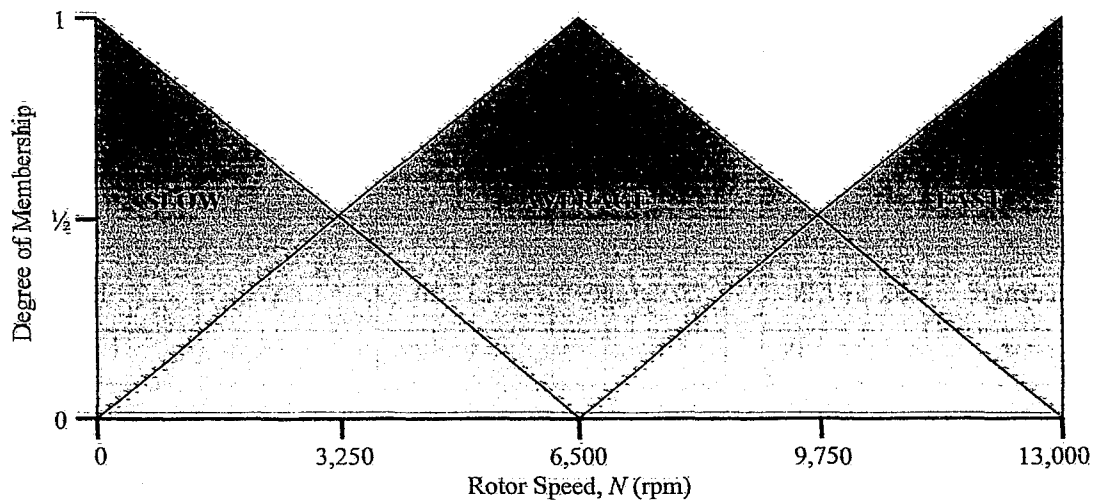


Figure 2.12: MFs for blade speed

2.5.2 CONSTRUCTING THE RULE BASE

For the case of a three-input and one-output model, the rule base can be constructed by creating two matrices of options and solutions. The first matrix is based on the mass flow

TURBOJET ENGINE MODELING

coefficient, where as a guide line Φ should be within the range of 0.4 and 0.7 (Archer, 1996). The input variable axial flow velocity is along the top of the matrix and the input variable blade speed along the side (see Table 2.7). The entries in the matrix are the desired response of the system, or in this case the probability of surge or rotating stall. The second matrix utilizes the work coefficient as a guideline, predicting safe operation if the coefficient is kept within the range of 0.35 and 0.5 (Archer, 1996). The pressure ratio is across the top of this matrix and the blade speed is along the side, and once again, the entries in this two-by-two matrix are the probabilities of either surge or rotating stall occurring.

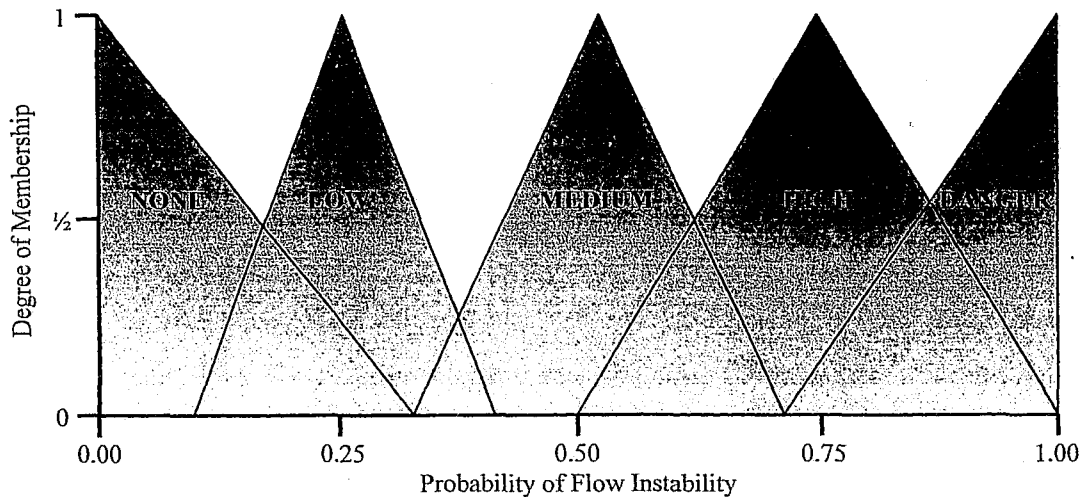


Figure 2.13: MFs for the probability of a flow instability

From the two rule base matrices eighteen rules are created, one for each matrix entry and hence the combination of the membership functions and the rule base create the fuzzy logic model. Additional rules can be added to couple the values of stage pressure and axial flow velocity to further adjust the model. The method used to develop a fuzzy logic model is presented in more detail in Chapter 3.

FUZZY LOGIC CONTROL OF COMPRESSOR SURGE IN A TURBOJET ENGINE MODEL

Blade Speed			
Slow	High	Danger	Danger
Average	Medium	Low	High
Fast	Low	None	Low
Probability of Flow Instability			

Blade Speed			
Slow	Low	Medium	Danger
Average	None	None	Medium
Fast	Medium	Low	Low
Probability of Flow Instability			

Table 2.7: Rule base matrices for three-input / one-output system

CHAPTER 3

FUZZY LOGIC CONTROLLERS

This chapter outlines the theory behind fuzzy logic decision-making utilized in the fuzzy logic controllers. A full description of the fuzzy logic controllers are presented within this chapter. First, the active controllers based on the turbojet engine model are given, and then the detection avoidance controllers based on the Moore-Greitzer models are presented.

3.1 FUZZY LOGIC CONTROL

The fuzzy logic controller is a rule-based system that controls the operation of the simulated engine system. The FLC receives current engine data fed back from the simulated system as it operates. These crisp values from the engine simulation are fuzzified (converted into fuzzy values) that are then processed by the fuzzy knowledge base. The fuzzy output is defuzzified (converted back to a crisp value) in order to update the engine simulator's operating conditions. The FLC process is summarized in Figure 3.1.

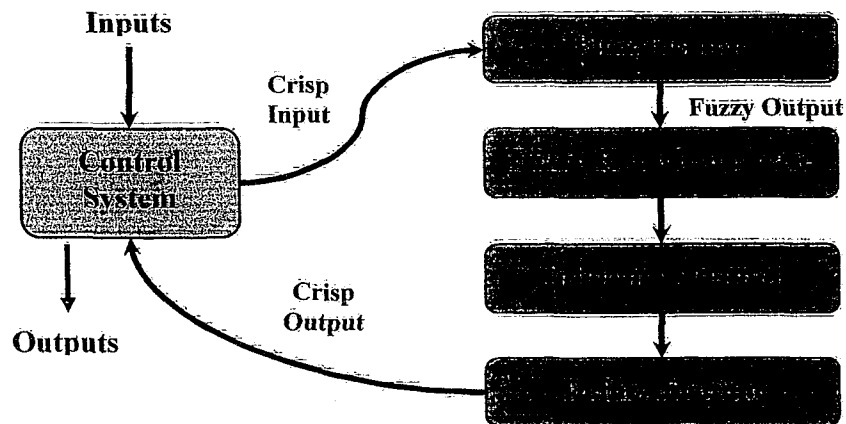


Figure 3.1: Fuzzy control logic flowchart

A fuzzy rule is created by combining various fuzzy statements to form the premise and the consequence of the rule. A fuzzy rule appears no different than an ordinary rule; however, the difference arises when clauses take on partial truths. These partial truths are evaluated based on the membership function. This value, referred to as the *rule alpha*, is used to indicate the significance of the rule and the significance of the consequence. A rule that is not completely true will still be able to convey information toward the final outcome. A collection of these fuzzy rules makes up the rule-base for the decision making processor. Traditionally, these assembled rules are designed such that no two contradicting rules are true. However, in fuzzy logic it is common for a multiple of rules to take on non-zero values (degrees of truth). After the variables have been passed through the rule base, the result is interpreted as a numerical result.

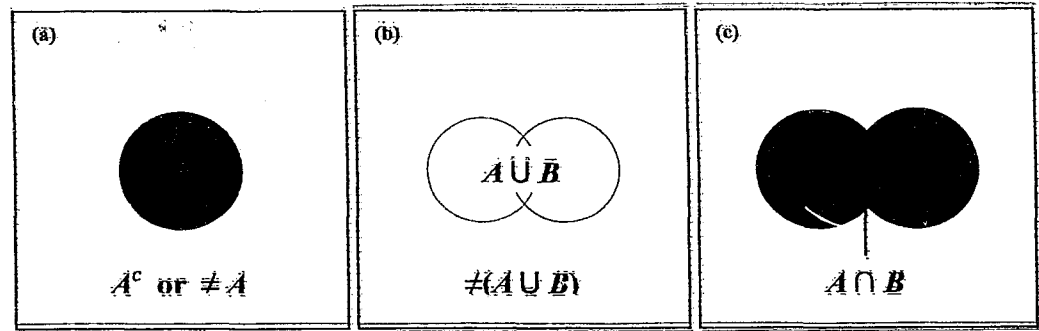
FUZZY LOGIC CONTROLLERS

The standard method of creating a fuzzy control system involves identifying and naming the fuzzy inputs and outputs, creating the fuzzy membership functions for each, constructing the rule base, and then deciding how the action will be carried out. A collection of these fuzzy rules makes up the *knowledge* base of the decision-making processor, shown earlier in Chapter 2.

3.1.1 FUZZY SETS

The purpose of a set is to single out its elements from those in its domain. The relationship between two sets has two possibilities, either they are partners merged in a larger entity or the relationship consists of the elements that they have in common. Sets that are partners are called disjunctions or unions. The union of A and B , denoted as $A \cup B$, is defined to be the set of all elements within A and B . In the fuzzy world, this partnership expresses the maximum value for the two sets involved. The intersection of A and B , denoted as $A \cap B$, is defined to only the set of elements that are found in both A and B . In the fuzzy world a conjunction is expressed as the minimum value for the two fuzzy sets. Fuzzy rules are either 'and' or 'or' rules, where 'and' rules set the rule alpha value to the maximum value of the set while the 'or' rule defines the rule alpha value as the minimum value of the set. By using the 'or' rules, the increase in step size of the gain is smaller so that it will reduce overshoot that was more commonly found when using the 'and' rules.

In classic set theory (see Figure 3.2) $A \rightarrow B$ is read as A implies B . Therefore if A is true it is inferred that B is also true or vice versa. If A is false, then $A \rightarrow B$ implies B is false. Now, let A and B be sets of fuzzy numbers. In fuzzy logic $A \rightarrow B$ is interpreted as A is contained in B and B is true if $A > B$. The statement $\neq A$ (not A) or A^C (compliment of A) in both crispy and fuzzy logic is defined as all elements in the domain that are not in the set of A . In crisp logic $A^C \cup A$ would contain the entire domain while $A^C \cap A$ is impossible since both sets are mutually exclusive. In fuzzy terms $A^C \cup A = \max(A^C, A)$, which would not contain the entire domain and $A^C \cap A = \min(A^C, A)$ is possible and would not be equal to an empty set. The differences between fuzzy and classical set theory are summarized in Table 3.1.


 Figure 3.2: Crisp set theory (a) A and not A (b) A union B (c) A intersection B

$A \cup B$	The set of all elements within A and B	$A \cup B = \max(A, B)$
$A \cap B$	The set of elements that are found in both A and B	$A \cap B = \min(A, B)$
$\neq A$	All elements in the domain that are not in the set of A	$\neq A = A^c = 1 - A$
$A \Rightarrow B$	If A is true it is implied that B is also true	$A \Rightarrow B$ is true if $A \geq B$

Table 3.1: Crisp theory compared with fuzzy set theory

3.1.2 MEMBERSHIP FUNCTIONS

The simplest membership functions (MFs) are formed using straight lines. The triangle MF, shown in Figure 3.3(a), is the most practical and commonly used function as it is easily represented, as seen in Chapter 2. Three numbers taking the form (a, b, c) represent the triangle MF where b is the apex of the triangle and the base of the triangle extends across the numerical range of fuzziness that is in the possible range from a to c . The trapezoidal MF is a truncated triangle curve which has a flat top, as shown in Figure 3.3(b).

Another commonly used MF is shown in Figure 3.3(c), which is built by the Gaussian distribution curve. These types of functions have the advantage of being nonzero at all points. Although the Gaussian MF achieve smoothness, they are unable to specify asymmetric MFs, unlike the triangle and trapezoid MFs that can be skewed. However, an open ended Gaussian MF, either open left or right can be used where half of the Gaussian

FUZZY LOGIC CONTROLLERS

function is utilized and the second half of the function is replaced with a flat top as seen in Figure 3.3(d).

Any polynomial-based curve can also be used as a membership function. However, the four types of membership functions outlined above more than adequately meet the thesis requirements without moving into more exotic membership functions. This chapter will present fuzzy logic controllers that were created using only triangular membership functions as well as controllers that use multiple membership functions.

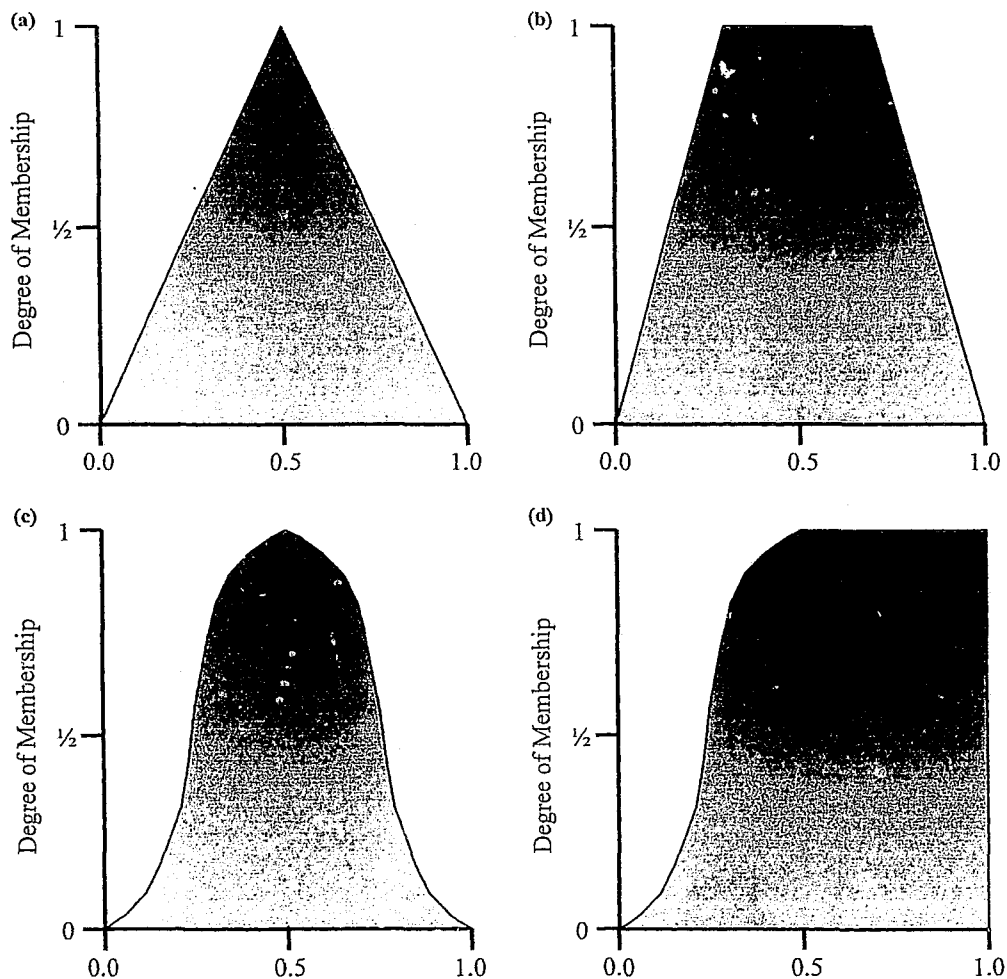


Figure 3.3: Membership functions (a) Triangle MF (b) Trapezoidal MF (c) Gaussian MF (d) Open ended Gaussian MF

3.1.3 FUZZY INFERENCE AND DEFUZZIFICATION

The process of interpreting a fuzzy logic result involves first the fuzzy inference step followed by the process known as defuzzification. The two most common inference methods are the “max-min” inference method and the “max-dot/product-sum” inference method, and the most common defuzzification method is the “centroid” defuzzification. For simple cases the two inference methods will produce the same results, but in complex situations can produce drastically different results. (Tanaka, 1997)

To illustrate the differences in the above methods, the following simplistic Rule Base and membership functions will be utilized:

$$\begin{aligned} &\text{IF (x is hot) AND (y is large) THEN (z is fast)} \\ &\text{IF (x is warm) AND (y is large) THEN (z is slow)} \\ &\text{IF (y is medium) THEN (z is slow)} \end{aligned} \quad 3.1$$

The Rule Base has been evaluated with the following clauses:

$$\begin{aligned} &(x \text{ is hot}) = 0.7 \quad (x \text{ is warm}) = 0.5 \\ &(y \text{ is large}) = 0.6 \quad (y \text{ is medium}) = 0.4 \end{aligned} \quad 3.2$$

The output membership functions are triangular as illustrated in Figure 3.4, and defined by the following:

$$\begin{aligned} &\text{slow} = (25, 100, 175) \\ &\text{fast} = (125, 200, 275) \end{aligned} \quad 3.3$$

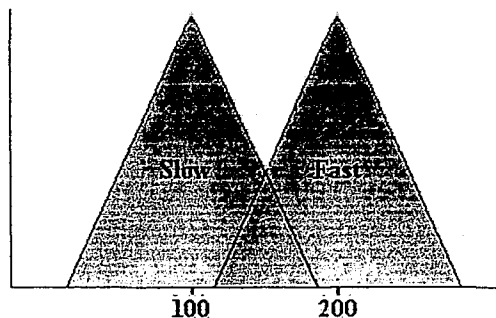


Figure 3.4: Triangular membership functions of output

FUZZY LOGIC CONTROLLERS

The max-min method truncates each output membership function appearing in the consequence of that rule by the rule alpha value. All the rules in the rule base are processed and the resultant shapes are combined as seen in Figure 3.5. Instead of truncating the output membership functions, the max-dot product and product-sum methods scale the output membership functions by the rule alpha value in the vertical direction. The max-dot method combines the results through absorption, as shown in Figure 3.6(a), while the product-sum method combines the results through summation, as seen in Figure 3.6(b). The product-sum method is considered more accurate since no information is lost via absorption.

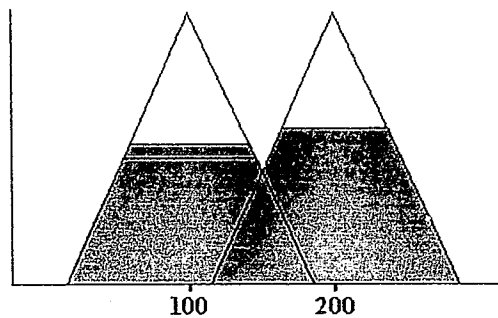


Figure 3.5: Max-min inference method

The Centroid Method of defuzzification is analogous to finding the center of mass of the output composition. Every piece of information is accounted for in the final defuzzified value, which is determined at the location of the centroid. All the simulations in this thesis use the product-sum method of inference and the centroid method of defuzzification.

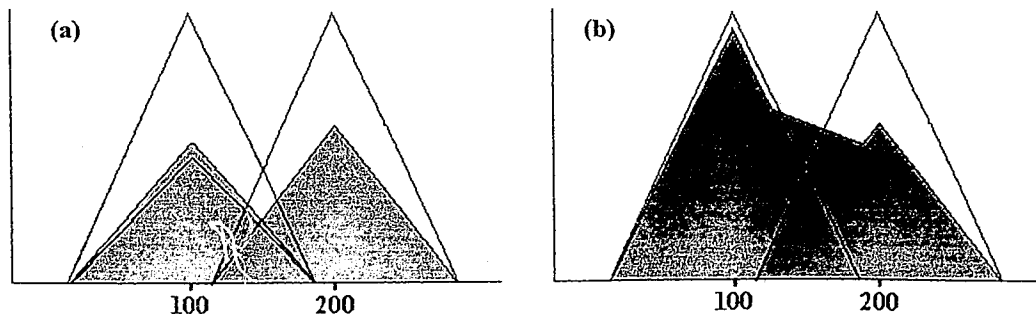


Figure 3.6: (a) Max-dot Inference Method (b) Product-sum inference method

3.2 SPOOL SPEED CONTROLLER

The first fuzzy controller was developed to adjust the spool speed with respect to the airspeed (the axial flow velocity entering the inlet) and altitude. A third input variable can be added to incorporate the desired thrust, and thus increase the spool speed to increase the thrust output. As the input values vary, the spool speed is varied accordingly by the fuzzy logic controller.

The fuzzy logic controller is provided with normalized input values for both the airspeed and the altitude. The simulated altitude is normalized over the specified maximum aircraft ceiling which is inputted by the user. The axial-flow velocity is normalized over the maximum allowable velocity that is based upon a user-selected Mach number.

The controller outputs a scaling factor from 0 to 1 which is multiplied by the maximum allowable spool speed.

$$N = N_{\max} f(v, h) \quad 3.4$$

The maximum allowable spool speed is calculated by solving the compressor tip speed at a given maximum Mach number:

$$N_{\max} = \frac{M_u a_1}{\pi r_{tip}} \quad 3.5$$

When modeling membership functions it is often easier to start with simple symmetric triangular functions for the controller inputs as seen in Figure 3.7, along with the use of a straightforward one-to-one rule base as shown in Table 3.2. The sensitivities of the controller can be adjusted by massaging the output membership functions to achieve the desired control surface (see Figure 3.8).

FUZZY LOGIC CONTROLLERS

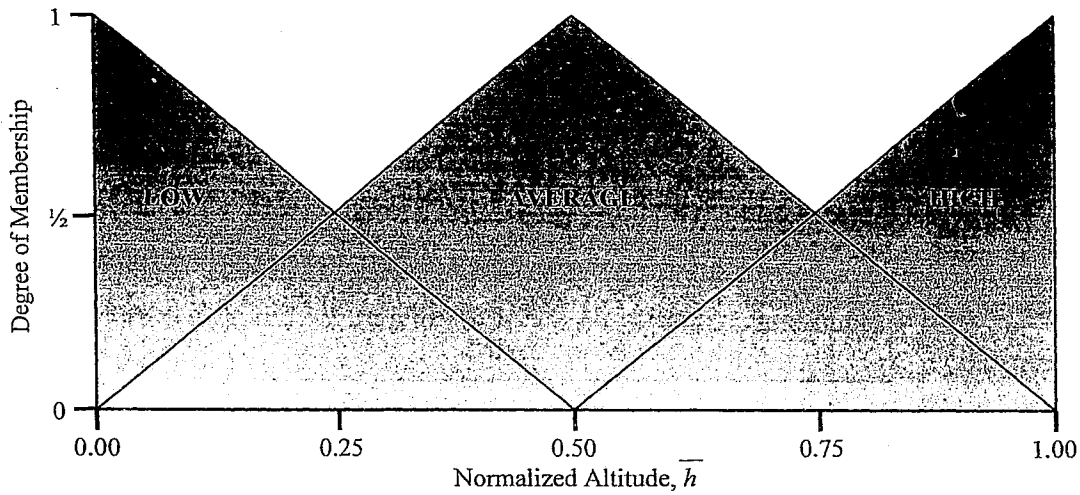


Figure 3.7: Simple symmetric triangular membership functions for altitude input

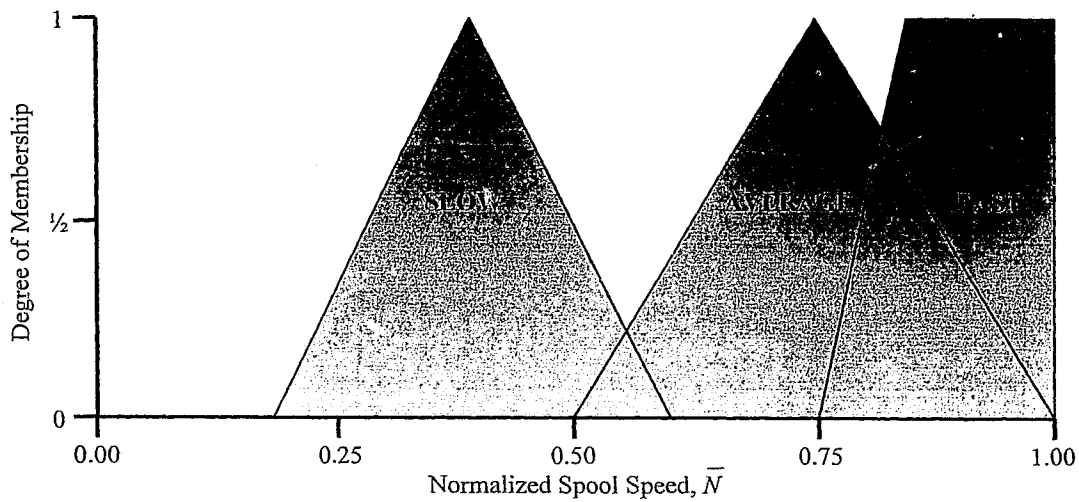


Figure 3.8: MF for spool speed scaling factor

The resulting control surface, in Figure 3.9, shows three distinct operation zones: a rapid increase occurs in spool speed as the flight speed and altitude increase at low operating conditions; a gradual increase in spool speed occurs in the middle regions of the surface; and the spool speed is increased slowly as the maximums in flight speed and altitude are reached.

FUZZY LOGIC CONTROL OF COMPRESSOR SURGE IN A TURBOJET ENGINE MODEL

Altitude		
Low	Average	High
Slow	Average	Fast
Blade Speed		
Low	Average	High
Slow	Average	Fast
Blade Speed		

Table 3.2: Rule base matrices for three-input / one-output system

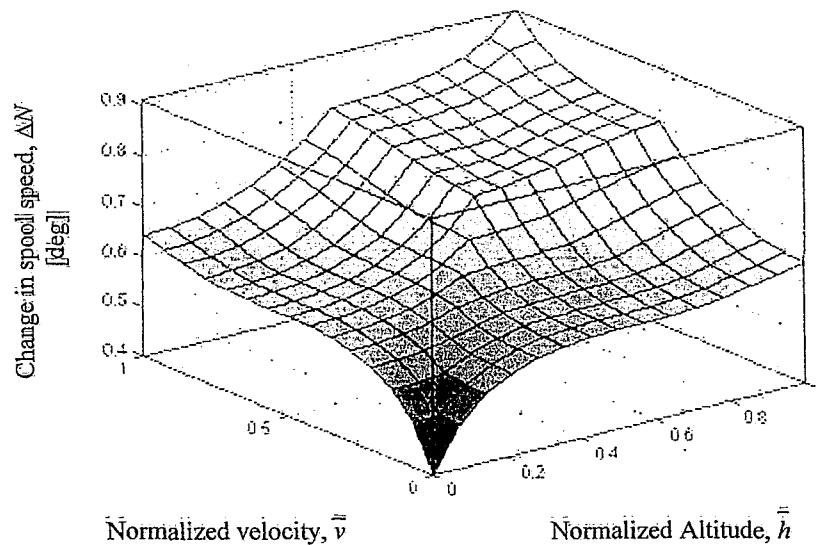


Figure 3.9: Three-dimensional control surface for spool speed controller

As well, the controller automatically installs a safety factor that is determined by the shapes of the membership functions (usually 10 to 20%), as the output of the scaling factor can be adjusted to always be less than 80 to 90%.

Spool speed can also be variable with regards to active surge control. A variation on the above spool speed control was created to adjust the spool speed with respect to current conditions of the mass flow coefficient as well as setting a limit on the maximum blade-tip speed. Both spool speed controllers can be run simultaneously, combining to create a

FUZZY LOGIC CONTROLLERS

controller that will govern spool speed with respect to all of the previously mentioned aspects.

Figure 3.10 expresses the acceptable range of the mass flow coefficient as membership functions. The use of the trapezoid membership functions keeps the controller idle until the set limits are breached, after which the outputted spool speed scaling factor will be altered according to the control surface shown in Figure 3.11. The maximum allowable value for the spool speed scaling factor of ± 0.5 results from the apex of the triangle membership functions 'decrease' and 'increase', which appears in the output membership functions shown in Figure 3.12. The rule base for this FLC is summarized as follows:

IF (Φ is SMALL) THEN (N is DECREASED)

IF (Φ is OKAY) THEN (N is OKAY)

IF (Φ is BIG) THEN (N is INCREASED)

IF (N / N_{MAX} is BIG) THEN (N is FAST DECREASE)

3.6

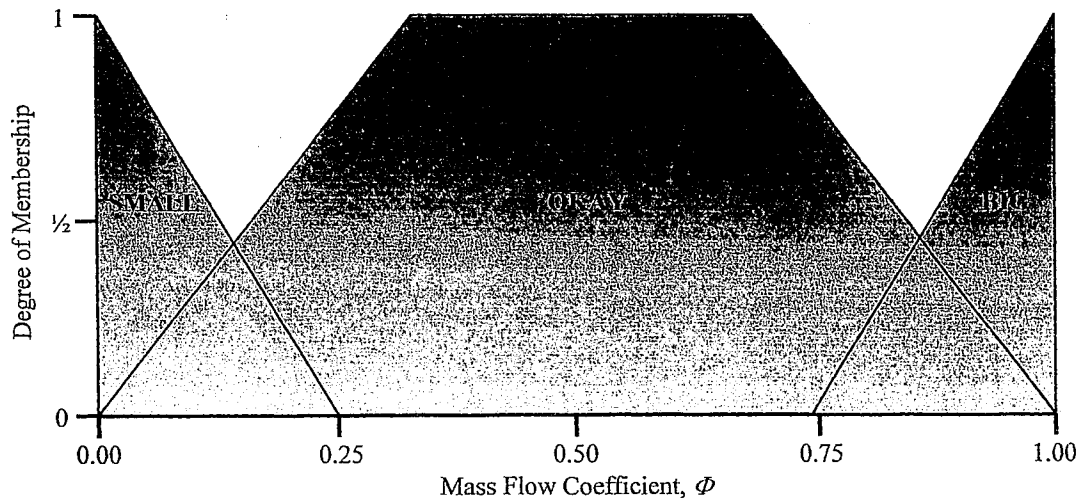


Figure 3.10: Acceptable values for the mass flow coefficient expressed as a MF

The 'fast decrease' membership function shown in Figure 3.12 is called into play if the ratio of spool speed over the maximum allowable spool speed approaches unity. This membership function will override the changes caused by the membership functions

FUZZY LOGIC CONTROL OF COMPRESSOR SURGE IN A TURBOJET ENGINE MODEL

dedicated to the mass flow coefficient, in order to guarantee that shock waves will not occur around the rotating blade tips, resulting in the combined three-dimensional control surface shown in Figure 3.13.

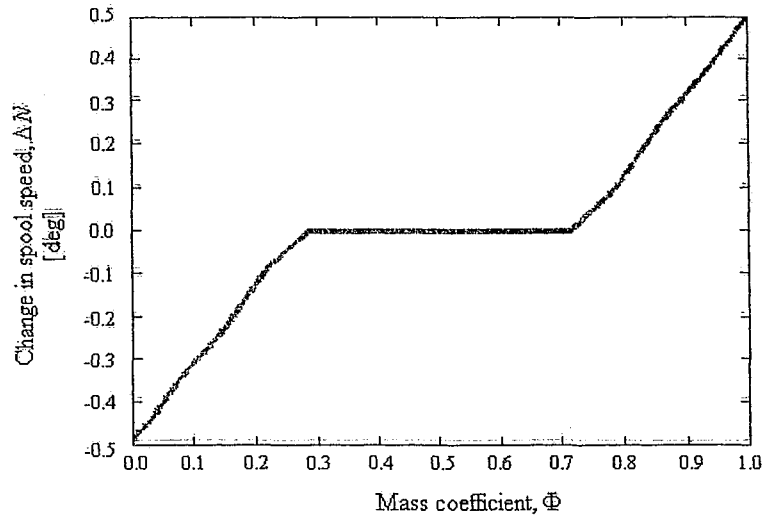


Figure 3.11: Two-dimensional control surface for spool speed control of mass coefficient

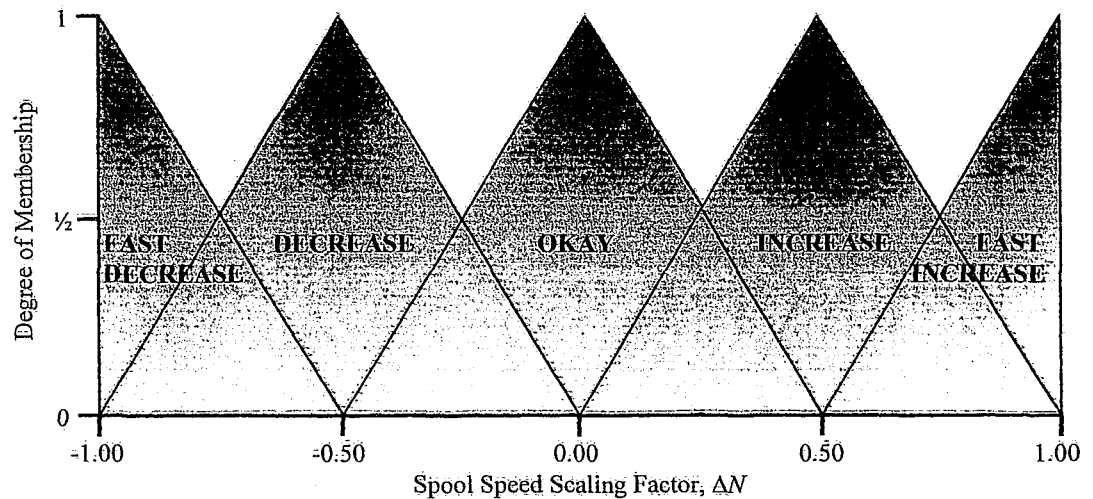


Figure 3.12: MF for outputted spool speed scaling factor

FUZZY LOGIC CONTROLLERS

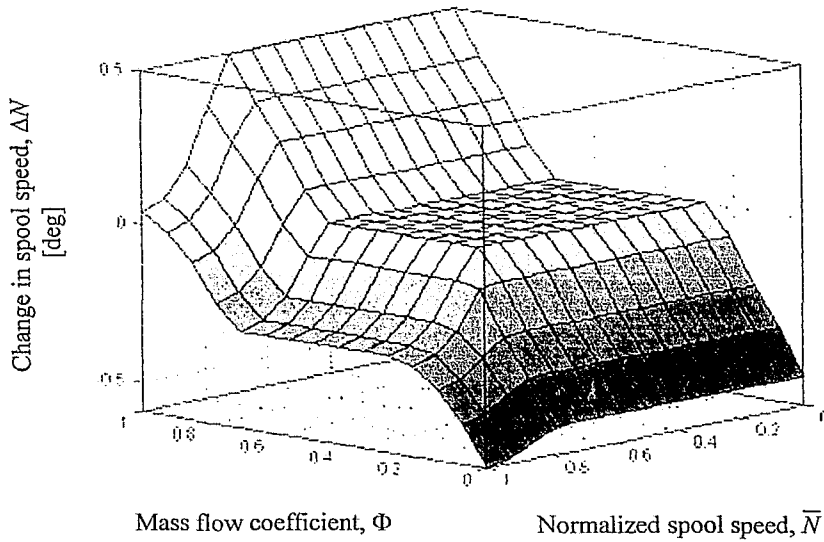


Figure 3.13: Three-dimensional control surface for spool speed control of mass coefficient

3.3 IGV AND STATOR BLADE ANGLE CONTROLLERS

The design angle of attack α_o defines the near-optimum inlet flow angle for the blade cascade. An empirical model by Aungier (2003) based on the design charts of Herrig et al. (1957) for NACA 65-series blades was developed to calculate this design value:

$$\alpha^* = \left[3.6K_{sh}K_{t,i} + 0.3532\theta \left(a/c \right)^{\frac{1}{4}} \right] \sigma^{0.65-0.002\theta} \quad 3.7$$

The blade shape parameter, K_{sh} assumes the value of 1.0 for NACA profiles, 1.1 for the C4-series profiles and 0.7 for the double-circular-arc profile (Aungier, 2003). The design incidence angle thickness correct factor, $K_{t,i}$ provided in Johnsen and Bullock (1965) is expressed empirically as a function of the blade maximum thickness-to-chord ratio, t_b/c :

$$K_{t,i} = \left(10t_b/c \right)^{0.28 \left[0.1 + (t_b/c)^{0.3} \right]} \quad 3.8$$

3.3.1 ADJUSTABLE IGV TO OPERATE AT DESIGN INCIDENCE ANGLE

The IGV metal angle can be adjusted to control the airflow entering the first rotor stage of the compressor. In order to avoid flow separation the air flow should pass the blade at

an angle close to the physical metal angle of the blade. The difference between the actual angle at which the flow passes the blade and the blade angle is defined as the incidence angle:

$$i = \alpha_{in} - \beta_{in} \quad 3.9$$

The design incidence angle for each cascade is related to the design angle of attack by the following relationship, where ζ is the blade stagger angle (Horlock, 1982):

$$i^* = \alpha^* + \zeta - \beta_{in} \quad 3.10$$

Using Lieblein's (1960) correlation, with all angles in degrees, an iterative solution can be used to compute the design incidence angle with the following:

$$i^* = K_{sh} K_{t,i} i_o^* + n\theta \quad 3.11$$

$$i_o^* = \frac{\alpha^{0.914+\sigma^3/160}}{5+46e^{-2.3\sigma}} - 0.1\sigma^3 e^{[(\alpha-70)/4]} \quad 3.12$$

$$n = 0.025\sigma - 0.06 - \frac{(\alpha/90)^{1+1.2\sigma}}{1.5+0.43\sigma} \quad 3.13$$

Separation is liable to occur if the incidence angle is more than $\pm 10^\circ$ different then the design incidence angle (Archer, 1996). The difference between the simulated actual incidence angle and the design incidence angle becomes the input to the FLC:

$$e_i = i^* - i \quad 3.14$$

The output of the FLC is the amount in radians that the IGV must be adjusted. The iterative nature of Lieblein's correlation works well within the loop of the simulation model. With each simulation step, one iteration of Lieblein's correlation is calculated, and then the FLC is called to adjust the IGVs, which results in a new flow angle and a smaller difference between the design and actual incidence angle.

As before, a one-to-one rule base is used for this controller: if the error term is negative then a large positive adjustment occurs in the IGV; if the error term is about zero then a

FUZZY LOGIC CONTROLLERS

small adjustment occurs in the IGV; and if the error term is positive then a negative adjustment occurs in the IGV. The same triangle membership functions shown in Figure 3.7 are utilized for both the input error term and the output term; the only difference being the domain has been changed to $[-1,1]$ in order to compensate for situations where the design incidence angle is smaller than the actual incidence angle. The resulting symmetrical two-dimensional control surface is shown in Figure 3.14, resulting from the rule base given by:

IF (e_i is POSITIVE) THEN (β_{IGV} is DECREASED)

IF (e_i is ZERO) THEN (β_{IGV} is OKAY)

3.15

IF (e_i is NEGATIVE) THEN (β_{IGV} is INCREASED)

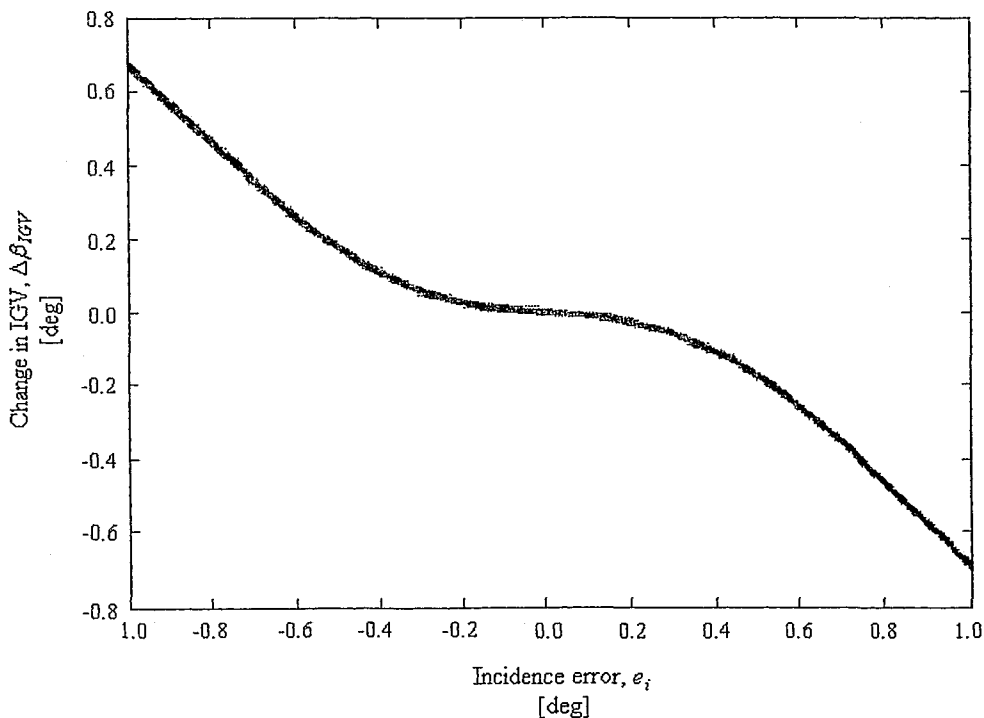


Figure 3.14: Two dimensional control surface for adjustable IGV to operate at design incidence angle

The identical strategy can be applied to controlling separation over the flow exiting a blade. The difference between the actual angle at which the flow leaves the blade and the blade angle is defined as the deviation angle:

$$\delta = \alpha_{out} - \beta_{out} \quad 3.16$$

Lieblein's (1960) iterative solution can be used to compute the design deviation angle as follows:

$$\delta^* = \bar{K}_{sh} \bar{K}_{t,i} \delta_o^* + m\theta \quad 3.17$$

where the zero-camber design deviation angle is calculated from:

$$\delta_o^* = \alpha 0.01\sigma + (0.74\sigma^{1.9} + 3\sigma) \left(\frac{\alpha}{90} \right)^{1.67+1.09\sigma} \quad 3.18$$

and the slope factor is calculated from:

$$m = \frac{0.17 - 0.0333 \left(\frac{\alpha}{100} \right) + 0.333 \left(\frac{\alpha}{100} \right)^2}{\sigma^b} \quad 3.19$$

$$b = 0.9625 - 0.17 \left(\frac{\alpha}{100} \right) - 0.85 \left(\frac{\alpha}{100} \right)^3 \quad 3.20$$

3.3.2 ADJUSTABLE IGV TO OPERATE AT DEFINED REACTION

The degree of reaction for a compressor is defined as the ratio of the static enthalpy increase across the rotor to the increase in static enthalpy for the stage. When the degree of reaction is 0.5, the increase in static enthalpy is evenly divided between the rotor and stator. This configuration is optimal for the present application, as it will minimize the tendency of the blade boundary layer to separate. Using the velocity triangles defined in Chapter 2, the degree of reaction can be defined as (Horlock, 1982):

$$R' = 0.5 - \frac{v_1}{2u} [\tan \alpha_{r3} + \tan \beta_{IGV}] \quad 3.21$$

The FLC outlined in Section 3.3.1 can be used to adjust the IGV in order to achieve a degree of reaction of 0.5. Now the inputted error term will become:

FUZZY LOGIC CONTROLLERS

$$e = 0.5 - R' \quad 3.22$$

The deHaller number is a measurement of the amount of diffusion, noting that both the rotor and stator act as diffusers. If the rate of diffusion is very slow, the blade length becomes excessive, resulting in large friction losses, and if the rate of diffusion is very large, boundary layer separation may occur (Harman, 1981). Based on the velocity triangle compressor model outlined in Chapter 2, the deHaller number can be calculated as follows:

$$\text{deH} = \frac{v_{r3}}{v_{r2}} \quad 3.23$$

Many designers use 0.707 as a target deHaller number (Cumpsty, 1989). Once again, the same methodology described above can be used to tune the deHaller number of a compressor stage.

3.3.3 STATOR CONTROL AT DESIGN INCIDENCE ANGLE

Stator blades can be treated the same as inlet guide vanes with respect to the two controller examples above. Either the stator blade turn angle, β_s , can be adjusted, or the entire stator blade can be rotated, hence adjusting the stagger angle, ζ_s , of the blades. These controllers can be run simultaneously on the IGVs and the stator blades of any stage.

3.3.4 COMBINATION CONTROL

The controller outlined in Section 3.3 can be run in parallel with any combination of the abovementioned controllers. Now the IGVs are tuned to simultaneously meet more than one condition (shown in Figure 3.15a). A natural middle ground is found where all the conditions are partially met according to the condition weighting. A multiple-input FLC can be used in place of running the controllers in parallel; as shown in Figure 3.15b, any number of error values can be passed to the fuzzy logic controller, which will output a change in the IGVs.

3.3.5 MULTIPLE STAGE CONTROL

Any number of compressor stages can be linked in series to create a multi-stage compressor within the turbojet model. The stator cascade of the previous stage becomes the IGV stage of the current stage, and thus the flow properties are based from stage to stage. Each stage can be controlled separately, or the stage control can be linked to a stage either before or after it. The IGV and the stator blades of the first few stages can be linked to tune variables throughout the remaining stages.

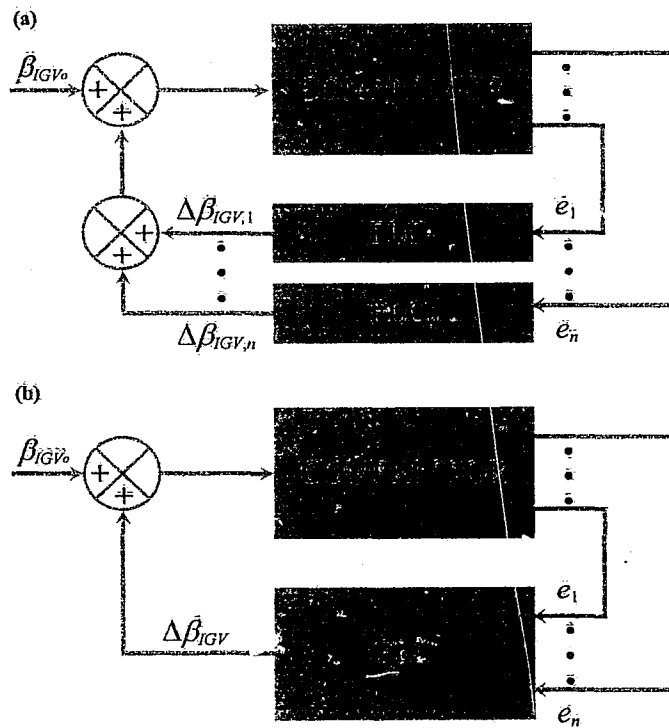


Figure 3.15: Combination control flow chart: (a) multiple error / single controller
(b) multiple error / multiple controller

3.4 IGV WITH ADJUSTABLE RPM

The spool speed controller outlined in Section 3.2 can be run in parallel with any of the above-mentioned controllers. Now two control variables, spool speed and IGV angles, are tuned simultaneously to achieve the desired results from the engine simulation, as shown in Figure 3.16.

FUZZY LOGIC CONTROLLERS

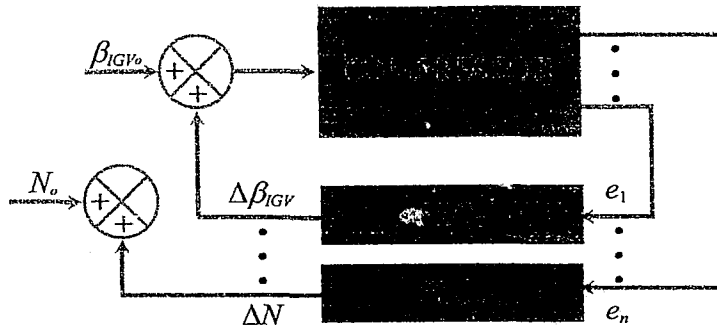


Figure 3.16: Multiple control surfaces flow chart

3.5 ACTIVE SURGE CONTROLLER

This controller uses the same feedback-loop fuzzy decision-making method as the above-mentioned controllers. The goal of this control is to show that engine operation can occur along the surge line, as any disturbance that pushes the operation point into the surge region will be quickly corrected.

This method of control requires knowledge of the surge line, and for this example a generic quadratic surge line is defined as follows for the design work coefficient:

$$\psi^* = \frac{\Phi^2}{3} + 0.35 \quad 3.24$$

By lowering the y-intercept in Equation 3.24 a surge margin can be placed on the above-mentioned defined surge line, both the surge line and margin line are plotted in Figure 3.17. An upper and lower bound is required for the mass flow coefficient, Φ . The second controller outlined in Section 3.2 will be run for this example, to obtain the desired limitations on the mass flow coefficient.

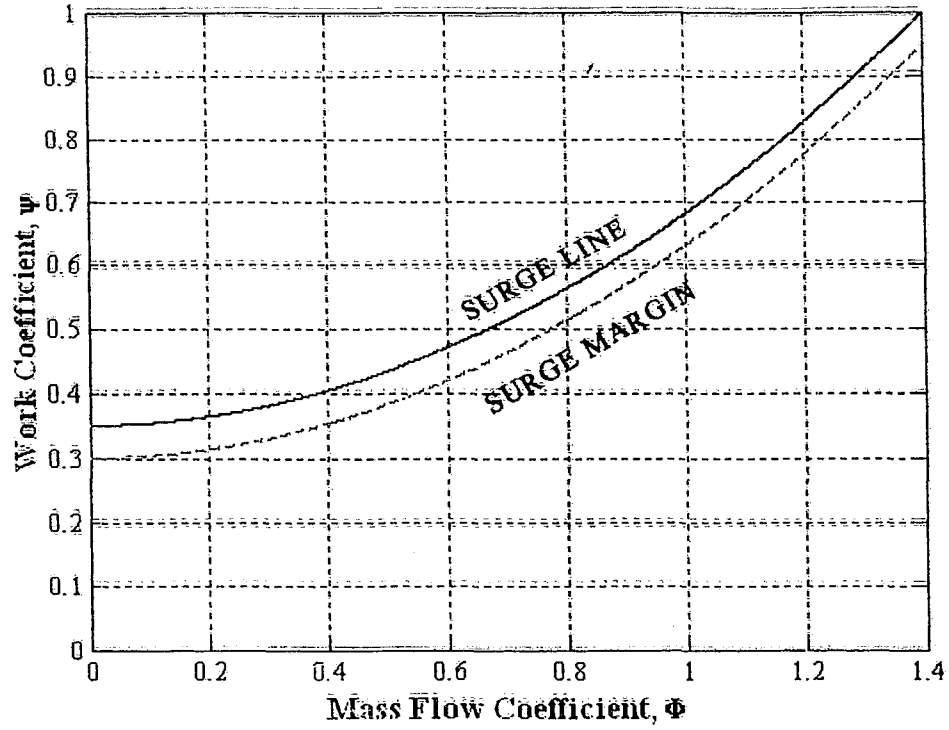


Figure 3.17: Surge line and surge margin

The design work coefficient, ψ^* , is solved for at the model's current mass flow coefficient using the quadratic surge line characteristic (Equation 3.24), and then the actual work coefficient ψ is solved from the compressor stage velocity triangles:

$$\psi = \frac{\Delta h_o}{u^2} = \frac{(w_3 - w_2)}{u} \quad 3.25$$

Now the FLC error term can be calculated using the design work coefficient and the actual work coefficient:

$$e_\psi = \psi^* - \psi \quad 3.26$$

If the error term is greater than zero, the compressor is operating safely below the surge line and the work coefficient can be slowly raised till the error is zero and the compressor is operating on the surge line. If the error term is less than zero the compressor is operating above the surge line, which is undesired behaviour, and the controller will very

FUZZY LOGIC CONTROLLERS

rapidly move the operating point back below the surge line by lowering the work coefficient.

In order to raise the work coefficient the whirl velocity across the IGV, w_2 , must be lowered and the whirl velocity entering the stator cascade, w_3 , must be raised. The IGV whirl, w_2 , will change proportionately to the IGV angle, and w_3 can be adjusted by changing the rotor turn angle (this can be tuned in the simulation, but is not commonly done in practice).

From Equation 2.39 the whirl velocity across the IGV can be expressed in terms of the axial velocity and the IGV angle:

$$w_2 = v_1 \tan \beta_{IGV} \quad 3.27$$

Combining Equations 2.44, 2.46, and 2.47, the whirl velocity entering the stator cascade can be expressed in terms of the blade speed, the axial velocity, the flow angle entering the rotor stage and the rotor turn angle:

$$w_3 = u + v_1 \tan(\alpha_{r2} + \theta_r) \quad 3.28$$

where α_{r2} , the angle at which the flow enters the rotor, can be expressed in terms of blade speed, axial velocity, and IGV angle as:

$$\alpha_{r2} = \arctan\left(\tan \beta_{IGV} - \frac{u}{v_1}\right) = \arctan\left(\tan \beta_{IGV} - \frac{1}{\Phi}\right) \quad 3.29$$

Substituting Equations 3.27 and 3.28 into Equation 3.25 yields the following relationship for the work coefficient:

$$\psi = \frac{(u + v_1 \tan(\alpha_{r2} + \theta_r) - v_1 \tan \beta_{IGV})}{u} = 1 + \Phi \tan(\alpha_{r2} + \theta_r) - \Phi \tan \beta_{IGV} \quad 3.30$$

FUZZY LOGIC CONTROL OF COMPRESSOR SURGE IN A TURBOJET ENGINE MODEL

Equations 3.29 and 3.30 illustrate that the work coefficient is dependent on the mass flow coefficient, the IGV blade angle, and the rotor turn angle. As previously mentioned, the mass flow coefficient will be governed by the controller outlined in Section 3.2, leaving the need for a FLC that will update the IGV angle and the rotor turn angle.

3.5.1 IGV SURGE CONTROL

In this section, a FLC is created using only the IGVs as the actuators for active surge control. The need to oversee the rotor and stator blade incidence angles (in order to avoid stall as seen in Section 3.3.1) is still a major concern. The avoidance of surge is given a heavier weighting, and thus the FLC will settle at an operating point that best meets the surge conditions while staying within the larger allowable boundaries for the stall condition.

The MF for the incidence angle error term, e_i , from Equation 3.14 is shown in Figure 3.18. The IGV is only altered if the flow entering the rotor blade is in danger of separating or more specifically if $|e_i| \geq 6^\circ$. Figure 3.19 shows the two-dimensional plot of the control surface created by the first two rules from the following rule base:

- IF (e_i is NEGATIVE) THEN ($\Delta\beta_{IGV}$ is INCREASED)
- IF (e_i is POSITIVE) THEN ($\Delta\beta_{IGV}$ is DECREASED)
- IF (e_w is NEGATIVE) THEN ($\Delta\beta_{IGV}$ is LARGE INCREASE) 3.31
- IF (e_w is ZERO) THEN ($\Delta\beta_{IGV}$ is ZERO)
- IF (e_w is POSITIVE) THEN ($\Delta\beta_{IGV}$ is DECREASED)

The work coefficient error e_w thus has more weight in the settling position of the IGV blades. If the work coefficient error is negative, then the system has crossed over into the surge region, and the IGV angle is quickly increased. If the work coefficient error is positive, then the system is working safely below the surge line, and the IGV angle can be slowly decreased. The lower limit of the IGV angle will be dictated by the incidence angle error.

FUZZY LOGIC CONTROLLERS

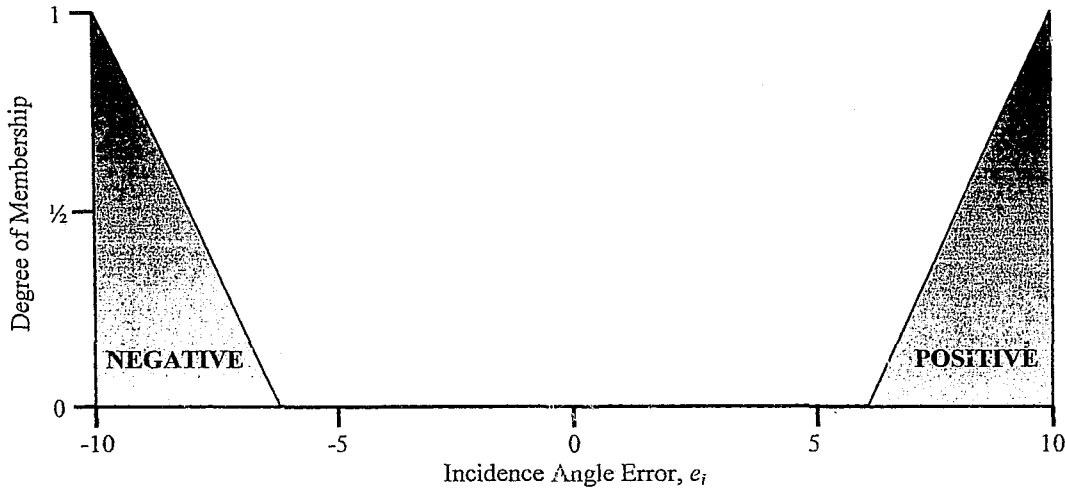


Figure 3.18: MF for incidence angle error for IGV surge controller

This non-symmetrical controller is created by combining non-symmetrical membership functions shown in Figures 3.20 and 3.21. The output MF contains one trapezoid MF which will slew the results quickly to the positive side if the work coefficient error becomes negative. The trapezoid MF in FLC input creates the step increase seen in the control surface (see Figure 3.22) as e_ψ becomes negative. In comparison, the gentler slope, as e_ψ becomes positive, is created by using an open-ended Gaussian membership function. In both cases, if $|e_\psi| > 0.4$, the maximum displacement for the IGV results; this range is set by the base of the triangular MF in the FLC input.

The triangular MF in the FLC input is required to settle the error term to zero. Any shift of the triangle's apex will result in a shift of the same magnitude of the controller's final settling point for the error value. The same relationship is found in shifting the apex of the central triangular MF in the FLC output with respect to the final settling point of the IGV displacement (both apexes are located above the zero, resulting in an equilibrium point of zero IGV displacement at a zero error).

FUZZY LOGIC CONTROL OF COMPRESSOR SURGE IN A TURBOJET ENGINE MODEL

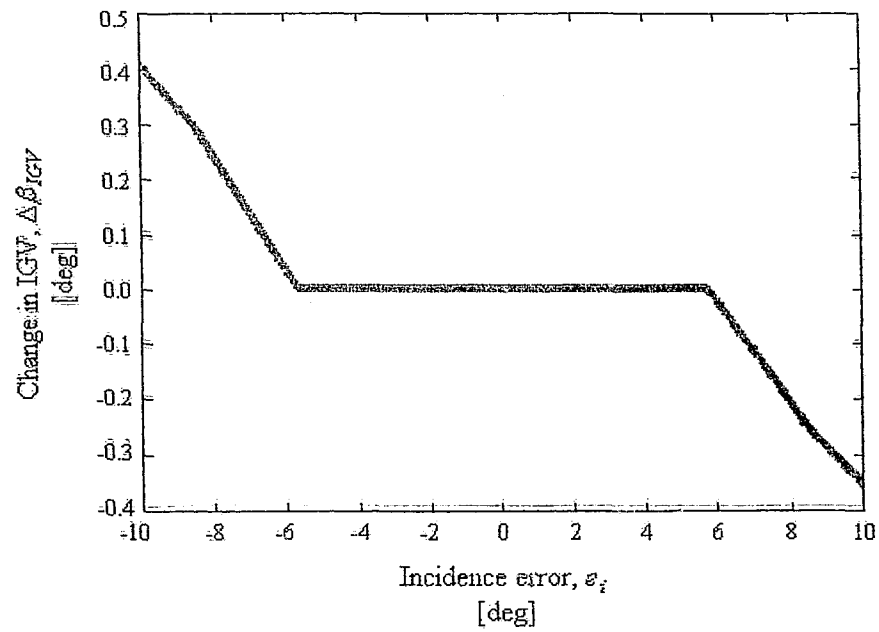


Figure 3.19: Two-dimensional plot of incidence error controller

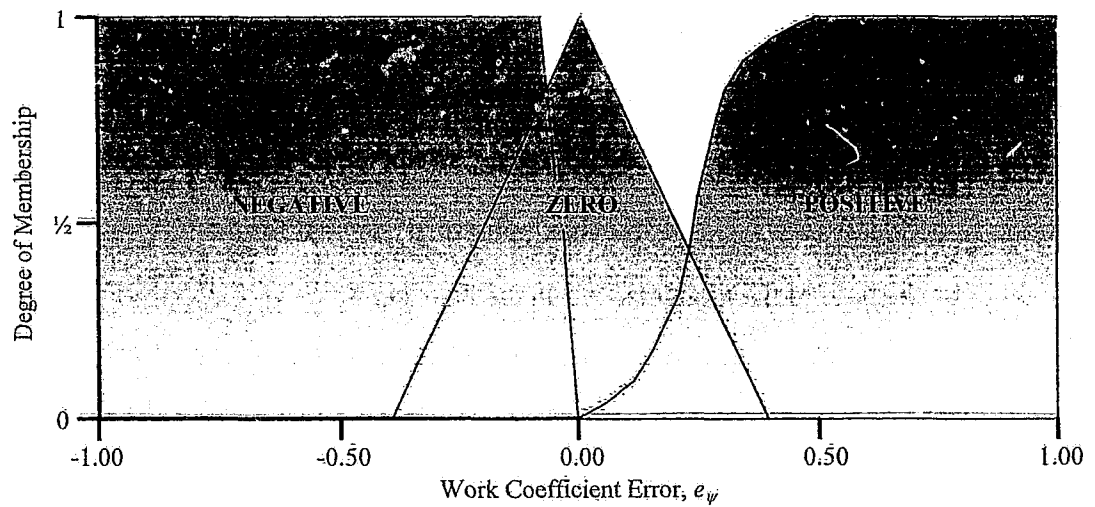


Figure 3.20: Input MF of work coefficient error for IGV surge controller

FUZZY LOGIC CONTROLLERS

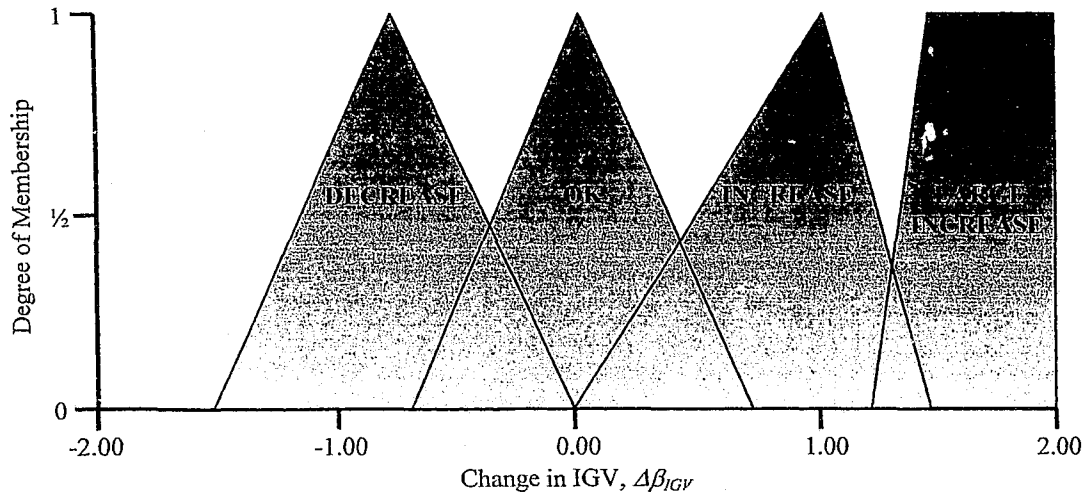


Figure 3.21: Output MF for change in IGV for surge controller

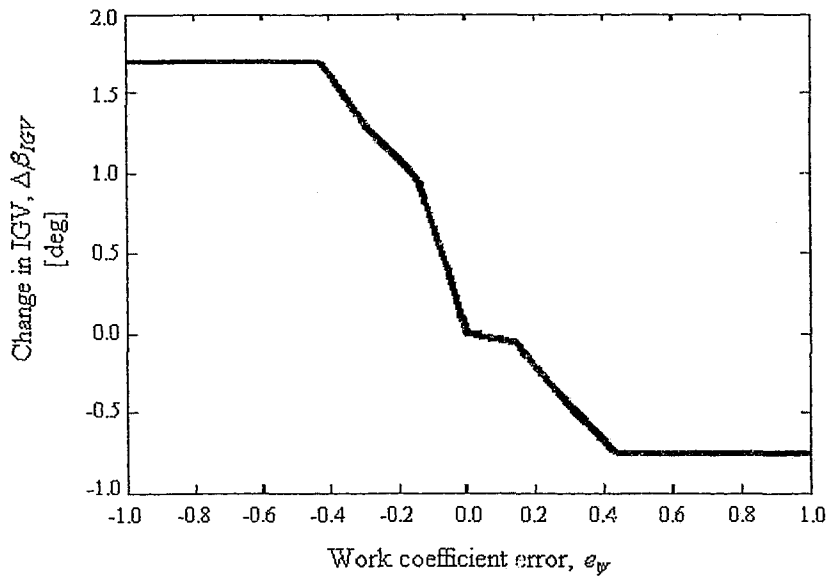


Figure 3.22: Two-dimensional control surface for IGV surge controller

Both two-dimensional control surfaces shown in Figure 3.19 and Figure 3.22 are combined to create the three-dimensional control surface shown in Figure 3.23.

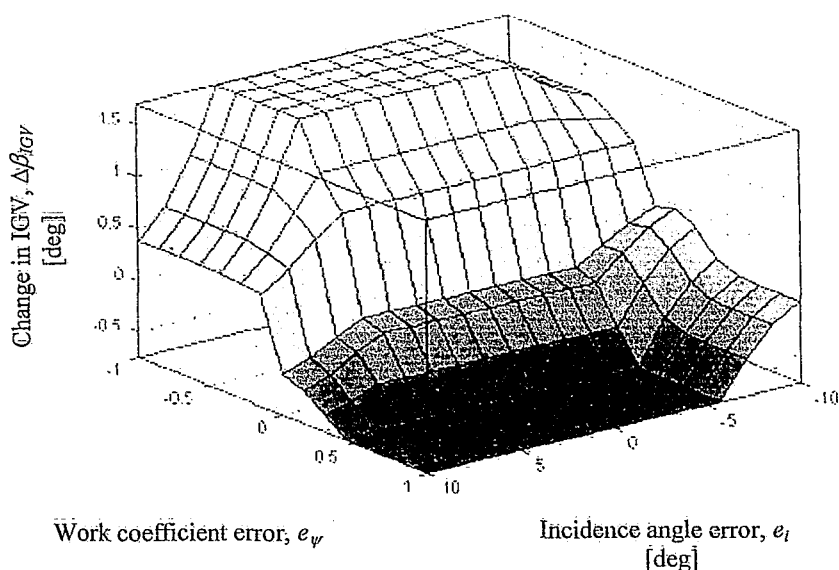


Figure 3.23: Three-dimensional control surface for IGV surge control

3.5.2 IGV AND VARIABLE ROTOR GEOMETRY CONTROL

The IGV positioning is often restricted by stall that occurs over the rotor blade. By introducing variable geometry to the rotor blade, the blade can be turned into the flow, reducing the limitations caused by stall, while increasing the operation range of the IGVs. A second FLC is created to run simultaneously with, yet independently of, the controller outlined in Section 3.5.1. This second controller is only concerned with rotating the rotor blade into the air flow and thus setting the incident angle and the deviation angle to the design value as outlined in Section 3.3. Just like the stator blade shown in Figure 3.1, the rotor blade can be rotated as a whole by altering just the blade stagger angle and keeping the turn angle constant, or by altering both the inlet and outlet blade angle independently and thus altering the rotor turn angle. As seen in Equations 3.11 and 3.17, altering the rotor turn angle results in changing both the design incidence angle and the design deviation angle. The same design strategy used in Section 3.3 to manoeuvre the IGV is applied to the rotor blade.

3.6 DETECTION/AVOIDANCE CONTROLLER

This control does not require any knowledge of the compressor characteristic. Instead, the controller analyses the fluctuations of the axial mass flow coefficient, $\Delta\Phi$, and

FUZZY LOGIC CONTROLLERS

pressure coefficient, $\Delta\Psi$. The response of the MG model is drawn upon for modeling the control system. Increasing the control gains will stabilize the system, however, at a penalty of pressure lost across the system.

The fluctuations of the axial mass flow coefficient, $\Delta\Phi$, and pressure coefficient $\Delta\Psi$ are normalized before being sent to the FLC as the crisp input by the following:

$$\Delta\Psi_i = \frac{|\Psi_i - \Psi_{i+\Delta t}|}{\max(\Psi_i, \Psi_{i+\Delta t})} \quad 3.32$$

$$\Delta\Phi_i = \frac{|\Phi_i - \Phi_{i+\Delta t}|}{\max(\Phi_i, \Phi_{i+\Delta t})} \quad 3.33$$

Samples of the coefficients are taken at regular time-step intervals. The crisp output from the FLC adjusts the throttle and/or the CCV gain by the following:

$$\gamma_{i+\Delta t} = \gamma_i + \Delta\gamma_i \quad 3.34$$

Triangular membership functions were defined for each classified category of input and output as shown in Table 3.3. The base of each triangular membership function rests on the intervals of each category, and the apex of the triangle is located above the midpoint of the interval.

$\Delta\Psi$ and $\Delta\Phi$		$\Delta\gamma$ and $\Delta\gamma_i$	
Small	0.00 – 0.25	Small	0.00 – 0.25
Medium	0.00 – 1.00	Medium	0.25 – 0.50
Large	0.50 – 1.00	Large	0.50 – 1.00

Table 3.3: Operating ranges of fuzzy inputs and output

For the case of two inputs and one output, the rule base was constructed by creating a matrix of options and solutions. The matrix has the input variable along the top side (see Table 3.4). The entries in the matrix are the desired response of the system, the changes in either throttle or CCV gain.

FUZZY LOGIC CONTROL OF COMPRESSOR SURGE IN A TURBOJET ENGINE MODEL

$\Delta\Psi$			
Small	Small	Small/Medium	Small/Large
Medium	Small/Medium	Medium	Medium/Large
Large	Small/Large	Medium/Large	Large
	$\Delta\gamma_v$ and $\Delta\gamma_T$		

Table 3.4: Rule base matrix for two-input / one-output system

From Table 3.4 the following 3-rule base was created (one for each entry along the diagonal):

IF ($\Delta\Psi$ is SMALL) OR ($\Delta\Phi$ is SMALL) THEN ($\Delta\gamma_v$ AND $\Delta\gamma_T$ is SMALL)

IF ($\Delta\Psi$ is MEDIUM) OR ($\Delta\Phi$ is MEDIUM) THEN ($\Delta\gamma_v$ AND $\Delta\gamma_T$ is MEDIUM) **3.31**

IF ($\Delta\Psi$ is LARGE) OR ($\Delta\Phi$ is LARGE) THEN ($\Delta\gamma_v$ AND $\Delta\gamma_T$ is LARGE)

The non-linear control surface created by this rule base is depicted in Figure 3.24.

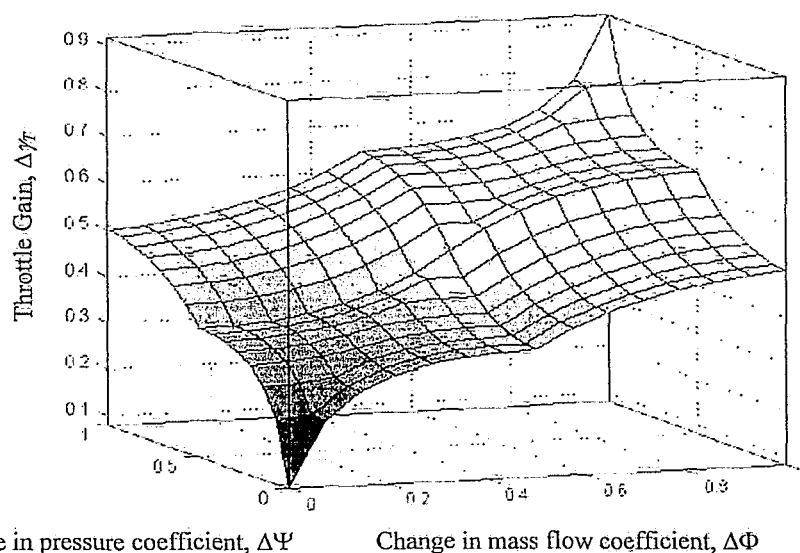


Figure 3.24: Three-dimensional control surface for MG surge detection model

CHAPTER 4

SIMULATION RESULTS

In this chapter, the proposed controllers from the previous chapter are simulated. Results for active stall and surge control are shown using the turbojet model. Detection and avoidance surge control is shown using the Moore-Greitzer model and the modified Moore-Greitzer CCV model.

4.1 IGV AND STATOR BLADE ANGLE CONTROLLERS

The simulations in this section alter the IGV exit blade angle and/or the stator turn angle or the stator stagger angle. The compressor variable geometry is illustrated in Figure 4.1. The axial velocity entering the engine is subsonic, and thus a subsonic diffuser inlet is used. No afterburner is present. The numerical values used in the following simulations are summarized in Table 4.1.

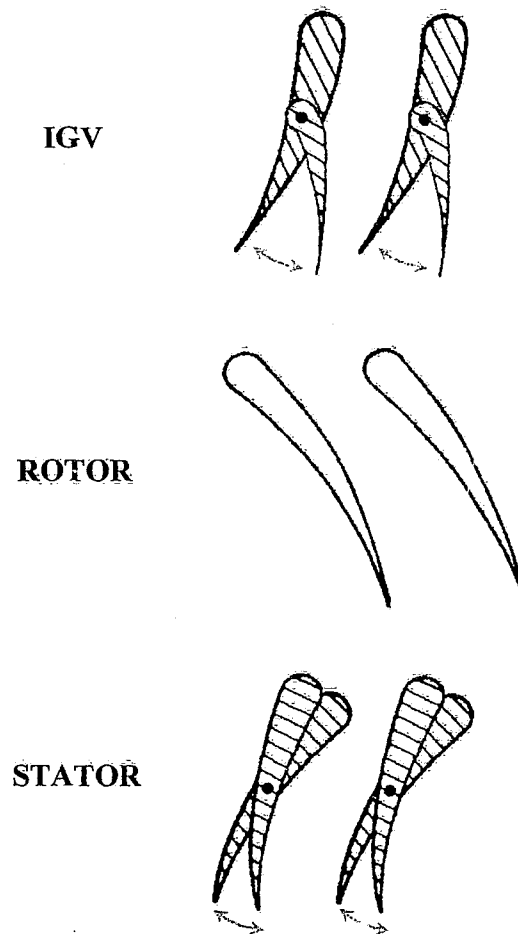


Figure 4.1: IGV and stator blade variable geometry

4.1.1 ADJUSTABLE IGV TO OPERATE AT DESIGN INCIDENCE ANGLE

Figure 4.2 shows the convergence of the actual rotor blade incidence angle with the design incidence angle, and Figure 4.3 shows the corresponding change in the IGV angle. When the error term is very large, the control will move the IGV the maximum amount per time step until the error is within approximately one degree, whereupon the control

SIMULATION RESULTS

will slow up and gently nudge the IGV into the final position. This method results in a smooth transition, with zero overshoot.

Variable	Value
Altitude, h	0 m
Axial velocity, v	180 m/s
Diffuser entrance radius, $r_{d,ent}$	0.62 m
Diffuser exit radius, $r_{d,exit}$	0.64 m
Diffuser length, L_d	0.8 m
Ratio of specific heats in diffuser, k_d	1.4
Gas constant for air in diffuser, R_d	287 J/kg · K
Intake efficiency, η_d	90 %
IGV initial position, β_{IGV_0}	0°
Rotor speed, N	8000 rpm
Ratio of specific heats in compressor, k_c	1.4
Gas constant for air in compressor, R_c	287 J/kg · K
Rotor blade angle at inlet, $\beta_{r,in}$	-53°
Rotor blade angle at outlet, $\beta_{r,out}$	-38°
Stator blade angle at inlet, $\beta_{s,in}$	50°
Stator blade angle at outlet, $\beta_{s,out}$	35°
Thickness-to-chord ratio, t_b / c	0.1
Solidity, σ	1
Rotor blade tip-to-tip diameter, d_t	0.660 m
Rotor hub diameter, d_h	0.457 m
Ratio of specific heats for burner, k_b	1.4
Gas constant for air, R_b	287 J/kg · K
Gas constant for fuel-air mixture, R_{ab}	293 J/kg · K
Mass flow of fuel into burner, $\dot{m}_{f,b}$	0.0238 kg/s
Burner efficiency, η_b	95 %
Heat of reaction in burner, q_r	44×10^6 J/kg fuel

Table 4.1: Numerical values for simulations

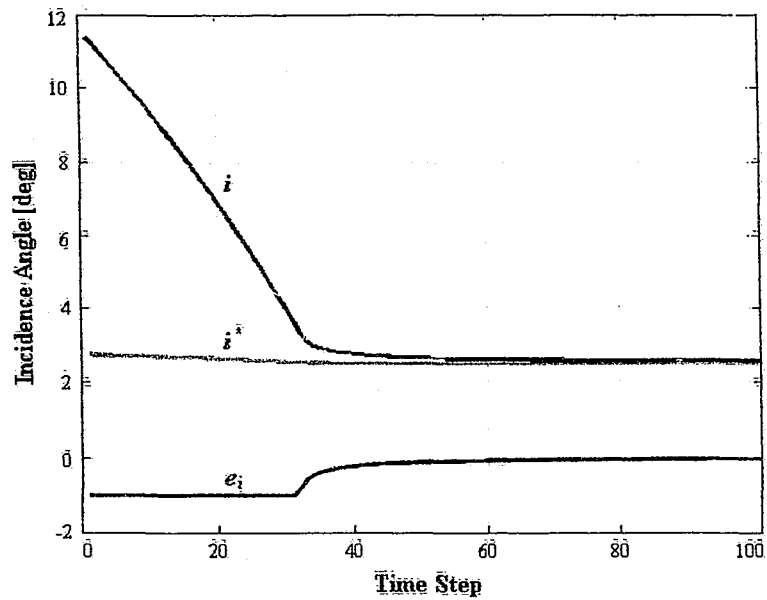


Figure 4.2: Change in rotor blade incidence angle

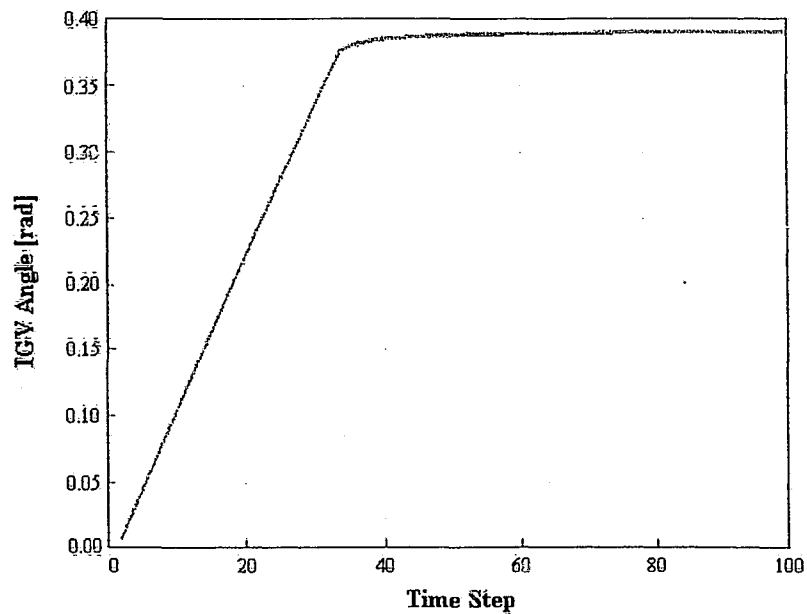


Figure 4.3: Change in IGV angle

While running, the simulation displays on screen the changes in the velocity triangles and blade angles. Figure 4.4(a) shows the velocity triangles at time zero and Figure 4.4(b) shows the velocity triangles at the simulation's end where the change in the IGV angle is

SIMULATION RESULTS

apparent. A more detailed breakdown of the turbojet engine data at the final equilibrium position is presented in Appendix A.

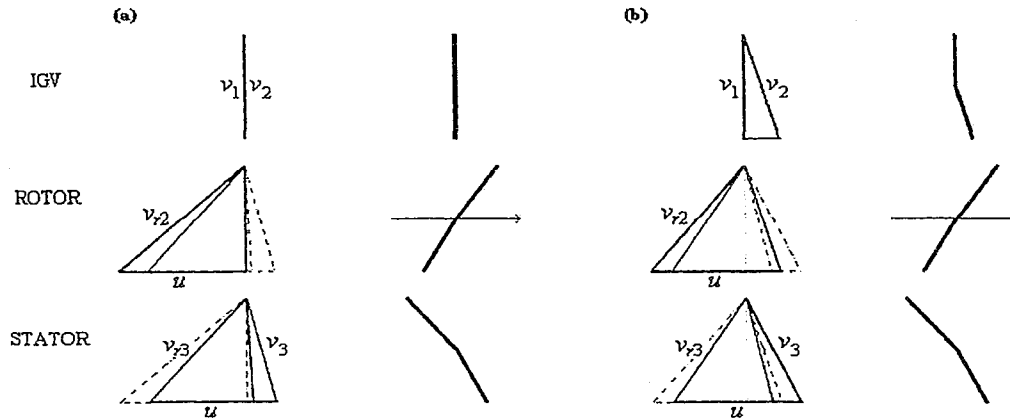


Figure 4.4: Velocity triangles and blade geometry for adjustable IGV operating at design incidence angle: (a) time zero (b) simulation end

4.1.2 ADJUSTABLE IGV TO OPERATE AT DEFINED REACTION

Figure 4.5 shows the result of a simulation run that optimizes the rate of reaction to 50% by adjusting the IGVs. The plotted velocity triangles are symmetrical, thus obtaining the defined rate of reaction goal.

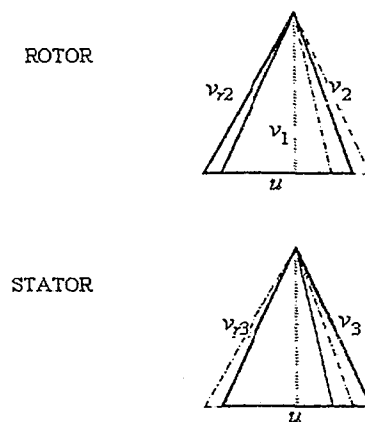


Figure 4.5: Velocity triangles for an optimized rate of reaction (50%)

4.1.3 ADJUSTABLE STATOR TO OPERATE AT DESIGN INCIDENCE ANGLE

In this example the same controller is used concurrently to control the stator stagger angle as well as the IGV angle. The resulting velocity triangles are shown in Figure 4.6.

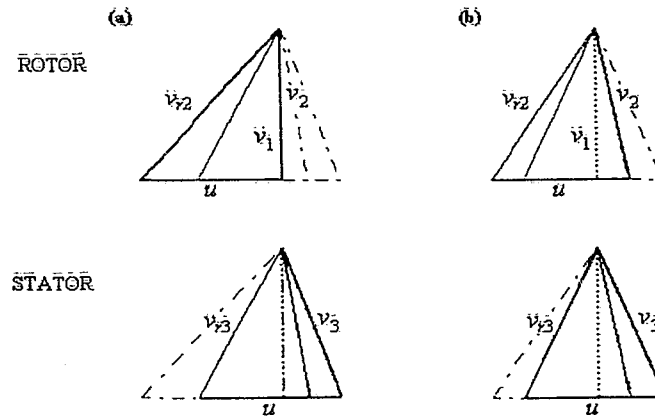


Figure 4.6: Velocity triangles and blade geometry for adjustable stator operating at design incidence angle: (a) time zero (b) simulation end

Figures 4.7 and 4.8 show the change in incidence angle as flow enters the rotor and stator blade respectively. The effect of altering the IGV to correct the rotor incidence can be seen in the flow entering the stator stage, thus creating a slight overshoot in the stator incidence error. This overshoot can be seen in Figure 4.9, which plots the actual change of the stator angle.

4.1.4 COMBINED CONTROL

In this example, the two controllers run concurrently, both the rotor blade incidence angle FLC and the defined rate of reaction FLC. Since both controllers use the IGV as an actuator there is a very low probability that both conditions can be met. Instead what results is a compromise as both conditions are partially met. Figure 4.10 shows that the rotor incidence angle error is reduced to within approximately one-third a degree and Figure 4.11 shows the degree of reaction is reduced to within 10% of the desired goal.

SIMULATION RESULTS

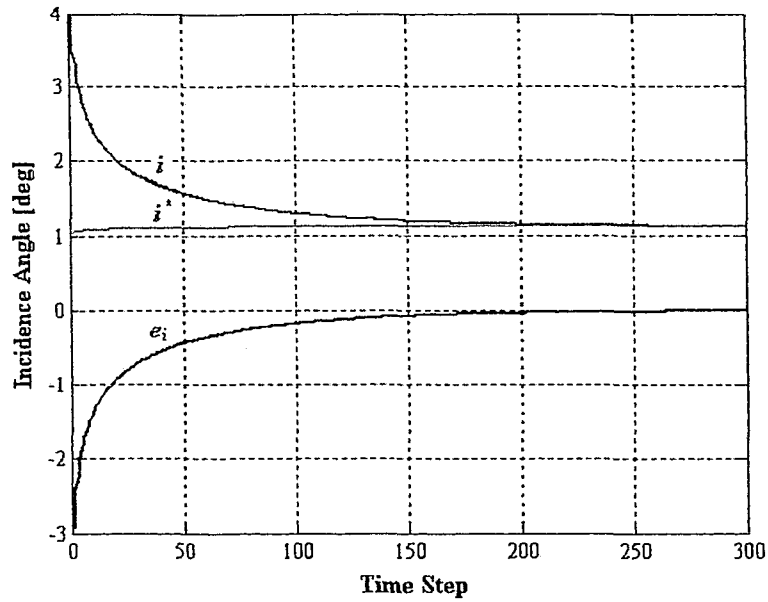


Figure 4.7: Incidence angles resulting from flow entering the rotor blades

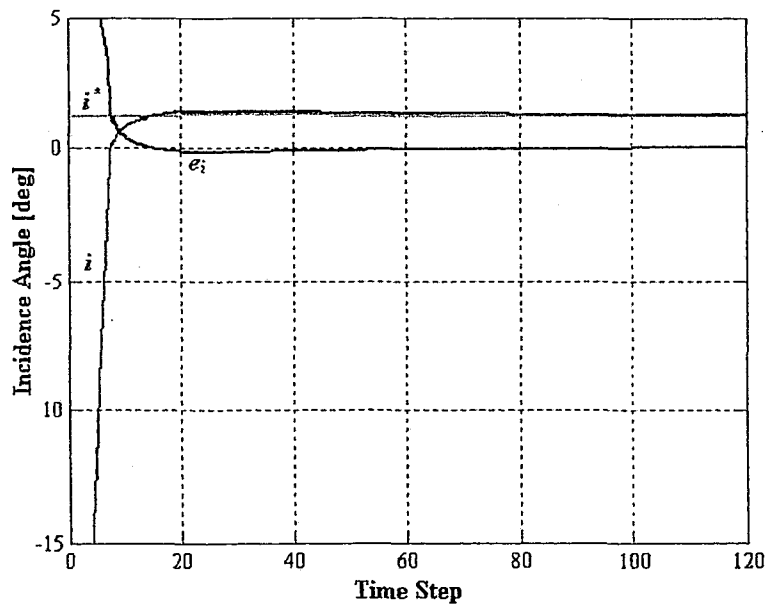


Figure 4.8: Incidence angles resulting from flow entering the stator blades

FUZZY LOGIC CONTROL OF COMPRESSOR SURGE IN A TURBOJET ENGINE MODEL

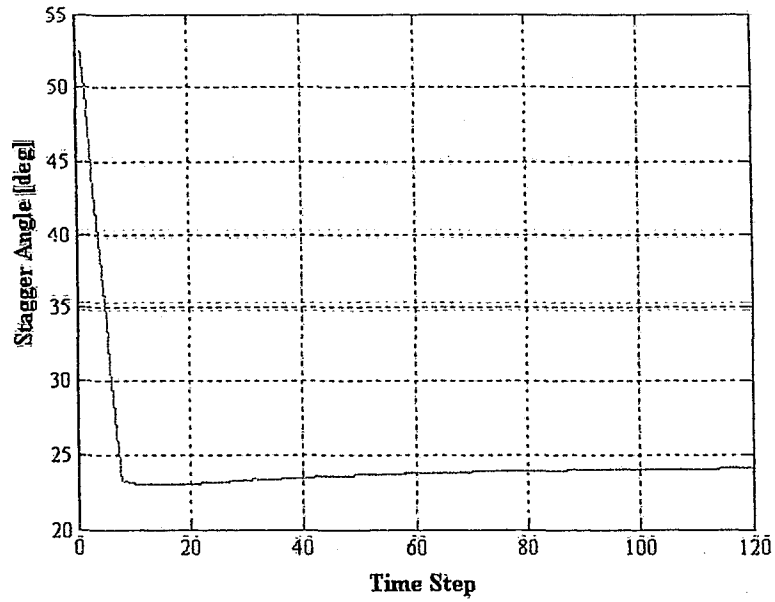


Figure 4.9: Change in stator blade stagger angle

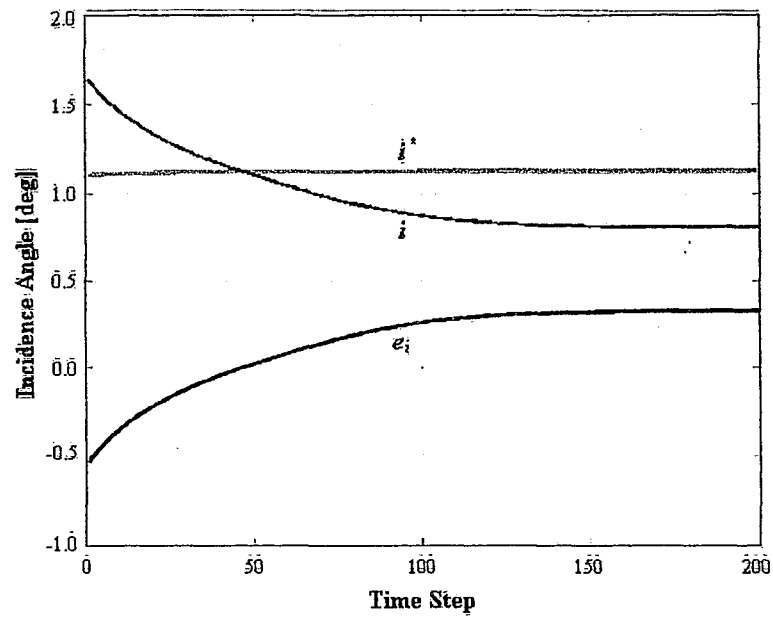


Figure 4.10: Incidence angles resulting from flow entering the rotor blades

SIMULATION RESULTS

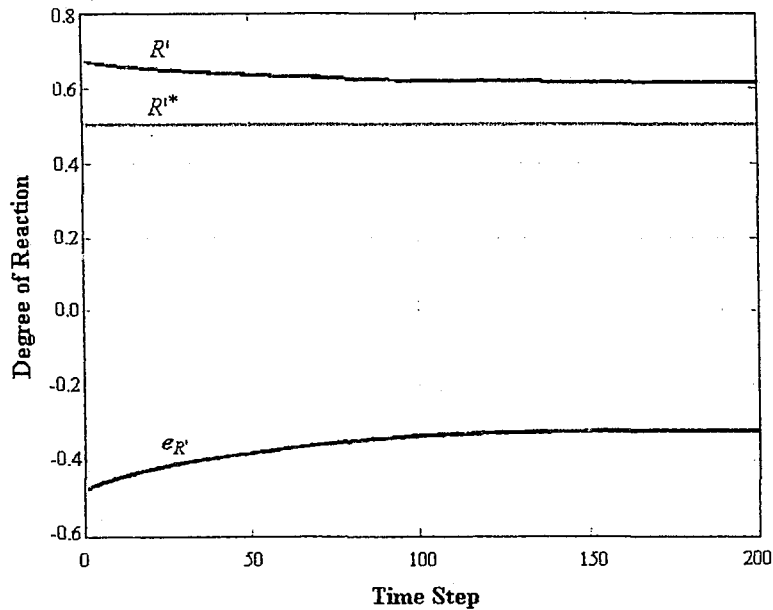


Figure 4.11: Degree of reaction

4.2 SPOOL SPEED CONTROL

The following example shows a trial run of the spool speed controller for an altitude of 10,000 m and a velocity of 200 m/s.

```

*****
Maximum Rotor Speed = 9985.39 rpm
Scale Factor = 0.697973
Rotor Speed = 6969.53 rpm
Blade Tip Speed = 240.85 m/s
Blade Mean Speed = 203.81 m/s
Mach Number = 0.697973
Max Blade Tip Speed = 345.07 m/s
*****

```

4.3 SURGE LINE CONTROLLER

The following three simulations demonstrate the controller working to maximize the performance of the compressor stage by pushing the operation limits to the defined surge margin. The first simulation shows the attempts to raise the work coefficient by adjusting the IGV. The second and third simulations show the use of variable rotor geometry to reach the desired operation point. A disturbance in the mass flow coefficient is added in

FUZZY LOGIC CONTROL OF COMPRESSOR SURGE IN A TURBOJET ENGINE MODEL

the third controller in the form of an increase in the axial flow velocity, and the corresponding adjustment to the spool speed is measured.

The simulations in this section use the same values as defined in Table 4.1, with the exception of the rotor inlet blade angle, $\beta_{r,in} = -45^\circ$, the rotor outlet blade angle, $\beta_{r,out} = -38^\circ$, and the spool speed $N = 6000 \text{ rpm}$.

4.3.1 IGV ONLY

From the results of this simulation it can be seen that adjusting the IGV alone is limited in its ability to increase the work coefficient. Figure 4.12 shows that the opposite desired behaviour occurs and the work coefficient is lowered in order to avoid stalling across the rotor blade. This controller is still deemed a success because the IGV is adjusted to avoid stall over the rotor blade while obtaining the highest available work coefficient. Figure 4.13 illustrates this point, since the incidence error over the rotor blade settles at the furthest allowable location in order to maximize the work coefficient.

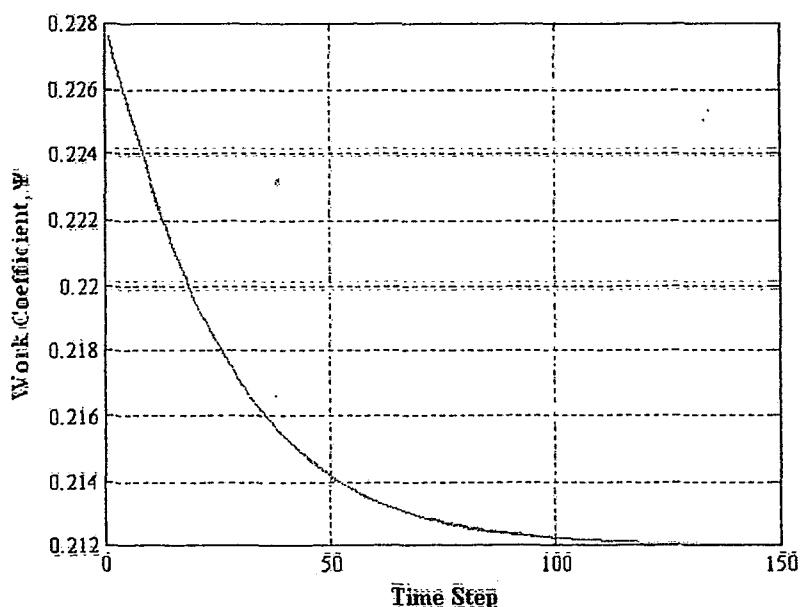


Figure 4.12: Change in work coefficient

SIMULATION RESULTS

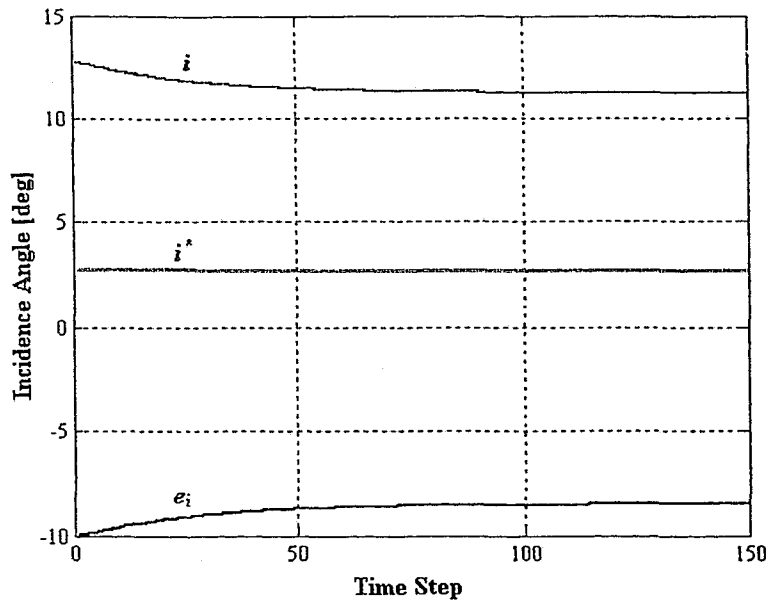


Figure 4.13: Incidence angles resulting from flow entering the rotor blades

4.3.2 IGV AND VARIABLE ROTOR GEOMETRY

This simulation tunes the rotor blade angles in order to free up the limitations that stall places on the IGVs. The change in the IGV angle is plotted in Figure 4.14. Since the system is operating at a safe distance from the surge margin, the FLC first takes care of the threat of blade stall by adjusting the rotor blade geometry and the IGV. Since the mass coefficient was held constant, the resulting system behaviour plotted against the compressor characteristic is a straight line from the starting point to the surge margin, as shown in Figure 4.15.

After the adjustment are made to avoid blade stall, the IGV finetunes the work coefficient error to a zero value as seen in Figure 4.16. Convergence of the incidence and deviation angles begins to occur around the 60th time interval as seen in Figure 4.17 and Figure 4.18 respectively. The change in velocity triangles and blade geometry is illustrated in Figure 4.19, and more detailed results from this simulation are summarized in Appendix A.

FUZZY LOGIC CONTROL OF COMPRESSOR SURGE IN A TURBOJET ENGINE MODEL

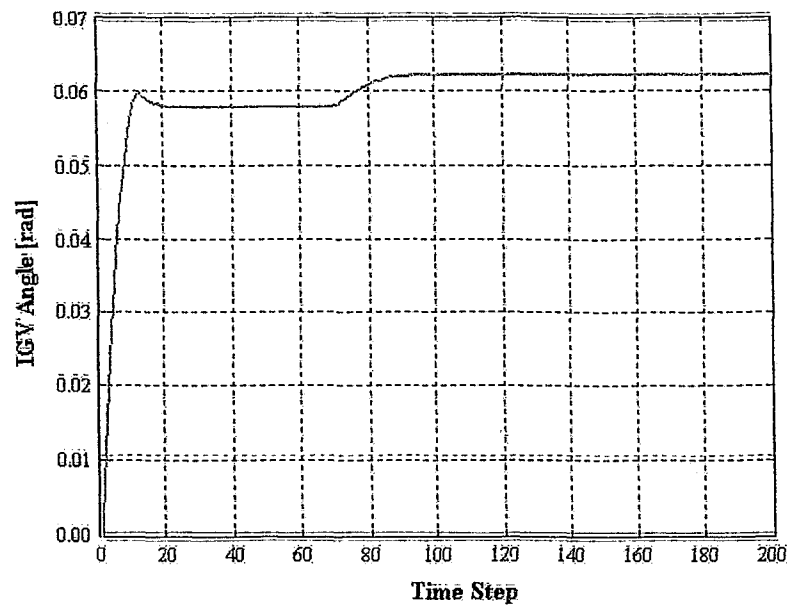


Figure 4.14: Change in IGV angle

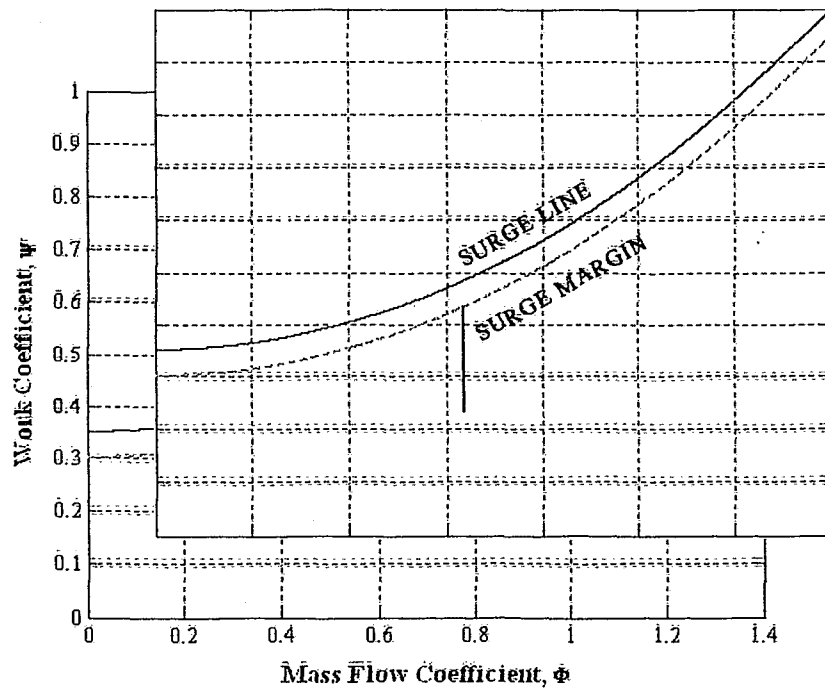


Figure 4.15: Compressor characteristic

SIMULATION RESULTS

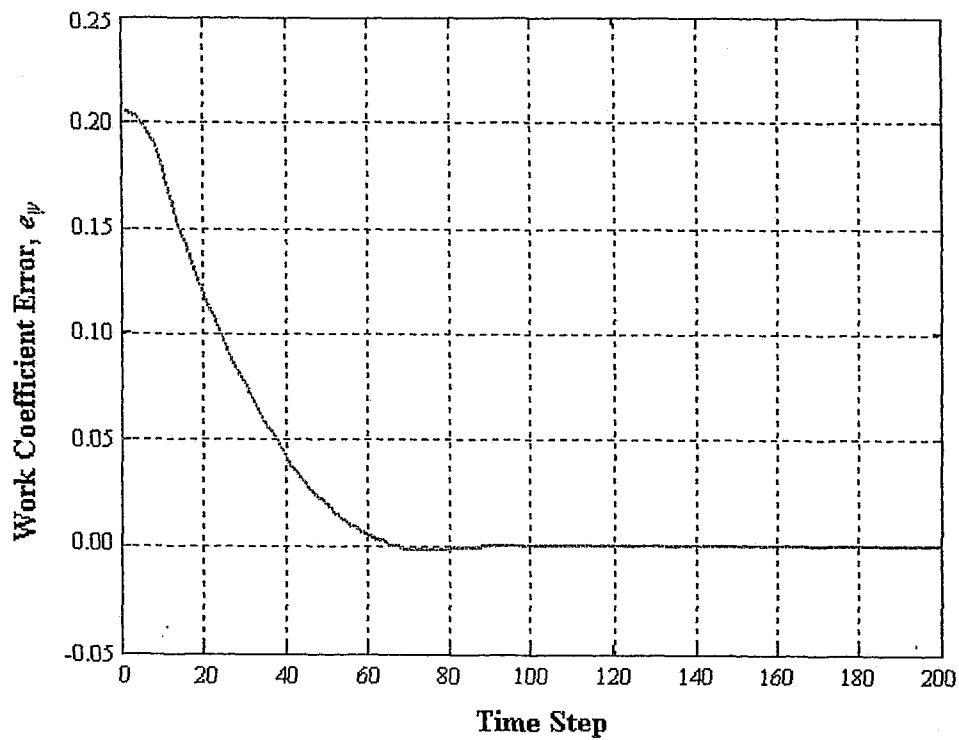


Figure 4.16: Change in work coefficient error value

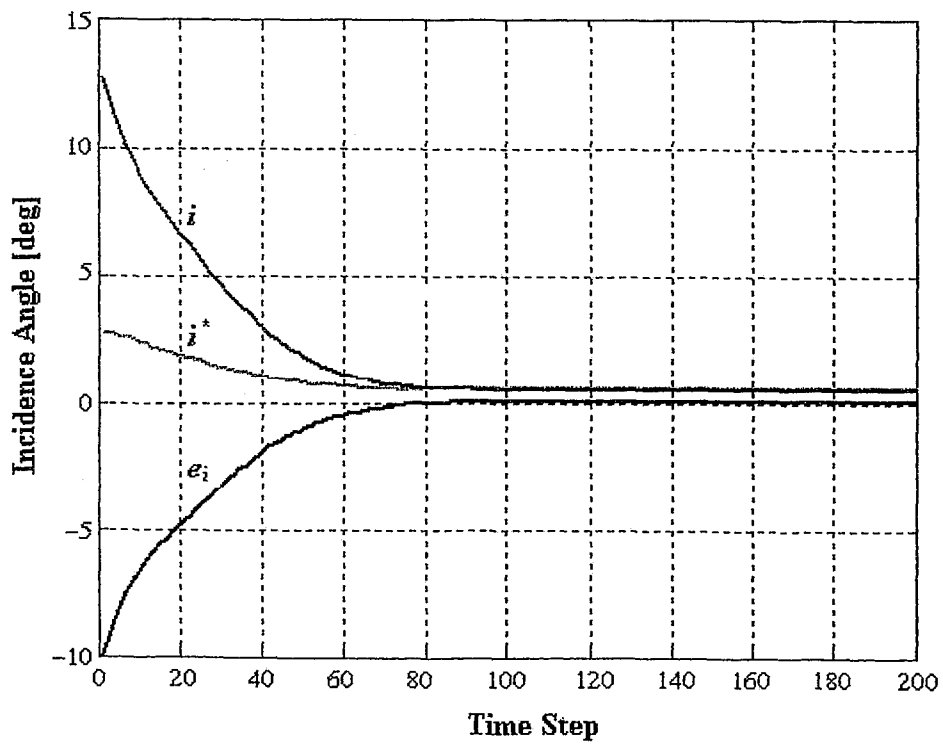


Figure 4.17: Change in incidence angle of flow entering rotor blade

FUZZY LOGIC CONTROL OF COMPRESSOR SURGE IN A TURBOJET ENGINE MODEL

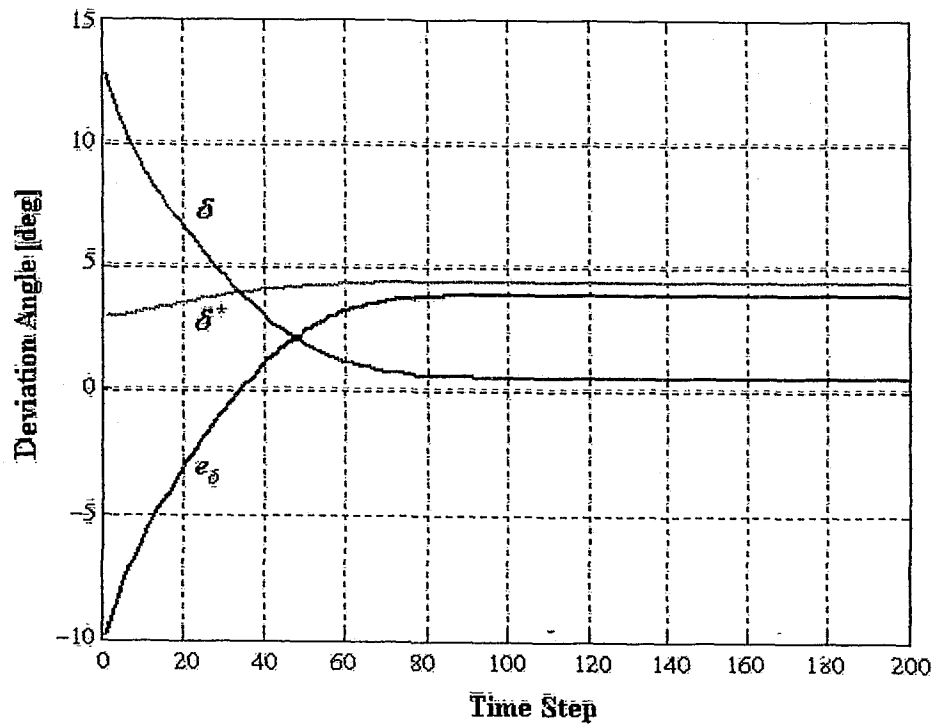


Figure 4.18: Change in deviation angle of flow leaving rotor blade

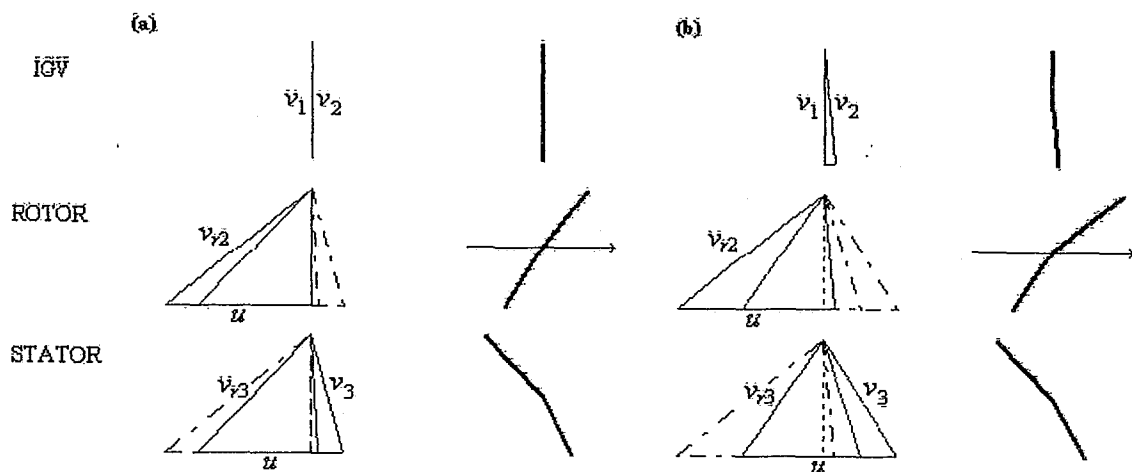


Figure 4.19: Velocity triangles and blade geometry for adjustable IGV and variable rotor geometry: (a) time zero (b) simulation end

4.3.3 IGV AND VARIABLE ROTOR GEOMETRY WITH DISTURBANCE

The same simulation from Section 4.3.2 is run but this time a disturbance occurs at the 50th time interval. The disturbance is a decrease in axial velocity which causes the

SIMULATION RESULTS

compressor to cross the surge line. The spool speed is automatically adjusted by the previously outlined controller. Figure 4.20 shows the change in the work coefficient error value, which turns negative at the 50th time step. The system's behaviour is plotted against the compressor characteristic in Figure 4.21. First the controller is pushing the compressor slowly towards the surge margin line, then after the disturbance occurs, the FLC quickly brings the system back to a safe operating point along the surge margin line.

This simulation relies on the IGV to bring the system out of the dangerous surge region. Figure 4.22 shows the plot of the IGV changing over time. Also included are the plots of the incidence and deviation angles of the rotor blade in Figure 4.23 and Figure 4.24, respectively. More details from this simulation are summarized in Appendix A.

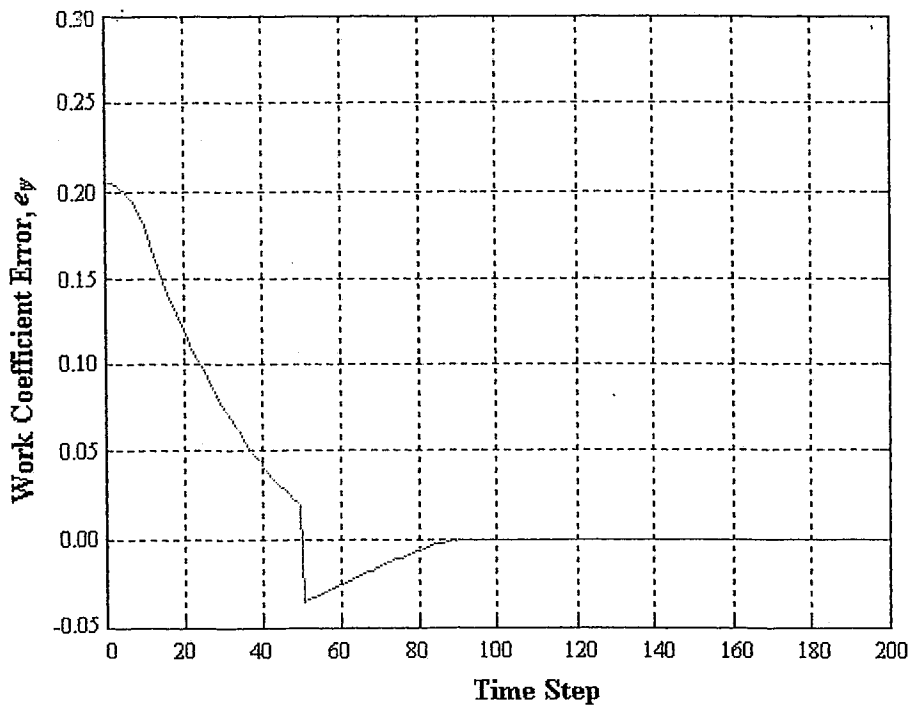


Figure 4.20: Change in work coefficient error for disturbed case

FUZZY LOGIC CONTROL OF COMPRESSOR SURGE IN A TURBOJET ENGINE MODEL

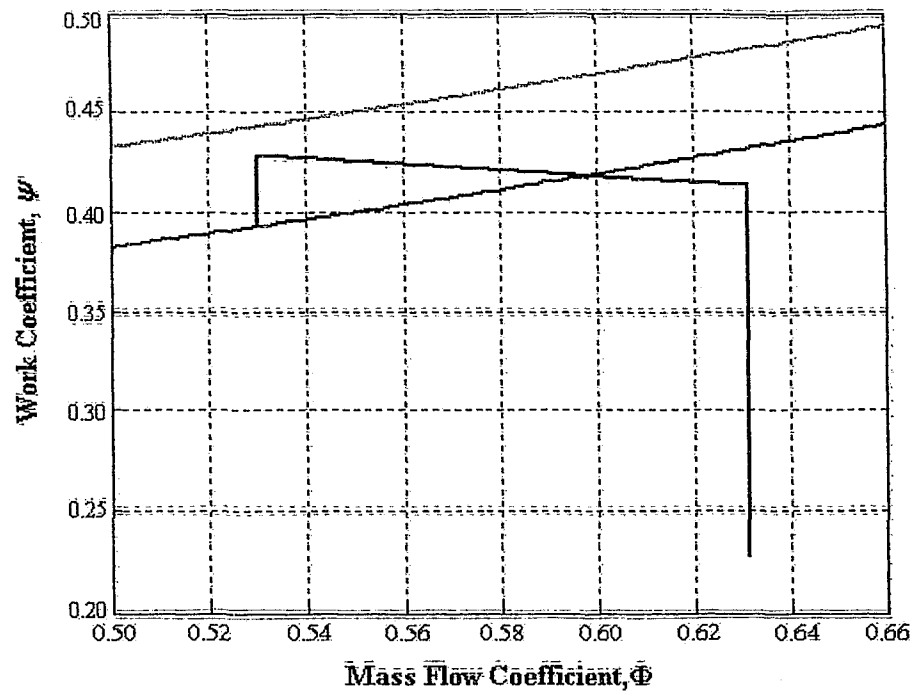


Figure 4.21: Compressor characteristic for disturbance case

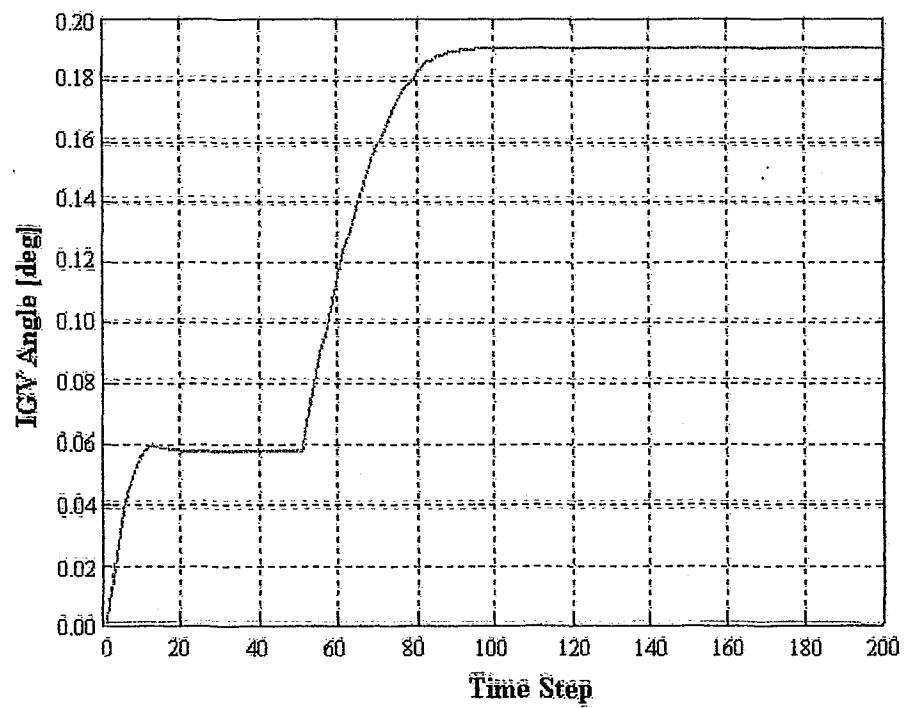


Figure 4.22: Change in IGV blade angle for disturbed case

SIMULATION RESULTS

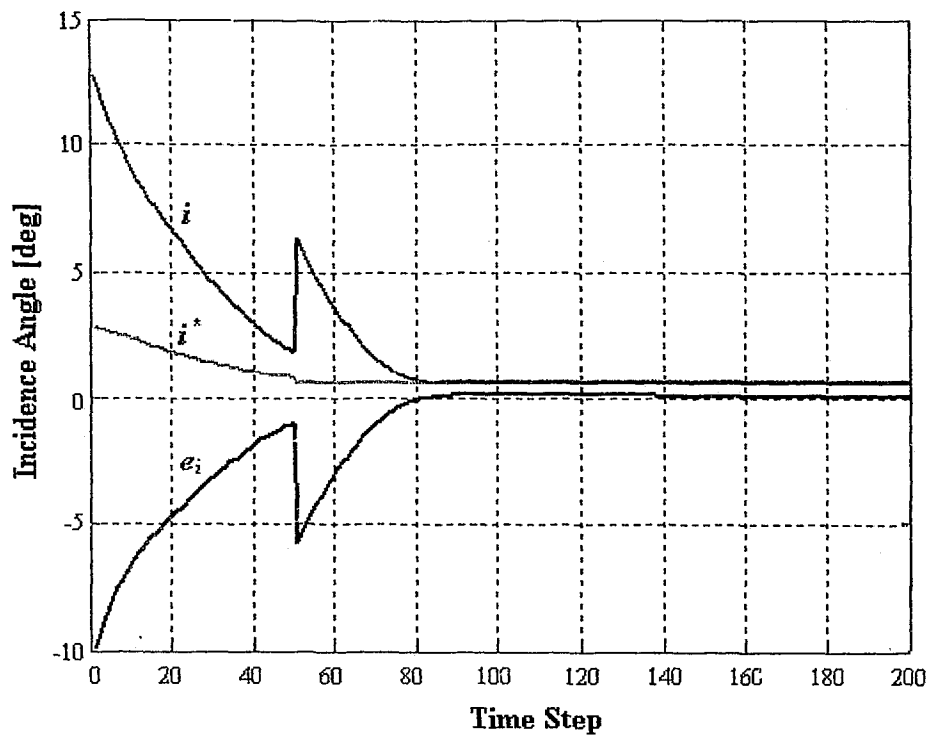


Figure 4.23: Change in rotor blade incidence angle for disturbed case

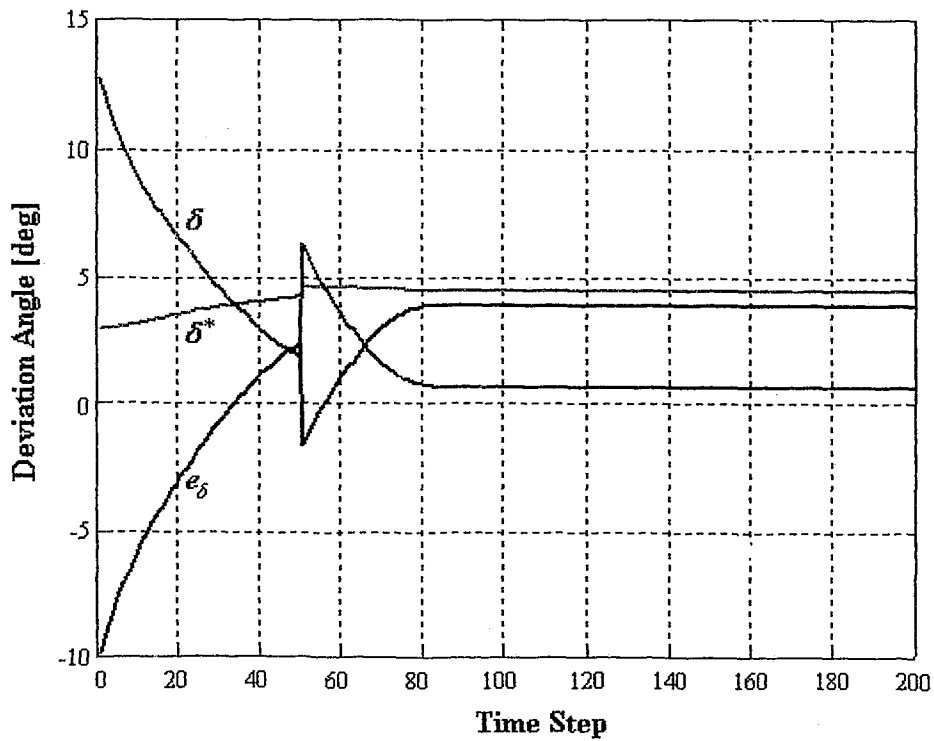


Figure 4.24: Change in rotor blade deviation angle for disturbed case

4.4 DETECTION/AVOIDANCE CONTROLLER

The results of two simulations are presented in this section. The first is the MG model without a CCV, and the second simulation is the MG model with the CCV. For both simulations the value of \bar{J} , the squared amplitude of rotating stall, has been set to zero. The Greitzer parameter $B = 1.8$, and the throttle gain has been set so that the intersection of the throttle line and the compressor characteristic is located on the part of the characteristic that has a positive slope, resulting in an unstable equilibrium (pure surge). The numerical values used in the simulations are listed in Table 4.2. Figure 4.25 shows the response of the system before the controller was switched on and after the controller was switched on at time $\xi \equiv 1000$. Before the controller was switched on, the mass flow and the pressure coefficients are fluctuating with a regular period and amplitude, and thus the system is surging.

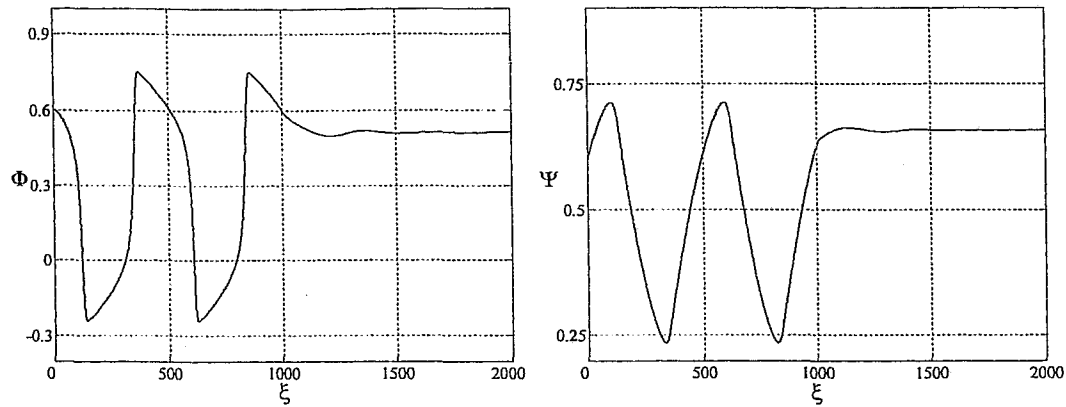
Both simulations pushed the design point along the compressor characteristic until it reaches a stable operation point without overshooting a stable equilibrium point. An overshoot of the equilibrium point would result in a pressure loss across the throttle or CCV. The gains are tuned back down towards the initial stable operation point in the case of overshoot. The optimal operating position is where the throttle characteristic intersects the compressor or equivalent compressor characteristic at a position just right of the maximum value of the compressor characteristic (slope of compressor characteristic is negative).

Figure 4.26 is a plot of the compressor and throttle characteristics in the first simulation. Initially the throttle gain was set to 0.41 which causes the plot of the throttle characteristic to cross into the unstable region of the compressor characteristic. The FLC has tuned the throttle gain up to the value of 0.63 which places the intersection point to the right of the maximum value of the compressor characteristic. The surge cycle is also plotted in Figure 4.26. The cycle begins at the intersection of the initial throttle characteristic and the compressor characteristic where the flow becomes unstable. It then jumps to the reverse flow characteristic on the negative side of the flow axis causing the mass flow to flow in the reverse direction. The cycle then jumps back to the compressor

SIMULATION RESULTS

characteristic until it reaches once again the unstable operation point. This cycle continues until the FLC pulls the operation point back to a stable position.

Case 1: Without CCV



Case 2: With CCV

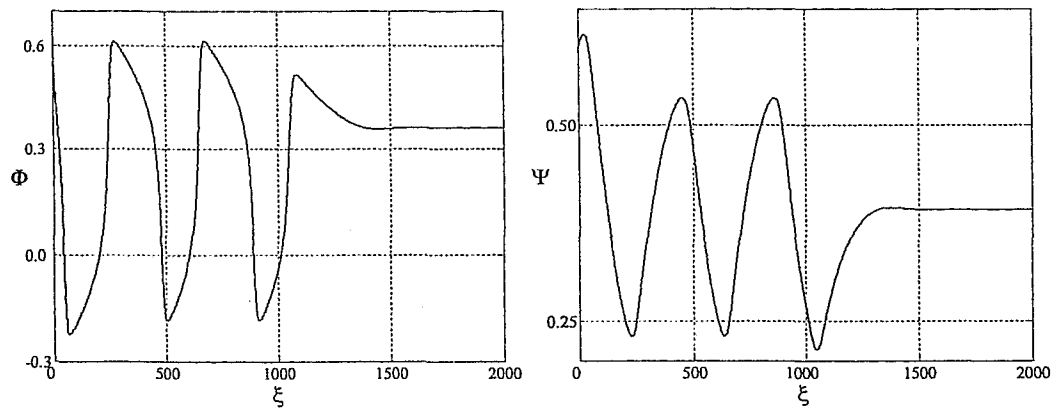


Figure 4.25: Response (controller turned on at $\xi = 1000$)

FUZZY LOGIC CONTROL OF COMPRESSOR SURGE IN A TURBOJET ENGINE MODEL

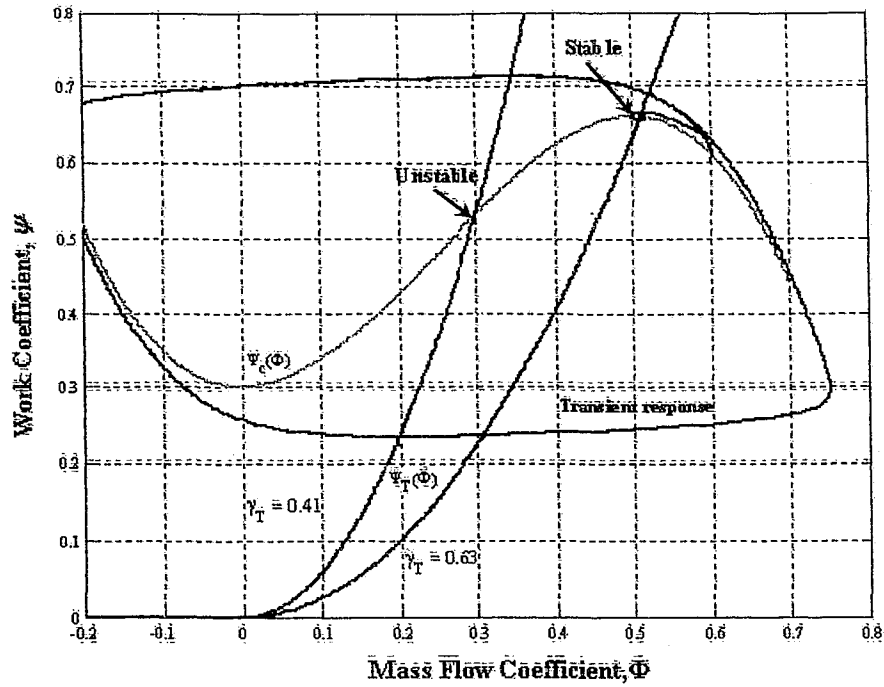


Figure 4.26: Compressor and throttle characteristics for Simulation 1 (no CCV)

Parameter	Value
Flow area, A_c	0.01 m^2
Speed of sound, a_s	340 m/s
Compressor characteristic semi height, H	0.18
Length of ducts and compressor, L_C	3 m
Length of exit duct, L_E	0.8 m
Length of inlet duct, L_I	0.2 m
Compressor duct flow parameter, m	1.75
Mean compressor radius, R	0.1 m
Tangential rotor speed, U	173.5 rps
Plenum volume, V_P	1.5 m^3
Compressor characteristic semi width, \bar{W}	0.25
Shut-off value of characteristic, ψ_{co}	0.3
Initial value axial mass flow coefficient, Φ_0	0.6
Initial value pressure coefficient Ψ_0	0.6

Table 4.2: Numerical values used in simulations

CHAPTER 5

CONCLUSIONS

This chapter outlines the contributions, and offers concluding remarks on the success of fuzzy logic towards surge detection and avoidance control, and active surge control. Future work that can be spring boarded by this thesis is outlined.

5.1 SUMMARY OF CONTRIBUTIONS

A fuzzy logic controller was developed for active surge and stall control of a compressor in a turbojet engine model with the objective of allowing the compressor to operate at close proximity to the stall line, in order to increase compressor performance. A turbojet engine model was created in MATLAB using velocity triangles to approximate the flow through the compressor. The actuator surfaces used in the controller are the inlet guide vanes, movable stator blades, and variable spool speed, and for design purposes, in the simulation, the rotor blade geometry is also variable.

Also, the stability and control of the Moore-Greitzer model, and Grävdahl and Egeland's close coupled valve active controller are examined. The MG model and the modified MG model are used as black boxes to create a surge detection and avoidance fuzzy logic controller that does not require a surge line. The controller responds to the fluctuations in the axial mass flow coefficient and the pressure coefficient across the compressor system, and adjusts the throttle characteristic or the close coupled valve characteristic in order to obtain a stable operation point.

The controllers make use of nonsymmetrical membership functions in order to create nonlinear and continuous control surfaces for usage at all operating conditions. The ease with which fuzzy logic can be adapted to these problems is demonstrated through the ability to allow one or more control surfaces to be simultaneously controlled by one or multiple inputs is established.

5.2 CONCLUSIONS

The main benefit of a fuzzy logic controller is the simple way in which a nonlinear and continuous control surface can be created. The instability problem of surge and rotating stall is dependent on the simulated compressor's operation point, thus requiring a controller with the ability to react differently to the various operating conditions. Most noteworthy are the following three situations: when the operation point crosses the surge margin into the surge region; when the operation point is well below the surge region; and when the operation point is just below the surge margin.

CONCLUSIONS

Section 4.3.2 illustrates a situation where the simulated compressor is working well below the surge margin. In this situation the IGV angle is primarily adjusted to ensure that stall will not occur over the stator blades with the secondary objective of raising the operation point towards the surge line. Simultaneously the rotor blade inlet angle and turn angle is altered to assure the stall will not occur across the rotor cascade, with the secondary objective of raising the operation point. Figure 4.15 shows the system's operation point, plotted against the compressor characteristic, successfully reaching then stabilizing on the surge margin with zero overshoot. Figure 4.17 and Figure 4.18 are plots of the incidence and deviation angles, respectively, across the rotor cascade. Clearly from these plots no separation will occur across the rotor blades as both error values are kept well within the $\pm 10^\circ$ range.

The same FLC that was used successfully in Section 4.1.1, to avoid stall across the stator blades, was applied in Section 4.3.2 to keep the rotor blades from stalling. An additional benefit of FLC is the ease with which controllers can be used for multiple applications, thus drastically cutting development time. Another example of controller capability is the three-dimensional control surface developed for the spool speed control in Section 3.2, which in turn was used for the detection/avoidance controller described in Section 3.6.

A decrease in axial velocity that pushes the operation point across the surge margin occurs in the simulation noted in Section 4.3.3. The plot of the work coefficient error in Figure 4.20 shows the error beginning to level off as it approaches zero before the disturbance occurs at the 50th time interval. As shown in previous simulations such as presented in Section 4.1.1 and Section 4.1.3, the rate of change of the control surface is maximized when the inputted error variable is large but will gently decrease as the error value approaches zero (see Figure 4.3). The spool speed is continuously monitored, before and after the disturbance occurs, by the control surface shown in Figure 3.13, to assure that the mass flow coefficient remains within the desired range. Figure 4.22 shows the immediate increase of the IGV angle as the simulation crosses the surge margin; again, the plot illustrates the nonlinear qualities of the FLC as the rate of change of the IGV angle lowers to zero as the work coefficient error approaches zero, hence leading to

FUZZY LOGIC CONTROL OF COMPRESSOR SURGE IN A TURBOJET ENGINE MODEL

zero overshoot. The FLCs successfully bring the simulation back to a stable operating point along the surge margin while avoiding stall over the rotor and stator blades. Therefore, this active surge control approach escalates the potential for increasing the efficiency of the compressor. Since the FLC can quickly recover from excursions into the surge region, the simulation can operate at a close proximity to the surge line.

The surge detection and avoidance approach, avoids the drawbacks of the loosely defined surge line. The MG models rely on a defined surge line; however, the FLC treats the MG models as a black box compressor models. The FLC controller is based exclusively on the fluctuations of the pressure and mass flow coefficients. The first simulation, without the CCV, begins operation at $(\Phi_0, \Psi_0) = (0.6, 0.6)$ and by adjusting the throttle gain shifts to a stable operation point of $(\Phi, \Psi) = (0.52, 0.65)$. The addition of the CCV shifts the stable operation point to the equivalent compressor characteristic. The simulation with the CCV active also starts with the initial conditions $(\Phi_0, \Psi_0) = (0.6, 0.6)$ but ends at a stable operation point $(\Phi, \Psi) = (0.32, 0.38)$. For this simulation the CCV gain and the throttle gain are adjusted to bring the system to a new operation point, at a much lower mass flow coefficient, that could not be reached in the first simulation. The addition of the CCV successfully extends the operation range of the compressor simulation. In both simulations the fuzzy logic controller successfully brings the system out of surge to a stable operation point.

Fuzzy logic control is conceptually easy to understand. The visual nature of the MFs and rule base allows for a trial and error approach that allows the user to massage the MFs in order to generate a desired control surface. The flexibility of such an approach allows for simple alterations in the controller in order to quickly adjust to the needs of various situations, without starting again from scratch.

Complex control problems were broken down into combinations of simple fuzzy logic controllers and these controllers were then layered; this approach was frequently adopted in this thesis. As well, this thesis demonstrates that fuzzy logic can model nonlinear functions of arbitrary complexity by virtue of MF adjustment. With respect to turbojet

CONCLUSIONS

engine control, via fuzzy logic the gap between the surge margin and the surge line can be closed, since both the simple velocity triangle and Moore-Greitzer models were able to rapidly recover from disturbances that pushed the system beyond the surge line. Using this detection and recovery strategy, the drawbacks of the loosely defined surge margin were avoided.

5.3 FUTURE WORK

The next step in this body of work would be to implement these controllers on a real working model. The approach of the active controllers is not limited to turbojet engines, and could be easily applied to other systems. With regards to the detection/avoidance controller, more research is required into the area of modeling pressure and mass flow sensors. The main challenge is to create a fuzzy logic controller that can decipher sensor noise from subtle pressure and mass flow fluctuations associated with surge.

As a learning tool, it would be beneficial to organize these turbojet engine modules and FLCs with a user interface that would allow students to easily witness the controllers in action.

REFERENCES

- Adomaitis (1995). Spatially Resolved Compressor Characteristics for Modeling and Control of Blade-Scale Flow Instabilities, in Proc. 1995 SPIE Int. Symp. Sensing, Actuation and Control in Aero propulsion, vol. 2492, pp. 36-36, Orlando, FL. April.
- Anderson, J.D. Jr. (1991). Fundamentals of Aerodynamics, Second Edition, McGraw Hill, United States of America.
- Archer, D. and Saarlal, M. (1996). An Introduction to Aerospace Propulsion, Prentice-Hall Inc., New Jersey.
- Aungier, R.H. (2003). Axial-Flow Compressors: A Strategy for Aerodynamic Design and Analysis, The American Society of Mechanical Engineers, New York.
- Badmus, O.O., Eveker, K.M. and Nett, C.N. (1995a). Control-Oriented High-Frequency Turbomachinery Modeling: General 1D Modeling Development, ASME J. Turbomachinery, vol. 117, no. 3. pp. 320-335, July.
- Badmus, O.O., Chowdhury, S., Eveker, K.M., Nett, C.N., and Rivera, C.J. (1995b). Simplified Approach for Control of Rotating Stall, Part 1: Theoretical Development, Part 2: Experimental Results, Journal of Propulsion and Power, 11(6), Nov.
- Bathie, W.W. (1996). Fundamentals of Gas Turbines, Second Edition, John Wiley & Sons, Inc., United States of America.
- Blumel, A.L., Hughes, E.J., and White, B.A. (1999). Design of robust fuzzy controllers for aerospace applications, 18th International Conference of the North American Fuzzy Information Processing Society, pp. 438-442, June.

REFERENCES

- Botros, K. (1994). Transient Phenomena in Compressor Stations During Surge, ASME J. Engine Gas Turbines and Power, vol. 116, no. 1, pp. 122-142, January.
- Chipperfield, A.J., Bica, B., and Fleming, P. J. (2002). Fuzzy scheduling control of a gas turbine aero-engine: A multiobjective approach, IEEE Transactions on Industrial Electronics, VOL. 49, NO. 3, pp. 536-548, June.
- Cohen. H., Rogers, G.F.C., and Saravanamutto, H.I.H. (1987). Gas Turbine Theory, 3rd Edition, Longman Scientific & Technical, John Wiley & Sons, Inc., New York.
- Cumpsty, N.A. (1989). Compressor Aerodynamics, Longman Scientific & Technical, Longman Group UK Limited, England.
- Cumpsty. N.A. (1997). Jet Propulsion: A simple guide to the aerodynamic and thermodynamic design and performance of jet engines, Cambridge Engine Technology Series, Cambridge University Press, United Kingdom.
- de Jager, B. (1995). Rotating stall and surge control: A survey, In Proceedings of the 34th IEEE Conference on Decision and Control, volume 2, pages 1857-1862, New Orleans.
- Epstein, A.H. and Ffowcs Williams, J.E., and Greitzer, E.M. (1989). Active suppression of aerodynamic instabilities in turbomachines. Journal of Propulsion and Power 5, 204-211.
- Ffowcs Williams, J.E. and Huang, X.Y. (1989). Active stabilization of compressor surge. Journal of Fluid Mechanics 204, 245-262.
- Fink, D.A, Cumpsty, N.A., and Greitzer, E.M. (1992). Surge Dynamics in a Free-Spool Centrifugal Compressor, ASME J. Turbomachinery , vol 114, no. 2, pp.321-332, April.

FUZZY LOGIC CONTROL OF COMPRESSOR SURGE IN A TURBOJET ENGINE MODEL

Fry, R.A. (1960). *The Principles and Construction of Aircraft Gas Turbines*, Sir Isaac Pitman & Sons, LTD., Great Britain.

Gravdahl, J.T. and Egeland, O. (1997a). A Moore-Greitzer axial compressor model with spool dynamics, *Proceedings of the 36th IEEE Conference on Decision and Control*, San Diego, CA, pp. 4714-4719.

Gravdahl, J.T. and Egeland, O. (1997b). Control of the three-state Moore-Greitzer compressor model using a close-coupled valve, *Proceedings of the 1997 European Control Conference*, Brussels, Belgium.

Gravdahl, J.T. (1998). *Modeling and control of surge and rotating stall in compressors*, PhD thesis, Norwegian University of Science and Technology.

Greitzer, E.M. (1976). Surge and rotating stall in axial compressors Part I: Theoretical compression system model, Part II: Experimental results and comparison theory, *ASME J. Engineering for Power*, 98(2): 191-217, April.

Greitzer, E.M. (1980). Review – Axial compression stall phenomena, *ASME J. Fluids Engineering*, 102(2): 134-151, June.

Guoxiang G., Sparks, A.G., and Siva, S. (1999). An overview of rotating stall and surge control for axial flow compressors, *IEEE*, 639-647, November.

Hansen, K.E., Jørgensen, P., and Larsen, P.S. (1981). Experimental and Theoretical Study of Surge in a Small Centrifugal Compressor, *ASME J. Fluids Eng.*, vol 103, no. 3, pp. 391-396, September.

Harman, R.T.C. (1981). *Gas Turbine Engineering: Application, cycles and characteristics*, The MacMillan Press Ltd., New York.

REFERENCES

Haynes, J.M., Hendricks, G.J., and Epstein, A.H. (1994). Active Stabilization of Rotating Stall in a Three-Stage Axial Compressor, ASME J. Turbomachinery, vol. 116, no. 2, pp. 226-239, April.

Hellendoorn, H., and Driankov, D. (1997). Fuzzy Model Identification, Springer-Verlag Berlin Heidelberg, Germany.

Hindmon, J. (1998). Fuzzy Logic: A Clear Choice for System Control, RSES Journal August.

Horlock, J.H. (1982). Axial Flow Turbines – Fluid Mechanics and Thermodynamics, Butterword and Company (Publishers) Limited, United States of America.

Lee, C.C. (1990). Fuzzy logic in control systems: Fuzzy logic controller—Parts I & II, IEEE Trans. Syst., Man, Cybern., vol. 20, pp. 404–435, March/April.

Liaw, D.C., and Abed, E.H. (1992). Stability Analysis and Control of Rotating Stall, IFAC Nonlinear Control System Design, Bordeaux, France, June.

Marks, R.J. II (1994). Fuzzy Logic Technology and Applications, IEEE Technical Activities Board, The Institute of Electrical and Electronics Engineers, INC, New York.

Mattson, Jr. H.F. (1993). Discrete Mathematics with Applications, John Wiley & Sons, Inc., United States of America.

Moore, F.K. (1984). A Theory of rotating stall of multistage axial compressors: Part I – Small disturbances & Part II – Finite Disturbances, ASME J. Engineering for Gas Turbines and Power, 106(2): 313-336, April.

Moore, F.K. and Greitzer, E.M. (1986). A theory of post-stall transients: Part I – Development of equations, ASME J. Engineering for Gas Turbines and Power, 108(1): 68-78, January.

FUZZY LOGIC CONTROL OF COMPRESSOR SURGE IN A TURBOJET ENGINE MODEL

Moran, M.J. and Shapiro, H.N. (1996). Fundamentals of Engineering Thermodynamics, 3rd Edition, John Wiley & Sons, Inc., United States of America.

Simon, J.S. and Valavani, L. (1991). A Lyapunov based nonlinear control scheme for stabilizing a basic compression system using a close-coupled control valve. In: Proceedings of the 1991 American Control Conference. pp. 2398-2406.

Simon, J.S. (1993). Feedback stabilization of compression systems. PhD thesis. MIT.

Spang, H.A. III and Brown, H. (1999). Control of jet engines, Control Engineering Practice 7, pp. 1043-1059, March.

Swaminathan, R., Prasad, J. V. R., Neumeier, Y., and Lal, L. (1997). Combined rule-based model-based control of compression system rotating stall, AIAA Paper 97-2659, July.

Tanaka, Y. (1997). An Overview of Fuzzy Logic, Togai Infra Logic, Inc, Irvine, CA.

Treager, I.E. (1979). Aircraft Gas Turbine Engine Technology, 2nd Edition, McGraw-Hill Inc., United States of America.

von Altrock, C. (1997). Fuzzy logic in automotive engineering, Circuit Cellar INK, The computer application journal, Issue 88, November.

White, F.M. (1999). Fluid Mechanics, Forth Edition, McGraw-Hill, United States of America.

Willems, F. and de Jager, B. (1998). Modeling and control of rotational stall and surge: Overview, In Proceedings 1998 IEEE Int. Conf. Control Applications, 331-333, Trieste, Italy, September.

Willems, F and de Jager, B. (1999) Modeling and control of compressor flow instabilities, IEEE Control Systems, 8=18, October.

APPENDIX A: ADDITIONAL SIMULATION DATA

SURGE CONTROL WITH IGV AND VARIABLE ROTOR GEOMETRY (§.4.1.1)

International Standard Atmosphere Calculations

Altitude = 0 m
Temperature = 288 K
Pressure = 101325 Pa
Speed of sound = 340.174 m/s

Subsonic Diffuser

Exit Temperature = 296.35 K
Exit Pressure = 104263 Pa
Inlet Mach Number = 0.529141
Exit Mach Number = 0.481507

Compressor with IGV Control

Exit Temperature = 309.733 K
Pressure Ratio = 1.25354
Inlet Mach Number = 0.481507
Exit Mach Number = 0.504782

Burner

Exit Stagnation Temperature = 1290.82 K
Exit Stagnation Pressure = 143324

Turbine

Exit Stagnation Temperature = 1161.07 K
Exit Stagnation Pressure = 92585.4
Exit Mach Number = 0.343684

Converging Nozzle

Nozzle is not choked
Exit Temperature = 1087.91 K
Exit Pressure = 101325 Pa
Exit Velocity = 342.161 m/s
Exit Mach Number = 0.515472
Thrust = 5107.07 N

ADJUSTABLE IGV TO OPERATE AT DESIGN INCIDENCE ANGLE (§.4.3.2)

International Standard Atmosphere Calculations

Altitude = 1000 m
Temperature = 281.499 K
Pressure = 89856.5 Pa
Speed of sound = 336.313 m/s

Subsonic Diffuser

Exit Temperature = 285.21 K
Exit Pressure = 91041.1 Pa
Inlet Mach Number = 0.356811
Exit Mach Number = 0.327214

Compressor with IGV Control

Exit Temperature = 308.327 K
Pressure Ratio = 1.35672
Inlet Mach Number = 0.327214
Exit Mach Number = 0.338921

Burner

Exit Stagnation Temperature = 1278.2 K
Exit Stagnation Pressure = 125373

Turbine

Exit Stagnation Temperature = 1220.16 K
Exit Stagnation Pressure = 103504
Exit Mach Number = 0.224061

Converging Nozzle

Nozzle is not choked
Exit Temperature = 1155 K
Exit Pressure = 89856.5 Pa
Exit Velocity = 356.662 m/s
Exit Mach Number = 0.52148
Thrust = 7352.37 N

SURGE CONTROL WITH IGV AND VARIABLE ROTOR GEOMETRY (§.4.3.3)

International Standard Atmosphere Calculations

Altitude = 1000 m
Temperature = 281.499 K
Pressure = 89856.5 Pa
Speed of sound = 336.313 m/s

Subsonic Diffuser

Exit Temperature = 285.21 K
Exit Pressure = 91041.1 Pa
Inlet Mach Number = 0.356811
Exit Mach Number = 0.327214

Compressor with IGV Control

Exit Temperature = 309.095 K
Pressure Ratio = 1.38482
Inlet Mach Number = 0.327214
Exit Mach Number = 0.324002

Burner

Exit Stagnation Temperature = 1278.89 K
Exit Stagnation Pressure = 127969

Turbine

Exit Stagnation Temperature = 1221.3 K
Exit Stagnation Pressure = 105820
Exit Mach Number = 0.1978

Converging Nozzle

Nozzle is not choked
Exit Temperature = 1158.02 K
Exit Pressure = 89856.5 Pa
Exit Velocity = 357.799 m/s
Exit Mach Number = 0.52246
Thrust = 7387.29 N

APPENDIX B: ACTIVE CONTROL SIMULATION CODE

Main.m

```
% *****
% This file is what the user calls to run the simulation. The user-defined variables are defined in
% this module, as well the user can select an inlet, an outlet and the option of an afterburner.
%
% Programmed by Mark Laderman, Ryerson University, 2004
% *****

clear all;

v = 120;           % initial axial velocity thru the engine [m/s]
h = 1000;          % initial altitude of the aircraft [m]
N = 6000;          % initial rotor rotation speed [rpm]

% *****
% INTAKE VARIABLES
% *****

Oblique1 = 20*pi/180; % initial deflection angle of inlet spike [rad]

% Diffuser variables
Diff_Area_in = 1.2;   % initial diffuser intake area [m^2]
Diff_Area_out = 1.3; % initial diffuser exit area [m^2]
Diff_Length = 0.8;    % initial length of diffuser [m]

k_i = 1.4;           % ratio of specific heats
R_i = 287;           % gas constant for air [J/kg*K]
eff_i = 0.90;         % Intake efficiency

% subsonic flight – subsonic_flag = 0
subsonic_flag = 0;    % toggle for output formatting

% super sonic flight – subsonic_flag = 1
subsonic_flag = 1;    % toggle for output formatting

% *****
% COMPRESSOR VARIABLES (for blade sign conventions see Figure 2.4)
% *****

k_c = 1.4;           % ratio of specific heat for air
R_c = 287;           % gas constant for air [J/kg*K]
cp_c = k_c/(k_c-1)*R_c; % specific heat for compressor

Bigv(1) = 0;         % IGV initial value

% *****
% Rotor Blade - Stage 1 (NACA 65-series)
% *****

% rotor blade angles and rotor spool speed to start simulation in surge
% B_ril = -56.6686;   % rotor inlet metal angle [deg]
% B_ror = -39.9249;   % rotor outlet metal angle [deg]
% N = 6.2878e+003;

B_ril = -45;          % rotor inlet metal angle [deg]
B_ror = -38;          % rotor outlet metal angle [deg]
```

Main.m

```

theta_r1 = B_ro1 - B_ril; % rotor camber (turn) angle [deg]
tbc_r1 = 0.1; % rotor thickness-to-chord ratio, tb/c
ae_r1 = 0.5; % rotor location of maximum camber-to-chord ratio, a/c
sigma_r1 = 1.0; % rotor solidity - chord-to-blade pitch ratio, c/s

td_r1 = 0.660; % rotor blade tip-to-tip diameter [m]
hd_r1 = 0.457; % rotor hub diameter [m]

Ksh_r1 = 1; % rotor blade shape parameter

% rotor design incidence angle thickness correction factor, Kt,i
Kti_r1 = (10*tbc_r1)^(0.28/(0.1+tbc_r1^0.3));

% rotor design deviation angle thickness correction factor, kt,d
Ktd_r1 = 6.25*(tbc_r1) + 37.5*(tbc_r1)^2;

% *****
% Stator Blade - Stage 1 (NACA 65-series)
% *****

B_si1 = 50; % stator inlet metal angle [deg]
B_so1 = 35; % stator outlet metal angle [deg]

stag_s1(1) = B_si1 - (theta_s1/2); % Stator stagger angle (deg)

theta_s1 = B_si1 - B_so1; % stator camber (turn) angle [deg]
tbc_s1 = 0.1; % stator thickness-to-chord ratio, tb/c
ae_s1 = 0.5; % stator location of maximum camber-to-chord ratio, a/c
sigma_s1 = 1.0; % stator solidity - chord-to-blade pitch ratio, c/s

Ksh_s1 = 1; % stator blade shape parameter

% stator design incidence angle thickness correction factor, Kt,i
Kti_s1 = (10*tbc_s1)^(0.28/(0.1+tbc_s1^0.3));

% stator design deviation angle thickness correction factor, kt,d
Ktd_s1 = 6.25*(tbc_s1) + 37.5*(tbc_s1)^2;

% *****
% BURNER VARIABLES
% *****

R_b = 287; % gas constant for air [J/kg*K]
k_b = 1.4; % ratio of specific heat for air
cp_b = k_b/(k_b-1)*R_b; % specific heat for burner

qr = 44E6; % heat of reaction [J/kg of fuel]
eff_b = 0.95; % burner efficiency
mass_flow_fuel = 1/42; % mass flow of fuel [kg/s]

f = mass_flow_fuel/mass_flow_air; % fuel/air ratio
cp_be = 2*cp_b-cp_c;

Tmax = 1400; % maximum temperature of burner [K]

% *****

```

Main.m

```
% *****
% TURBINE VARIABLES
% *****

R_t = 294;           % Gas constant for air [J/kgK]
k_t = 1.32;          % Ratio of specific heat for air
cp_t = k_t*R_t/(k_t-1);

% *****
% Nozzle (Stator) Blade - Stage 1
% *****

B_ni = 0;            % Nozzle inlet metal angle [deg]
B_no = 72;           % Nozzle outlet metal angle [deg]

% *****
% Rotor Blade - Stage 1
% *****

B_ri = 0;            % Rotor inlet metal angle [deg]
B_ro = -64.3521;     % Rotor outlet metal angle [deg]

Mean_blade_d = 0.483; % Mean blade diameter [m]

% *****

% *****
% AFTERBURNER VARIABLES
% *****

R_ab = 294;
k_ab = 1.32;
cp_ab = k_ab/(k_ab-1)*R_ab; % specific heat for afterburner

eff_ab = 0.95;        % afterburner efficiency
mass_flow_fuel_ab = 1/42; % mass flow of fuel [kg/s]

f_ab = mass_flow_fuel_ab/mass_flow_air; % fuel/air ratio
cp_ab = 2*cp_ab-cp_t;

% *****

% *****
% EXIT NOZZLE VARIABLES
% *****

k_n = 1.4;            % ratio of specific heat for air
R_n = 294;            % gas constant for air [J/kg*K]
cp_n = k_n/(k_n-1)*R_n;

A5_n = 0.05;          % Area of the nozzle at the inlet [m^2]
A6_n = 0.04;          % Area of the nozzle at the exit [m^2]

% *****

% Calculates the ambient conditions at the initial altitude
```

Main.m

Ambient_Conditions;

```
% user selects the desired inlet
Intake_Subsonic_Diffuser;    % subsonic diffuser
% Low_Supersonic_Intake;    % low supersonic intake with normal shock
% Supersonic_Intake_One_OS; % supersonic intake with one oblique shock

% the use selects the desired compressor control strategy
%Compressor_IGV_Only;        % IGV are controlled to avoid stall while maximizing reaction,
                             % deHallers number etc.
%Compressor_IGV_Surge;       % IGV only are used to actively control surge and stall
Compressor_IGV_Surge2;       % IGV and variable rotor geometry are used
                             % to actively control surge and stall
%Compressor_IGV_Surge2_dis;  % IGV and variable rotor geometry are used
                             % to actively control surge and stall with disturbances
```

Burner;

Turbine;

```
% user selects if simulation is run with or without an afterburner
```

```
% Afterburner_Yes;
```

```
Afterburner_No;
```

```
% user selects exit nozzle type
```

```
Converging_Nozzle;
```

```
% Con_Div_Nozzle;
```

Ambient_Conditions.m

```
% *****
% Calculates temperature [K], pressure [Pa] and speed of sound [m/s] at a user-defined altitude [m]
%
% Programmed by Mark Laderman, Ryerson University, 2004
% *****

fprintf('\n')
fprintf('*****')
fprintf('\n')
fprintf('*   International Standard Atmosphere Calculations   *')
fprintf('\n')
fprintf('*****')
fprintf('\n')

% Properties of air at standard sea level conditions
Po = 101325;           % pressure [Pa]
To = 288;              % temperature [K]
ao = 340;              % speed of sound [m/s]

k = 1.4;               % ratio of specific heats
R = 287;               % Gas constant for air [J/kg*K]

% troposphere, which extends from sea level to 11,000 m
if (h <= 11000)
    temp_ratio = 1 - (h/44300);
    T = To*temp_ratio;           % [K]
    P = Po*(temp_ratio^5.261);   % [Pa]

% lower stratosphere, which extends from 11,000 meters to 25,000 meters
elseif (h > 11000) & (h <= 25000)
    T = 216.576;                 % [K]
    P = 22.65 * exp(1.73 - .000157 * h); % [Pa]

% upper stratosphere, which extends upwards from 25,000 meters
else
    T = 141.94 + .00299 * h;      % [K]
    P = 2.488 * (T / 216.6) ^ 11.388; % [Pa]
end

% calculates the speed of sound at h [m/s]
a = sqrt(k * R * T);

% output results
fprintf('\n')
fprintf('          Altitude = %g m', h)
fprintf('\n')
fprintf('          Temperature = %g K', T)
fprintf('\n')
fprintf('          Pressure = %g Pa', P)
fprintf('\n')
fprintf('          Speed of sound = %g m/s', a)
fprintf('\n')
fprintf('*****')
fprintf('\n')
```

Intake_Subsonic_Diffuser.m

```

% *****
% Subsonic diffuser inlet to be used with flow less than Mach 1
%
% Calculates the exit temperature [K], exit pressure [Pa] and exit Mach number for flow entering
% a subsonic diffuser. If the flow entering the diffuser is > Mach 1 the simulation is halted. Flow
% separation is monitored and if separation occurs the simulation is halted.
%
% Programmed by Mark Laderman, Ryerson University, 2004
% *****

% this module is called by both supersonic inlets and thus a toggle is used to format the output;
% the following heading is printed only if the subsonic_flag = 0
if (subsonic_flag == 0)
    fprintf('\n')
    fprintf('*****')
    fprintf('\n')
    fprintf('          Subsonic Diffuser          ')
    fprintf('\n')
    fprintf('*****')
    fprintf('\n')

    % calculates inlet Mach number
    M = v/a;
end

% verifies the diffuser variables selected by the user are correct (see Figure 2.2 for diffuser geometry)
if (Diff_Area_in > Diff_Area_out)
    fprintf('Error: Subsonic diffuser inlet area is larger then outlet area. ');
    break;
end

% Checks for separation in the subsonic flow inlet duct. If separation occurs the simulation is halted.
% The upper limit on the divergence semi-angle of the duct cross-section is  $[(1-M^2)*5deg]$ 
% See Equation 2.1

% the radius of the diffuser inlet and outlet are calculated assuming a circular cross-section
ri = sqrt(Diff_Area_in)/pi;      % diffuser inlet radius [m]
re = sqrt(Diff_Area_out)/pi;     % diffuser outlet radius [m]

% checks diffuser for flow separation
if ((0.8*(atan((re-ri)/Diff_Length))) > ((1-M^2)*(5/180)*pi))
    fprintf('Error: Separation occurs in subsonic diffuser. ');
    break;      % if separation occurs simulation is halted
end

% checks Mach number of diffuser inlet flow the user is warned if the Mach number approaches sonic flow
if (M >= 1)
    fprintf('Error: Sonic flow occurs at the inlet of the subsonic diffuser.\n');
    break;
elseif (M >= 0.9)
    fprintf('Warning: Flow at subsonic diffuser inlet is approaching sonic speeds.\n');
end

% air density at inlet - Ideal Gas Law [Pa] (see Equation 2.2)
rho = P / (R_i * T);

% mass flow through diffuser (assumed constant) [kg/s] (see Equation 2.3)

```

Intake_Subsonic_Diffuser.m

```

diff_mass = rho * (M * (sqrt(k_i * R_i * T))) * Diff_Area_in;

% diffuser exit velocity [m/s] (see Equation 2.4)
v1 = diff_mass / (rho * Diff_Area_out);

% Calculate pressure at diffuser exit [Pa] - Bernoulli's Equation (see Equation 2.5)
P1 = (v^2 - v1^2) * (rho/2) + P;
T1 = (P1/P)*T; % [K] (see Equation 2.6)

% exit Mach Number
M1 = v1 / sqrt(k_i * R_i * T1);

% stagnation pressure and temperature (see Equation 2.7 and 2.8)
T01 = T*(1+((k_i-1)/2)*M^2); % [K]
P01 = P*(1 + eff_i*((T01/T) - 1))^(k_i/(k_i-1)); % [Pa]

% checks Mach number of diffuser exit flow and warns user if flow entering compressor is close to sonic
if (M1 >= 1)
    fprintf('Error: Sonic flow occurs at the exit of the subsonic diffuser.')
    break;
elseif (M1 >= 0.85)
    fprintf('Warning: Flow at subsonic diffuser exit is approaching sonic speeds.')
end

% output results
fprintf('\n')
fprintf('      Exit Temperature = %g K', T1)
fprintf('\n')
fprintf('      Exit Pressure = %g Pa', P1)
fprintf('\n')
fprintf('      Inlet Mach Number = %g ', v/a)
fprintf('\n')
if (subsonic_flag == 1)
    fprintf('      Diffuser Inlet Mach Number = %g ', M)
    fprintf('\n')
end
fprintf('      Exit Mach Number = %g ', M1)
fprintf('\n')
fprintf('\n')
fprintf('*****')
fprintf('\n')

```

Low_Supersonic_Intake.m

```
% *****
% Low supersonic pitot tube intake to be used with low supersonic flow (Mach < 1.4)
%
% Calculates the exit temperature [K], exit pressure [Pa] and exit Mach number for passing through
% a normal shock at the mouth of a subsonic diffuser. The values after the normal shock are passed
% to Intake_Subsonic_Diffuser.m to calculate the flow at the intakes exit.
%
% Programmed by Mark Laderman, Ryerson University, 2004
% *****

fprintf('\n')
fprintf('*****')
fprintf('\n')
fprintf('*           Low Supersonic Pitot Intake           *')
fprintf('\n')
fprintf('*****')
fprintf('\n')

% inlet Mach number
M = v/a;
subsonic_flag = 1;      % output format toggle see Intake_Subsonic_Diffuser.m for details

% if the Mach number is less then 1 (subsonic) no shock wave occurs intake is a subsonic diffuser
if M < 1
    Intake_Subsonic_Diffuser;

elseif M < 1.4
    if M >= 1.3
        fprintf('Warning: Flow at Low Supersonic Intake is approaching Mach Limit.')
    end

    % Normal shock occurs at inlet (See Equations 2.9, 2.10, and 2.11)
    T = T * ((1+((2*k_i)/(k_i+1)) * (M^2-1)) * ((2+(k_i-1)*(M^2))/((k_i+1)*M^2)));
    P = P * (1+(2*k_i)/(k_i+1)*(M^2-1));
    M = sqrt((1+((k_i-1)/2) * M^2) / ((k_i*M^2) - ((k_i-1)/2)));

    % Flow behind the normal shock is now subsonic and the subsonic diffuser module is called
    Subsonic_Diffuser;

% if the flow entering the diffuser is > 1.4 Mach the simulation is halted
else
    fprintf('Error: Flow at Low Supersonic Intake has surpassed Mach Limit.')
    break;
end
```

Supersonic_Intake_One_OS.m

```
% *****
% Supersonic intake with one oblique shock and one normal shock
% to be used with supersonic flow (Mach > 1.4)
%
% Calculates the exit temperature [K], exit pressure [Pa] and exit Mach number for passing through
% an oblique shock then a normal shock at the mouth of a subsonic diffuser.
% The values after the normal shock are passed to Intake_Subsonic_Diffuser.m to calculate the
% flow at the intakes exit (See Figure 2.3 for intake geometry).
%
% Programmed by Mark Laderman, Ryerson University, 2004
% *****

fprintf('\n')
fprintf('*****')
fprintf('\n')
fprintf('*      Supersonic Intake with One Oblique Shock      *')
fprintf('\n')
fprintf('*****')
fprintf('\n')

% inlet Mach number
M = v/a;
subsonic_flag = 1;      % output format toggle see Intake_Subsonic_Diffuser.m for details

if M < 1
    % Mach number is subsonic no shock wave occurs intake is a subsonic diffuser
    Intake_Subsonic_Diffuser;
else
    % Oblique Shock
    % Step Method for theta-beta-mach solution for an oblique shock wave (see Section 2.1.1.3)

    % first test that the deflection angle is <= 45.5 deg
    if Oblique1 >= (45.5*pi/180)
        fprintf('Error: Delection angle of inlet spike is to large. ');
        break;
    end

    % the Mach Angle is uses as the initial guess [rad] (see Equation 2.13)
    x = asin(1/M);

    % solves theta-beta-mach relationship at 'x = Mach Angle' (see Equation 2.12)
    A = ((M*sin(x))^2) - 1;
    B = (M^2) * (k_i + (cos(2*x))) + 2;
    a = 2*cot(x);
    b = A / B;

    fx = (a * b) - tan(Oblique1);
    found = 0;

    % finds the sign of fx at the Mach Angle
    if (fx > 0)
        sign = 1;
    elseif (fx < 0)
        sign = 0;
    else
        found = 1;
    end
end
```

Supersonic_Intake_One_OS.m

```

Beta1 = x;
end

% increases the step size
step = 0.0001;
MaxX = pi/2;

if (~found)
    while (x < MaxX)

        x = x + step;
        % Solves theta-beta-mach relationship at 'x+step'
        A = ((M*sin(x))^2) - 1;
        B = (M^2) * (k_i + (cos(2*x))) + 2;
        a = 2*cot(x);
        b = A / B;

        fx = (a * b) - tan(Oblique1);

        if (fx == 0)
            found = 1;
            Beta1 = x;
            break;
        end

        % value begins as positive - program searches for first negative
        if (sign)
            if fx < 0
                found = 1;
                Beta1 = ((x - step) + x)/2;
                break;
            end
        end

        % value begins as a negative - program searches for first positive number
        if (~sign)
            if fx > 0
                found = 1;
                Beta1 = ((x - step) + x)/2;
                break;
            end
        end
    end

    if (~found)
        fprintf('Error: Wave Angle Solver failed');
        break;
    end

    % calculates temperature and pressure behind the oblique shock (see Equations 2.14 to 2.18)
    Mn1 = M*sin(Beta1);
    Mn2 = sqrt((1+((k_i-1)/2)*Mn1^2)/((k_i*Mn1^2)-((k_i-1)/2)));
    M = Mn2/(sin(Beta1-Oblique1));

    rho_ratio = ((k_i + 1) * Mn1^2)/(2 + (k_i - 1) * Mn1^2);
    P_ratio = (1 + ((2 * k_i)/(k_i + 1)) * (Mn1^2 - 1));

```

Supersonic_Intake_One_OS.m

```

in_rho_ratio = 1/rho_ratio;

T = T * P_ratio * in_rho_ratio; % [K]
P = P * P_ratio; % [Pa]

% flow now pass through a normal shock at diffuser inlet
T = T * ((1+((2*k_i)/(k_i+1)) * (M^2-1)) * ((2+(k_i-1)*(M^2))/((k_i+1)*M^2)));
P = P * (1+(2*k_i)/(k_i+1)*(M^2-1));
M = sqrt((1+((k_i-1)/2) * M^2) / ((k_i*M^2) - ((k_i-1)/2)));

% flow is now subsonic and the subsonic diffuser module is called
subsonic_flag = 1;
Subsonic_Diffuser;
end

```

Compressor_IGV_Surge.m

```
% *****
% One compressor stage with variable inlet guide vanes
% Optional      - variable rotor geometry
%              - disturbances
%              - variable stator geometry
%              - spool speed control
%              - degree of reaction or deHaller number control
%
% Programmed by Mark Laderman, Ryerson University, 2004
% *****

fprintf('\n')
fprintf('*****')
fprintf('\n')
fprintf('*          Compressor with IGV Control          *')
fprintf('\n')
fprintf('*****')
fprintf('\n')

% check that axial velocity entering the compressor is subsonic
if M1 >= 1
    fprintf('Error: Compressor inlet velocity is sonic')
    break;
end

% for variable rotor blade geometry – stores the values of the changing rotor blade
% Rotor_In_Angle(1) = B_r1;
% Rotor_Out_Angle(1) = B_ro1;
% theta(1) = B_ro1 - B_r1;

% constants used for scaling velocity triangle plotting
X0 = 100;
Y0 = 150;
Sc = v1/40;

% loads fuzzy logic controller

% IGV control for active surge avoidance and active stall avoidance
Controller_A = readfis('igv_Surge2');

% spool speed control
%Controller_B = readfis('NSurgeControl');

% controls rotor inlet angle (also can be used for rotor outlet angle control)
Controller_C = readfis('RotorInAngle');

% adjust rotor turn angle
%Controller_D = readfis('RotorTurnAngle');

% adjusts IGV to lower error value to zero (used for controlling incidence angles, reaction, deHaller,
% deviation angle)
%Controller_E = readfis('igv_1');

% control loop (if control loop is in main program then comment out this control loop)
for j = 1 : 200
```

Compressor_IGV_Surge.m

```

% calculates rotor blade turn angle (if constant this can be removed from control loop)
theta_r1 = B_r01 - B_r11;

% Rotor local blade speed @ mid-blade [m/s]
u = (td_r1 + id_r1)*N*pi/120;

% VELOCITY TRIANGLES (see Sections 2.1.2.2, 2.1.2.3, and 2.1.2.4)

% Flow leaving the IGV at the trailing edge (assume flow leaves at blade exit angle)
v2 = v1/cos(B1gv(j));
% Stationary frame (absolute) tangential velocity
w2 = v1*tan(B1gv(j));
% Subtract the speed of the blade to determine the tangential velocity in the moving frame
vru2 = w2 - u;
% Calculate the relative velocity entering the rotor stage
vr2 = sqrt(v1^2 + vru2^2);
% Flow angle into rotor blade [deg]
Alpha2 = (atan(vru2/v1))*180/pi;
% Turns air across rotor blade [deg]
B_r1 = Alpha2 + theta_r1;

% see Section 3.3
% zero-camber design incidence angle for Rotor Blade [deg] (see Equation 3.12)
p_r1 = 0.914 + sigma_r1^3/160;
io_r1 = (((-Alpha2)^p_r1)/(5+46*exp(-2.3*sigma_r1))) - 0.1*sigma_r1^3*exp((-Alpha2)-70)/4;

% zero-camber design deviation angle for Rotor Blade [deg]
do_r1 = 0.01*sigma_r1*(-B_r1) + (0.74*(sigma_r1^1.9) + 3*sigma_r1) *
        (B_r1/90)^(1.67+1.09*sigma_r1);

% slope factors for Rotor blade, n (see Equation 3.13)
n_r1 = 0.025*sigma_r1 - 0.06 - (((-Alpha2/90)^(1+1.2*sigma_r1)) / (1.5 + 0.43*sigma_r1));
m_r1 = (0.17 - 0.0333*(-B_r1/100) + 0.333*(-B_r1/100)^2)/(sigma_r1^(0.9625 - 0.17*(-B_r1/100) -
        0.85*(-B_r1/100)^3));

% calculates design incidence angle developed from Lieblein's design incidence angle correlation [deg]
% (see Equation 3.11)
idesign_r1(j) = Ksh_r1 * Kti_r1 * io_r1 + (n_r1 * theta_r1);

% calculates design deviation angle developed from Lieblein's design incidence angle correlation [deg]
% (see Equation 3.17)
ddesign_r1(j) = Ksh_r1 * Ktd_r1 * do_r1 + (m_r1 * theta_r1);

% calculates incidence angle for Rotor blade [deg]
i_r1(j) = B_r1 - Alpha2;

% calculates the deviation angle for Rotor blade [deg]
d_r1(j) = B_r01 - B_r11;

vr3 = v1/cos(B_r1*pi/180);
vru3 = v1*tan(B_r1*pi/180);
w3 = u + vru3;

W3(j) = w3;
W2(j) = w2;
w3w2(j) = w3-w2;

```

Compressor_IGV_Surge.m

```

% flow angle into stator blade [deg]
Alpha3 = (atan(w3/v1))*180/pi;
v3 = v1/cos(Alpha3*pi/180);

% velocity exiting the stator blade [rad]
Alpha4 = (Alpha3 - theta_s1)*pi/180;
v4 = v1/cos(Alpha4);
w4 = v1 * sin(Alpha4);

% calculates Reaction (see Equation 3.21)
Reaction(j) = 0.5 * (v1/(2*u))*(tan(B_rt1*pi/180) + tan (Bigv(j)));

% calculates DeHaller Number (see Equation 3.23)
DeHaller(j) = vr3/vr2;

% calculates mass flow [kg/s] (see Equation 2.54)
mass_flow(j) = ((P1*v1*pi)/(4*R_c*T1))*(td_r1^2 - hd_r1^2);

% calculates torque [Nm] (see Equation 2.53)
Torque(j) = mass_flow(j)*((td_r1+hd_r1)/2)*(w2-w3);

% power required [J/kg] (see Equation 2.55)
power(j) = (Torque(j)*2*pi*N)/(60*mass_flow(j));

% static temperature across stage [deg C]
T015 = T1 + (v1^2)/(2*cp_c);
T02 = T015 - power(j)/cp_c;
T2(j) = T02 - (v3^2)/(2*cp_e);

% pressure ratio (see Equation 2.58)
Pr(j) = (T02/T015)^(k_e/(k_e-1));
V2 = v4;
M2 = V2/sqrt(k_c * R_c * T2(j));
Po2 = Po1*Pr(j);

% variable used for plotting graphs
count(j) = j;

% error term inputted into FLC – rotor incidence angle error
error_r1(j) = (idesign_r1(j) - i_r1(j));

% the error is bounded to be with in the range of [-10 to 10]
if error_r1(j) > 10
    error_r1(j) = 10;
end
if error_r1(j) < -10
    error_r1(j) = -10;
end

% error term inputted into FLC – rotor deviation angle error
error_d(j) = (ddesign_r1(j) - d_r1(j));

% the error is bounded to be with in the range of [-10 to 10]
if error_d(j) > 10
    error_d(j) = 10;
end
if error_d(j) < -10

```

Compressor_IGV_Surge.m

```

    error_d(j) = -10;
end

% used for surge controller
Phi(j) = v1/u;           % Mass Flow Coefficient
Psi(j) = (w3-w2)/u;      % Work Coefficient
Psi_Star(j) = ((Phi(j)^2)/3) + 0.3; % Surge Margin Line (compressor characteristic)

error_Psi(j) = Psi_Star(j) - Psi(j); % Work coefficient error used for FLC

% error is bounded between [-1 to 1]
if error_Psi(j) > 1
    error_Psi(j) = 1;
end
if error_Psi(j) < -1
    error_Psi(j) = -1;
end

%% Uncomment for spool speed control based on the ratio of the current spool speed to the maximum
%% spool speed and the current value of the work coefficient error
%% maximum allowable rotor speed [Mach]
%Mmax_U = 0.95;
%a1 = sqrt(T1*k_c*R_c);
%uu = Mmax_U*a1;
%Nmax = (uu*60)/(pi*td_r1);

%R_NMax = N/Nmax;
%% calls the FLC controller and updates the spool speed
% N = N + 100*(evalfis([Phi(j) R_NMax error_Psi(j)], Controller_B));

% *****
% DISTRUBANCE (uncomment to add disturbance)
% *****
%% add disturbances at time step 50 (rotor speed is increased and axial velocity is decreased)
%if j == 50
%    N = N + 500;
%    v1 = v1 - 10;
%end
%N_Holder(j) = N;
% *****

% calls the FLC and updated inlet guide vane blade angle [rad] based on the rotor incidence error
% and the work coefficient error
Bigv(j + 1) = Bigv(j) + ((evalfis([error_r1(j) error_Psi(j)], Controller_A))*pi/180);

% the IGV is bounded
if Bigv(j+1) < -0.5
    Bigv(j+1) = -0.5;
end

% FLC - rotor angle is adjusted based on the rotor incidence error
Rotor_In_Angle(j+1) = Rotor_In_Angle(j) + ((evalfis([error_r1(j)], Controller_C))/2);
B_r1 = Rotor_In_Angle(j+1);

% FLC - rotor outlet angle is adjusted based on the deviation error and the work coefficient error
Rotor_Out_Angle(j+1) = Rotor_Out_Angle(j) - ((evalfis([error_d(j) error_Psi(j)], Controller_A))/2);

```

Compressor_IGV_Surge.m

```

B_rot = Rotor_Out_Angle(j#1);

theta(j#1) = B_rot - B_ril;

% *****
% the following code is used to plot the velocity triangles and blade geometry
% *****

newplot

axis([0 Xo*2.5 0 Yo+Sc])
text(Xo/4, Yo=v1/(4*Sc), 'IGV', 'FontWeight','Bold', 'HorizontalAlignment', 'center')
text(Xo/4, 2*Yo/3=v1/(4*Sc), 'Rotor', 'FontWeight','Bold', 'HorizontalAlignment', 'center')
text(Xo/4, (Yo/3)=v1/(4*Sc), 'Stator', 'FontWeight','Bold', 'HorizontalAlignment', 'center')
% draw v1
line([Xo Xo], [Yo Yo-v1/Sc], 'Color', 'r', 'LineWidth', 2)
text(Xo, Yo-v1/(2*Sc), 'v_1', 'HorizontalAlignment', 'right')
line([Xo Xo], [2*Yo/3 2*Yo/3-v1/Sc], 'Color', 'm', 'LineWidth', 2, 'LineStyle', '-')
line([Xo Xo], [Yo/3 (Yo/3)-v1/Sc], 'Color', 'm', 'LineWidth', 2, 'LineStyle', '-')
% draw w3
line([Xo Xo+w3/Sc], [(2*Yo/3)-v1/Sc (2*Yo/3)-v1/Sc], 'Color', 'b', 'LineWidth', 1, 'LineStyle', '-')
% draw v2
line([Xo Xo+w2/Sc], [Yo Yo-v1/Sc], 'Color', 'r', 'LineWidth', 2)
text((2*Xo+w2/Sc)/2, Yo-v1/(2*Sc), 'v_2', 'HorizontalAlignment', 'left')
line([Xo Xo+w2/Sc], [2*Yo/3 2*Yo/3-v1/Sc], 'Color', 'r', 'LineWidth', 2)
line([Xo Xo+w2/Sc], [Yo/3 (Yo/3)-v1/Sc], 'Color', 'b', 'LineWidth', 1, 'LineStyle', '-')
% draw w2
line([Xo Xo+w2/Sc], [Yo-v1/Sc Yo-v1/Sc], 'Color', 'r', 'LineWidth', 2)
% draw u
line([Xo=Xo+w2/Sc Xo=Xo+w2/Sc-u/Sc], [2*Yo/3-v1/Sc 2*Yo/3-v1/Sc], 'Color', 'r', 'LineWidth', 2)
text((Xo=Xo+w2/Sc)-u/(2*Sc), 2*Yo/3 - (v1/Sc), 'u', 'HorizontalAlignment', 'center', 'VerticalAlignment',
'Top')
line([Xo=Xo+w2/Sc Xo=Xo+w2/Sc-u/Sc], [(Yo/3)-v1/Sc (Yo/3)-v1/Sc], 'Color', 'b', 'LineWidth', 1, 'LineStyle', '-')
% draw vr2
line([Xo=Xo+w2/Sc-u/Sc Xo], [2*Yo/3-v1/Sc 2*Yo/3], 'Color', 'r', 'LineWidth', 2)
text((Xo+w2/Sc-u/Sc+Xo)/2, 2*Yo/3-v1/(2*Sc), 'v_r_2', 'HorizontalAlignment', 'right')
line([Xo=Xo+w2/Sc-u/Sc Xo], [(Yo/3)-v1/Sc Yo/3], 'Color', 'b', 'LineWidth', 1, 'LineStyle', '-')
% draw vr3
line([Xo Xo+vru3/Sc], [2*Yo/3 2*Yo/3-v1/Sc], 'Color', 'm', 'LineWidth', 2)
line([Xo Xo+vru3/Sc], [(Yo/3) (Yo/3)=v1/Sc], 'Color', 'r', 'LineWidth', 2)
text((Xo+Xo+vru3/Sc)/2, (Yo/3)=v1/(2*Sc), 'v_r_3', 'HorizontalAlignment', 'right')
% draw v3
line([Xo Xo+w3/Sc], [2*Yo/3 (2*Yo/3)=v1/Sc], 'Color', 'b', 'LineWidth', 1, 'LineStyle', '-')
line([Xo Xo+w3/Sc], [Yo/3 (Yo/3)=v1/Sc], 'Color', 'r', 'LineWidth', 2)
text((Xo+Xo+w3/Sc)/2, (Yo/3)-v1/(2*Sc), 'v_3', 'HorizontalAlignment', 'left')
% draw v4
line([Xo Xo+w4/Sc], [(2*Yo/3) (2*Yo/3)-v1/Sc], 'Color', 'b', 'LineWidth', 1, 'LineStyle', '-')
line([Xo Xo+w4/Sc], [(Yo/3) (Yo/3)-v1/Sc], 'Color', 'm', 'LineWidth', 2)
text((Xo+Xo+w4/Sc)/2, (Yo/3)-v1/(2*Sc), 'v_4', 'HorizontalAlignment', 'left')
% draw u
line([Xo+vru3/Sc Xo+vru3/Sc+u/Sc], [(Yo/3)-v1/Sc (Yo/3)-v1/Sc], 'Color', 'r', 'LineWidth', 2)
text((Xo+vru3/Sc+u/(2*Sc)), (Yo/3) - (v1/Sc), 'u', 'HorizontalAlignment', 'center', 'VerticalAlignment',
'Top')

% plot blades
% IGV
line([2*Xo 2*Xo], [Yo Yo-(v1/Sc)/2], 'Color', 'k', 'LineWidth', 3)

```

Compressor_IGV_Surge.m

```

line([2*Xo 2*Xo + (w2/Sc)/2], [Yo-(v1/Sc)/2 Yo-(v1/Sc)], 'Color','k', 'LineWidth',3)
% Rotor
line([2*Xo - (u/(2*Sc)) 2*Xo + (u/(2*Sc))], [2*Yo/3-(v1/Sc)/2 2*Yo/3-(v1/Sc)/2], 'Color','r',
'LineWidth',1)
line([2*Xo + (u/(2*Sc)) 2*Xo + (u/(2*Sc))-(Sc/3)], [2*Yo/3-(v1/Sc)/2 2*Yo/3-(v1/Sc)/2+(Sc/3)],
'Color','r', 'LineWidth',1)
line([2*Xo + (u/(2*Sc)) 2*Xo + (u/(2*Sc))-(Sc/3)], [2*Yo/3-(v1/Sc)/2 2*Yo/3-(v1/Sc)/2-(Sc/3)],
'Color','r', 'LineWidth',1)
line([2*Xo - (v1/(2*Sc))*tan(B_r1*pi/180) 2*Xo], [2*Yo/3 2*Yo/3-(v1/Sc)/2], 'Color','k', 'LineWidth',3)
line([2*Xo 2*Xo + (v1/(2*Sc))*tan(B_r1*pi/180)], [2*Yo/3-(v1/Sc)/2 2*Yo/3-(v1/Sc)], 'Color','k',
'LineWidth',3)

% Stator
line([2*Xo - (v1/(2*Sc))*tan(B_s1*pi/180) 2*Xo], [Yo/3 Yo/3-(v1/Sc)/2], 'Color','k', 'LineWidth',3)
line([2*Xo 2*Xo + (v1/(2*Sc))*tan(B_s1*pi/180)], [Yo/3-(v1/Sc)/2 Yo/3-(v1/Sc)], 'Color','k',
'LineWidth',3)

% Captures image for future viewing
Movie_Triangles(j) = getframe;

% *****

end
% end of control loop

% output results
fprintf('\n')
fprintf('      Exit Temperature = %g K', T2(j))
fprintf('\n')
fprintf('      Pressure Ratio = %g', Pr(j))
fprintf('\n')
fprintf('      Inlet Mach Number = %g', M1)
fprintf('\n')
fprintf('      Exit Mach Number = %g', M2)
fprintf('\n')
fprintf('\n')
fprintf('*****')
fprintf('\n')

% graph plotting
figure(2)
plot(Bigv)
grid on
xlabel('Time Step','FontSize',12,'FontWeight','bold','FontName','Times New Roman')
ylabel('IGV Angle (rad)','FontSize',12,'FontWeight','bold','FontName','Times New Roman')
title('Change in IGV Angle Change', 'FontWeight','bold','FontSize',16,'FontName','Times New Roman')

figure(3)
plot(count, idesign_r1, count,i_r1,count,error_r1)
grid on
xlabel('Time Step','FontSize',12,'FontWeight','bold','FontName','Times New Roman')
ylabel('Angle (deg)','FontSize',12,'FontWeight','bold','FontName','Times New Roman')
title('Incidence Angles', 'FontWeight','bold','FontName','Times New Roman','FontSize',16)
h = legend('i*','i', 'Error', 1);

figure(4)
plot(Rotor_In_Angle)
xlabel('Time Step','FontSize',12,'FontWeight','bold','FontName','Times New Roman')

```

Compressor_IGV_Surge.m

```
ylabel('Rotor Inlet Angle (deg)', 'FontSize', 12, 'FontWeight', 'bold', 'FontName', 'Times New Roman')
title('Change in Rotor Inlet Angle', 'FontWeight', 'bold', 'FontName', 'Times New Roman')
grid on

figure(6)
plot(Rotor_Out_Angle)
xlabel('Time Step', 'FontSize', 12, 'FontWeight', 'bold', 'FontName', 'Times New Roman')
ylabel('Rotor Outlet Angle (deg)', 'FontSize', 12, 'FontWeight', 'bold', 'FontName', 'Times New Roman')
title('Change in Rotor Out Angle', 'FontWeight', 'bold', 'FontName', 'Times New Roman')
grid on

for i = 1:1400
    x = i/1000;
    y(i) = 0.33*x^2 + 0.35;
    z(i) = 0.33*x^2 + 0.30;
    ccount(i) = x;
end

figure(8)
plot(ccount, y, ccount, z, Phi, Psi)
grid on
axis([0 1.4 0 1])
xlabel('Mass Flow Coefficient, \Phi', 'FontSize', 12, 'FontWeight', 'bold', 'FontName', 'Times New Roman')
ylabel('Work Coefficient, \Psi', 'FontSize', 12, 'FontWeight', 'bold', 'FontName', 'Times New Roman')
title('Compressor Characteristic', 'FontWeight', 'bold', 'FontName', 'Times New Roman', 'FontSize', 16)

% figure(9)
% plot(count, W2, count, W3, count, w3w2)
% grid on
% g = legend('w_2', 'w_3', 'w_3=w_2', 1);

figure(10)
plot(Phi)
xlabel('Time Step', 'FontSize', 12, 'FontWeight', 'bold', 'FontName', 'Times New Roman')
ylabel('Mass Flow Coefficient, \Phi', 'FontSize', 12, 'FontWeight', 'bold', 'FontName', 'Times New Roman')
title('Change in Mass Flow Coefficient', 'FontWeight', 'bold', 'FontName', 'Times New Roman', 'FontSize', 16)
grid on

figure(11)
plot(Psi)
xlabel('Time Step', 'FontSize', 12, 'FontWeight', 'bold', 'FontName', 'Times New Roman')
ylabel('Work Coefficient, \Psi', 'FontSize', 12, 'FontWeight', 'bold', 'FontName', 'Times New Roman')
title('Change in Work Coefficient', 'FontWeight', 'bold', 'FontName', 'Times New Roman', 'FontSize', 16)
grid on

figure(12)
plot(error_Psi)
grid on
xlabel('Time Step', 'FontSize', 12, 'FontWeight', 'bold', 'FontName', 'Times New Roman')
ylabel('Error in \Psi', 'FontSize', 12, 'FontWeight', 'bold', 'FontName', 'Times New Roman')
title('Error value', 'FontWeight', 'bold', 'FontName', 'Times New Roman', 'FontSize', 16)

figure(13)
plot(count, ddesign_r1, count, d_r1, count, error_d)
grid on
xlabel('Time Step', 'FontSize', 12, 'FontWeight', 'bold', 'FontName', 'Times New Roman')
```

Compressor_IGV_Surge.m

```
ylabel('Angle (deg)', 'FontSize', 12, 'FontWeight', 'bold', 'FontName', 'Times New Roman')
title('Deviation Angle', 'FontWeight', 'bold', 'FontName', 'Times New Roman', 'FontSize', 16)
h = legend('\delta*_', '\delta', 'Error_\delta', 1);

figure(14)
plot(N_Holder)
xlabel('Time Step', 'FontSize', 12, 'FontWeight', 'bold', 'FontName', 'Times New Roman')
ylabel('Rotor Speed (rpm)', 'FontSize', 12, 'FontWeight', 'bold', 'FontName', 'Times New Roman')
title('Change in Rotor Speed', 'FontWeight', 'bold', 'FontName', 'Times New Roman')
grid on

figure(15)
plot(Reaction)
grid on
xlabel('Time Step', 'FontSize', 12, 'FontWeight', 'bold', 'FontName', 'Times New Roman')
ylabel('Reaction', 'FontSize', 12, 'FontWeight', 'bold', 'FontName', 'Times New Roman')
title('Degree of Reaction', 'FontWeight', 'bold', 'FontSize', 16, 'FontName', 'Times New Roman')

figure(16)
plot(DeHaller)
grid on
xlabel('Time Step', 'FontSize', 12, 'FontWeight', 'bold', 'FontName', 'Times New Roman')
ylabel('DeHaller Number', 'FontSize', 12, 'FontWeight', 'bold', 'FontName', 'Times New Roman')
title('Change in DeHaller Number', 'FontWeight', 'bold', 'FontName', 'Times New Roman', 'FontSize', 16)
```

Burner.m

```
% *****
% Burner - calculates the stagnation temperature [K] and pressure [Pa] at the burner exit
%
% Programmed by Mark Laderman, Ryerson University, 2004
% *****

% calculates the stagnation temperature [K] and pressure [Pa] at the burner exit
%(see Equation 2.59 and 2.60)

To3 = (eff_b*f*qr + cp_c*To2)/((1+f)*cp_be);
Po3 = pi_b * Po2;

% checks that the burner temperature is below the maximum specified value
if To2 >= Tmax
    fprintf('Error: Engine overheating at compressor outlet');
    break;
end

% output results
fprintf('\n')
fprintf('*****')
fprintf('\n')
fprintf('*          Burner          *')
fprintf('\n')
fprintf('*****')
fprintf('\n')
fprintf('\n')
fprintf('  Exit Stagnation Temperature = %g K', To3)
fprintf('\n')
fprintf('  Exit Stagnation Pressure = %g', Po3)
fprintf('\n')
fprintf('\n')
fprintf('*****')
fprintf('\n')
```

Turbine.m

```
% *****
% Turbine - One stage with nozzle (stator)
%
% Programmed by Mark Laderman, Ryerson University, 2004
% *****

% velocity triangles (see Compressor)
To30 = To3;           % [K]
Po30 = Po3;           % [Pa]

v30 = V2;             % gas entering nozzle row [m/s]
alpha30 = 0;          % angle of entering gas

va30 = v30*cos(alpha30); % axial velocity of entering gas [m/s]

va35 = va30;          % axial velocity entering rotor [m/s]

alpha35 = B_nol*pi/180; % air turn by nozzle [rad]

v35 = va35/cos(alpha35);
vu35 = v35*sin(alpha35);
wu35 = vu35 - U;
B35 = atan(wu35/va35);
w35 = sqrt(wu35^2 + va35^2);

va40 = va35;          % Assume axial velocity is constant [m/s]

B40 = B_rtol*pi/180;
w40 = va40 / cos(B40);
wu40 = w40*sin(B40);

vu40 = wu40 + U;
alpha40 = atan(vu40/va40); % exit angle [rad]
v40 = sqrt(vu40^2 + va40^2); % exit velocity [m/s]

% maximum velocity in the stage is the absolute velocity at the nozzle exit (stage 35)
% calculate Mach number at nozzle exit

ho30 = cp_t * To30;
ho35 = ho30;

h35 = ho35 + v35^2/2;
T35 = h35/cp_t;

a35 = sqrt(k_t*R_t*T35);
M35 = v35/a35;

% monitors turbine flow speeds
if M35 >= 1
    fprintf('Error: Turbine flow speeds are sonic. ');
    break;
elseif M35 > .90
    fprintf('Warning: Turbine flow speeds approaching sonic velocities. ');
end

% work done by turbine (must be greater then work required by the compressor)
w = U*(vu35 - vu40); % (Kj/kg)
```

Turbine.m

```

ho40 = ho30 - w;
To40 = ho40/cp_t;

Po40 = Po30 / ((To30/To40)^(k_t/(k_t-1)));

Pro = Po30/Po40;

Reaction_t = 0.5 * (va30/(2*U))*(tan(B40)+tan(alpha35));

h40 = ho40 - v40^2/2;
T40 = h40/cp_t;

To4 = To40;
Po4 = Po40;
V4 = v40;

% output results
fprintf('\n')
fprintf('*****')
fprintf('\n')
fprintf('*           Turbine           *')
fprintf('\n')
fprintf('*****')
fprintf('\n')
fprintf('\n')
fprintf('Exit Stagnation Temperature = %g K', To40)
fprintf('\n')
fprintf('Exit Stagnation Pressure = %g', Po40)
fprintf('\n')
fprintf('Exit Mach Number = %g', v40/sqrt(k_t * R_t * T40));
fprintf('\n')
fprintf('\n')
fprintf('*****')
fprintf('\n')

```

Afterburner_No.m

```
% *****  
% Afterburner - NO  
% The stagnation pressure and temperature at the turbine exit is equal to that at the nozzle entrance  
%  
% Programmed by Mark Laderman, Ryerson University, 2004  
% *****  
  
To5 = To4;  
Po5 = Pc4;  
V5 = V4;
```

Afterburner_Yes.m

```
% *****
% Afterburner - YES
% Engine contains an afterburner (see Section 2.1.3 same as burner calculations)
%
% Programmed by Mark Laderman, Ryerson University, 2004
% *****

To5 = (eff_ab*f_ab*qr + cp_t*To4)/((1+f_ab)*cp_abe);    % [K]
Po5 = pi_ab * Po4;                                     % [Pa]

% output results
fprintf('\n')
fprintf('*****')
fprintf('\n')
fprintf('*          After Burner          *')
fprintf('\n')
fprintf('*****')
fprintf('\n')
fprintf('\n')
fprintf('  Exit Stagnation Temperature = %g K, T05)')
fprintf('\n')
fprintf('  Exit Stagnation Pressure = %g, Po5)')
fprintf('\n')
fprintf('\n')
fprintf('*****')
fprintf('\n')
```

Converging_Nozzle.m

```
% *****
% Converging Nozzle
%
% Programmed by Mark Laderman, Ryerson University, 2004
% *****

fprintf('\n')
fprintf('*****')
fprintf('\n')
fprintf('          Converging Nozzle          ')
fprintf('\n')
fprintf('*****')
fprintf('\n')

P5 = 1.2*P; % (Pa)
T5 = To5 = (V5^2)/(2*cp_n);

% stagnation pressure
Po5 = P5*(To5/T5)^(k/(k-1));

% nozzle choke condition (see Equation 2.19)
P5_star = Po5*(2/(k_n+1))^(k_n/(k_n-1));

% if nozzle is choked
if P5_star > P
    fprintf('\n')
    fprintf('          Nozzle is choked')
    P6 = P5_star;
    T6 = To5*(2/(k_n+1));
    V6 = sqrt(k_n * R_n * T6);
else
    % if nozzle is not choked
    fprintf('\n')
    fprintf('          Nozzle is not choked')
    P6 = P;
    T6 = To5*(P6/Po5)^((k_n-1)/k_n);
    V6 = sqrt(2*(T5-T6)*cp_n);
end

M6 = V6/sqrt(k_n*R_n*T6);

% Calculate Thrust
Thrust = (P6-P)*A6_n + mass_flow_air*((1+f)*V6 - v);

fprintf('\n')
fprintf('          Exit Temperature = %g K', T6)
fprintf('\n')
fprintf('          Exit Pressure = %g Pa', P6)
fprintf('\n')
fprintf('          Exit Velocity = %g m/s', V6)
fprintf('\n')
fprintf('          Exit Mach Number = %g', M6)
fprintf('\n')
fprintf('          Thrust = %g N', Thrust)
fprintf('\n')
fprintf('*****')
```

Con_Div_Nozzle.m

```
% *****
% Converging-Diverging Nozzle
% Thrust is calculated assuming throat is always at critical sonic area
% and that no shock occurs in nozzle
%
% Programmed by Mark Laderman, Ryerson University, 2004
% *****

fprintf('\n')
fprintf('*****')
fprintf('\n')
fprintf('*          Converging-Diverging Nozzle          *')
fprintf('\n')
fprintf('*****')
fprintf('\n')

% calculates temperature [K], pressure [Pa] and Mach number and nozzle entrance
% (see Equations 2.27 and 2.28)
V5 = V4; % (m/s)
T5 = T05 - (V5^2)/(2*c_p_n);
P5 = P05/((T05/T5)^(k_n/(k_n-1)));
M5 = V5/sqrt(R_n * k_n * T5);

% Critical throat area [m^2] (see Equation 2.29)
A_star = A5_n/((1/M5)*((1+0.5*(k_n-1)*M5^2)/(0.5*(k_n+1)))^(0.5*(k_n+1)/(k_n-1)));

% step solver is run to find the nozzle exit Mach number using an initial guess of M = 1
% (see Equation 2.30)
M_exit = 1;
Error = ((1/M_exit)*((1+0.5*(k_n-1)*M_exit^2)/(0.5*(k_n+1)))^(0.5*(k_n+1)/(k_n-1)));
A_ratio = A6_n/A_star;

if (A6_n > A_star)
    while (A_ratio - Error) > 0.001
        M_exit = M_exit + 0.001;
        Error = ((1/M_exit)*((1+0.5*(k_n-1)*M_exit^2)/(0.5*(k_n+1)))^(0.5*(k_n+1)/(k_n-1)));
    end
    % simulation will halt if the nozzle exit area is smaller then the critical throat area
elseif (A6_n <= A_star)
    fprintf('Error: Nozzle exit area is smaller then throat area. ');
    break;
end

M6 = M_exit;

% exit temperature and pressure (see Equation 2.31 and 2.32)
T6 = T05/(1+((k_n-1)/2)*M6^2);
P6 = P05/(T05/T6)^(k_n/(k_n-1));

V6 = M6*sqrt(k_n*R_n*T6);

% calculates engine thrust (see Equation 2.26)
Thrust = (P6-P)*A6_n + mass_flow_air*((1+f)*V6 - v);

fprintf('\n')
fprintf('          Exit Temperature = %g K', T6)
```

Con_Div_Nozzle.m

```
fprintf('\n')
fprintf('      Exit Pressure = %g Pa', P6)
fprintf('\n')
fprintf('      Exit Velocity = %g m/s', V6)
fprintf('\n')
fprintf('      Entrance Mach Number = %g', M5)
fprintf('\n')
fprintf('      Exit Mach Number = %g', M6)
fprintf('\n')
fprintf('      Thrust = %g N', Thrust)
fprintf('\n')
fprintf('\n')
fprintf('*****')
fprintf('\n')
```